SANDIA REPORT

SAND97-1585 • UC-505
Unlimited Release
Printed July 1997

The Fireball Integrated Code Package

Dean Dobranich, Dana A. Powers, Frederick T. Harper

Prepared by
Sandia National Laboratories
Albuquerque, New Mexico 87185 and Livermore, California 94550

Sandia is a multiprogram laboratory operated by Sandia Corporation, a Lockheed Martin Company, for the United States Department of Energy under Contract DE-AC04-94AL85000.

Sandia National Laboratories

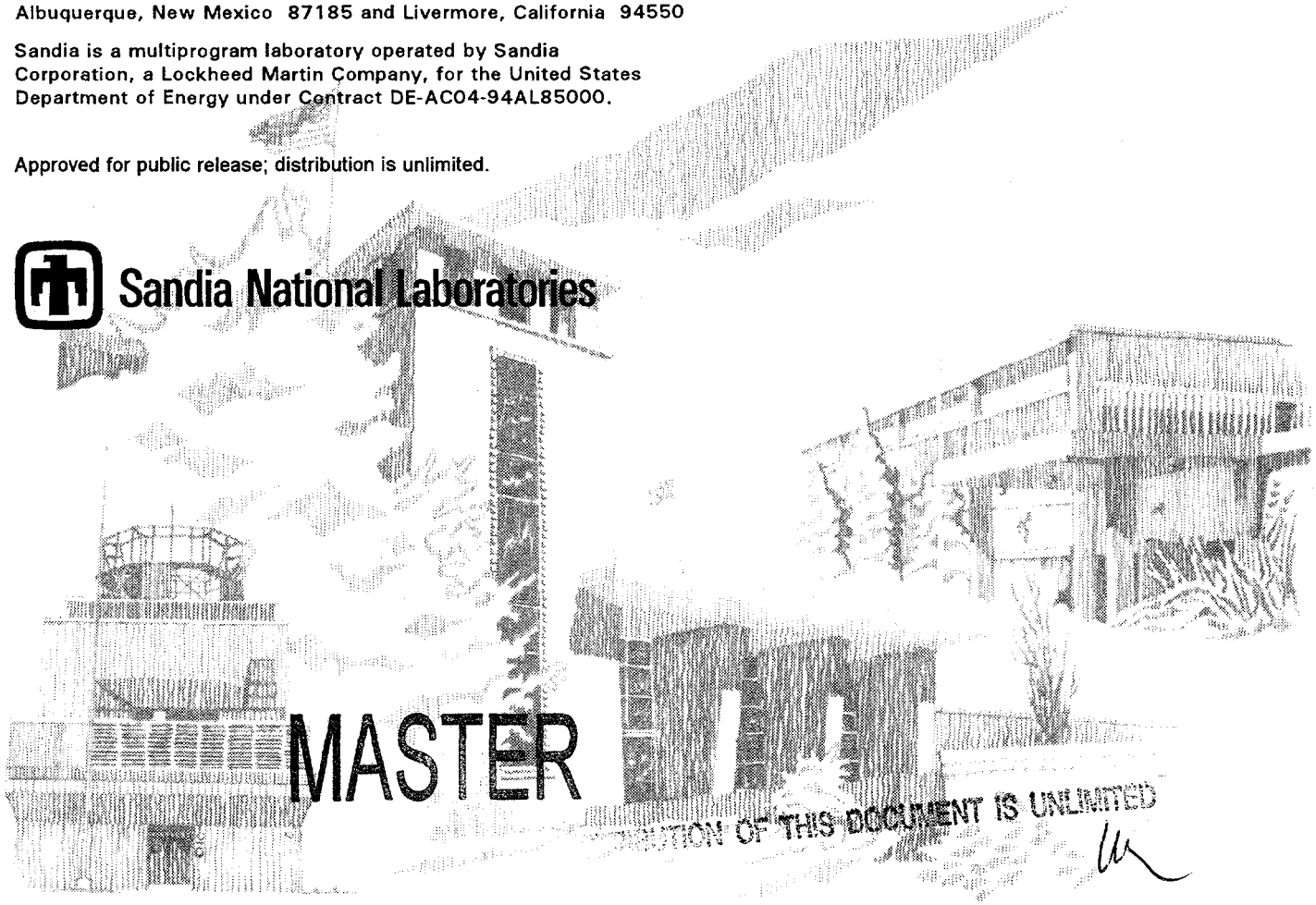

SF2900Q(8-81)

Issued by Sandia National Laboratories, operated for the United States Department of Energy by Sandia Corporation.

Available to DOE and DOE contractors from
Office of Scientific and Technical Information
P.O. Box 62
Oak Ridge, TN 37831

Prices available from (615) 576-8401, FTS 626-8401

Available to the public from
National Technical Information Service
U.S. Department of Commerce
5285 Port Royal Rd
Springfield, VA 22161

NTIS price codes
Printed copy: A06
Microfiche copy: A01

DISCLAIMER

SAND97-1585
Unlimited Release
July 1997

Distribution
Category UC-505

The Fireball Integrated Code Package

Dean Dobranich
Thermal Sciences Department

Dana A. Powers
Nuclear Facilities Safety Department

Frederick T. Harper
Accident Analysis and Consequence Assessment Department

Sandia National Laboratories
P. O. Box 5800
Albuquerque, NM 87185-0835

Abstract

Many deep-space satellites contain a plutonium heat source. An explosion, during launch, of a rocket carrying such a satellite offers the potential for the release of some of the plutonium. The fireball following such an explosion exposes any released plutonium to a high-temperature chemically-reactive environment. Vaporization, condensation, and agglomeration processes can alter the distribution of plutonium-bearing particles. The Fireball code package simulates the integrated response of the physical and chemical processes occurring in a fireball and the effect these processes have on the plutonium-bearing particle distribution. This integrated treatment of multiple phenomena represents a significant improvement in the state of the art for fireball simulations. Preliminary simulations of launch-abort scenarios indicate: (1) most plutonium vaporization occurs within the first second of the fireball; (2) large non-aerosol-sized particles contribute very little to plutonium vapor production; (3) vaporization and both homogeneous and heterogeneous condensation occur simultaneously; (4) homogeneous condensation transports plutonium down to the smallest-particle sizes; (5) heterogeneous condensation precludes homogeneous condensation if sufficient condensation sites are available; and (6) agglomeration produces larger-sized particles but slows rapidly as the fireball grows.

Acknowledgments

The advice of several experts from a diverse range of disciplines was essential to the creation of the Fireball code package within the very limited time frame allotted for development. The advice of the following individuals is greatly appreciated:

- Thermodynamics – Ronald C. Dykhuizen (9113)
- Fire Physics – Sheldon R. Tieszen (9116)
- Chemistry – David C. Williams (6421)
- Aerosol Physics – John E. Brockmann (9114)
- Chemistry – Michael L. Hobbs (9112)
- Chemistry – Maher E. Tadros (6472)

In addition, David K. Monroe (1276) provided code support for the conversion of Maeros2 into a callable subroutine for Fireball implementation, and Vincent J. Dandini (6412) and Kelly M. Hayes (6412) provided code testing support.

Contents

Figures

Tables

Executive Summary

Many deep-space satellites contain a plutonium heat source. An explosion, during launch, of a rocket carrying such a satellite offers the potential for the release of some of the plutonium. For such hypothetical explosions, it is desirable to predict the quantity and size distribution of plutonium-bearing particles released to the environment. The fireball following such an explosion exposes any released plutonium to a high-temperature, chemically-reactive environment. Vaporization, condensation, and agglomeration processes occurring within this environment can then alter the distribution of plutonium-bearing particles. The Fireball code package simulates the integrated response of the physical and chemical processes occurring in a fireball, and the effect these processes have on the plutonium-bearing particle distribution.

The Fireball code package provides a fast-running computational tool for assessing the impact of hypothetical launch-abort fireballs on the quantity and size distribution of plutonium-bearing particles. Examination of the Fireball code simulations indicate that an integrated approach is necessary to capture the complex nonlinear phenomena inherent in a fireball. An integrated approach, along with an increase in sophistication of the physics and chemistry submodels, provides a significant improvement over models used previously.

The intent of Fireball code development is to provide a first-order integrated model to enable parametric investigations of various launch-abort scenarios. A first-order fireball model is one that approximately captures the dominant physical and chemical processes occurring in the fireball. The many uncertainties inherent in the simulation of plutonium particle dispersal from a hypothetical explosion make it desirable to address these uncertainties parametrically. Thus many fireball simulations are required, necessitating a fast-running and flexible code. The objective here is to determine how the fireball environment modifies the size distribution of all plutonium-bearing particles.

The following list provides a summary of the key features of the Fireball code package:

- Fully-integrated thermodynamics, chemistry, heat and mass transfer, vaporization and condensation, and agglomeration models.
- Many user-selectable input parameters to facilitate parametric investigations.
- Adaptive time step control for the entire transient simulation.
- Sequential or concurrent combustion of multiple reactant mixes with a different combustion rate and pressure specified for each.
- Transient heat transfer solution for multiple aluminum-alloy structures, including melting, vaporization, and combustion of aluminum vapor.

- Quasi-static heat transfer solution for agglomerated aerosol particles with a coupled vaporization/condensation model.
- Transient heat transfer solution for non-aerosol particles (rocks) with a coupled vaporization/condensation model.
- Simultaneous heterogeneous and homogeneous condensation processes for plutonium based on both fireball temperature and chemical composition.
- Fireball emissivity based on the calculated composition of the combustion gases and on the concentration of all suspended particles.
- Fireball emissivity coupled to the structure and particle heat transfer models and to the fireball energy equation.
- Convection (based on the fireball properties) and radiation boundary conditions for all structure and particle heat transfer calculations, with the fireball treated as a semitransparent participating medium for radiation.
- Coupled aerosol physics model for the simulation of multicomponent particle agglomeration and gravitational settling.
- Five particle components considered for heat transfer and agglomeration: original plutonium, condensed plutonium, soot (equilibrium and supplemental), generated aluminum oxide, and entrained dirt.
- Non-spherical particles accounted for via user-specified shape factor that directly affects agglomeration, particle heat transfer, and fireball emissivity.
- Automatic update of agglomeration section coefficients based on user-specified time and temperature intervals.
- Time-varying control volume associated with fireball growth accounted for in agglomeration governing equations.
- Momentum equation for the fireball rise velocity accounts for buoyancy, drag, and time-varying volume effects.
- Calculation of entrained air for both the combustion and entrainment stages based on fireball size and velocity, and user-specified entrainment coefficients.
- Simple models of soot production and dirt entrainment allow parametric investigations of particle response in a fireball.

Preliminary simulations of launch-abort scenarios using the Fireball code package indicate: (1) most plutonium vaporization occurs within the first second of the fireball; (2) large non-aerosol-sized particles contribute very little to plutonium vapor production; (3) plutonium vaporization and both homogeneous and heterogeneous condensation occur simultaneously because of the different temperatures of the various-sized particles; (4) homogeneous condensation transports plutonium down to the smallest-particle sizes; (5) heterogeneous condensation precludes homogeneous condensation if sufficient condensation sites are available; and (6)

agglomeration produces larger-sized particles but slows rapidly as the fireball expands or cools.

Introduction

Many deep-space satellites make use of a what is referred to as a General Purpose Heat Source (GPHS), which contains substoichiometric plutonium dioxide fuel. The major constituent of this fuel is plutonium-238, which has an activity level of about 15 Curies/g and a half life of 87.7 years. For brevity, throughout this report, the term "plutonium" is often used in place of the technically-correct term "substoichiometric plutonium dioxide." The use of the term "plutonium" should be unambiguous in the context in which it is used. The term "plutonia" is now considered archaic and therefore is not used here.

Plutonium from the GPHS may be released to the environment following a hypothetical explosion of a space vehicle on the launch pad or during ascent. Three phases of calculations are needed to assess the impact of such an explosion: (1) the blast phase, (2) the fireball phase, and (3) the plume dispersion phase. Simulation of the blast phase is performed using other codes and is not addressed here. These other codes predict the particle-size distribution (the number of plutonium particles in each of several representative size bins) following an explosion. This particle-size distribution is then modified by the relevant fireball physics and chemistry. The modified distribution is then provided to a plume dispersion model, which calculates the dispersal of the released plutonium in the atmosphere. *This report addresses the Fireball code package used to model the fireball phase.*

The next section provides an overview of the Fireball code package. This overview is strictly qualitative and provides a concise description of the individual models in the code and how they are connected. In the sections to follow are detailed descriptions of each model, including all assumptions, governing equations, and their derivations. Following these detailed descriptions are sections describing model integration, code use, sample results, and summary comments with recommendations.

This report provides a detailed description of the code, which is essential for proper code assessment and results interpretation. This report also serves as a user's manual for the Fireball code. Because a large number of technical papers and books were reviewed in preparation for Fireball model development, an extensive bibliography is included. This bibliography, together with the references, provides a useful compendium of information sources for those interested in further pursuit of fireball modeling.

Fireball Model Overview

The Fireball code package consists of three codes integrated into a single fireball simulation code, referred to as Fireball. The CET89 code,[1,2] converted to a subroutine, is used to perform the combustion thermodynamic calculations. The Maeros2 code,[3] also converted to a subroutine, is used to perform the aerosol physics calculations. All the remaining calculations, such as fireball physics and particle heat transfer, are calculated by new routines written specifically for launch-abort fireball simulations. The entire fireball simulation is controlled in this new Fortran77 code.

The behavior of the fireball is assumed to consist of two stages for purposes of simulation: (1) the combustion stage, and (2) the entrainment stage. During the combustion stage, the fireball temperature and size increase as the propellant of the launch or space vehicle burns. This is countered by radiative and convective heat losses from the fireball to the ambient environment and to structures within the fireball. Air entrainment also occurs during this stage but is expected to have a small effect compared to combustion. Following the combustion stage, the fireball lifts from the ground and rises due to buoyant forces, resulting in entrainment of air and dirt. No propellant combustion is assumed to occur during the entrainment stage.

An overall description of the fireball model is depicted schematically in Figure 1. The arrows depict the general direction of information exchange between the various submodels. The initial plutonium particle size distribution is provided as input to the Fireball code. Such input could come from explosion/debris computer codes or from experimental data. The modified particle size distribution is part of the output of the Fireball code; this output can then be made available to a plume dispersal code if desired.

The initial plutonium particle distribution can be modified by the fireball via several temperature-driven mechanisms. Four such mechanisms are included in the current fireball model: (1) vaporization of plutonium particles followed by homogeneous and heterogeneous condensation; (2) agglomeration with entrained dirt particles; (3) agglomeration with soot particles arising from propellant combustion; and (4) agglomeration with aluminum oxide (Al_2O_3) particles arising from the vaporization of aluminum-alloy structures (such as the rocket) and subsequent combustion within the fireball. In addition to agglomeration, the introduction of particles into the fireball results in additional sites for heterogeneous condensation. These mechanisms are simulated to assess the impact of agglomeration, vaporization, and condensation on the size distribution and plutonium mass fraction of the released plutonium-bearing particles.

The intent of the Fireball code is to provide a first-order model to enable parametric investigations of various launch-abort scenarios. A first-order fireball model is one that approximately captures the dominant physical and chemical processes occurring in the fireball. The many uncertainties inherent in the simulation of plutonium particle dispersal from a hypothetical explosion make it desirable to address these uncertainties via parametric simulations. Thus many fireball simulations are required, necessitating a fast-running and flexible code.

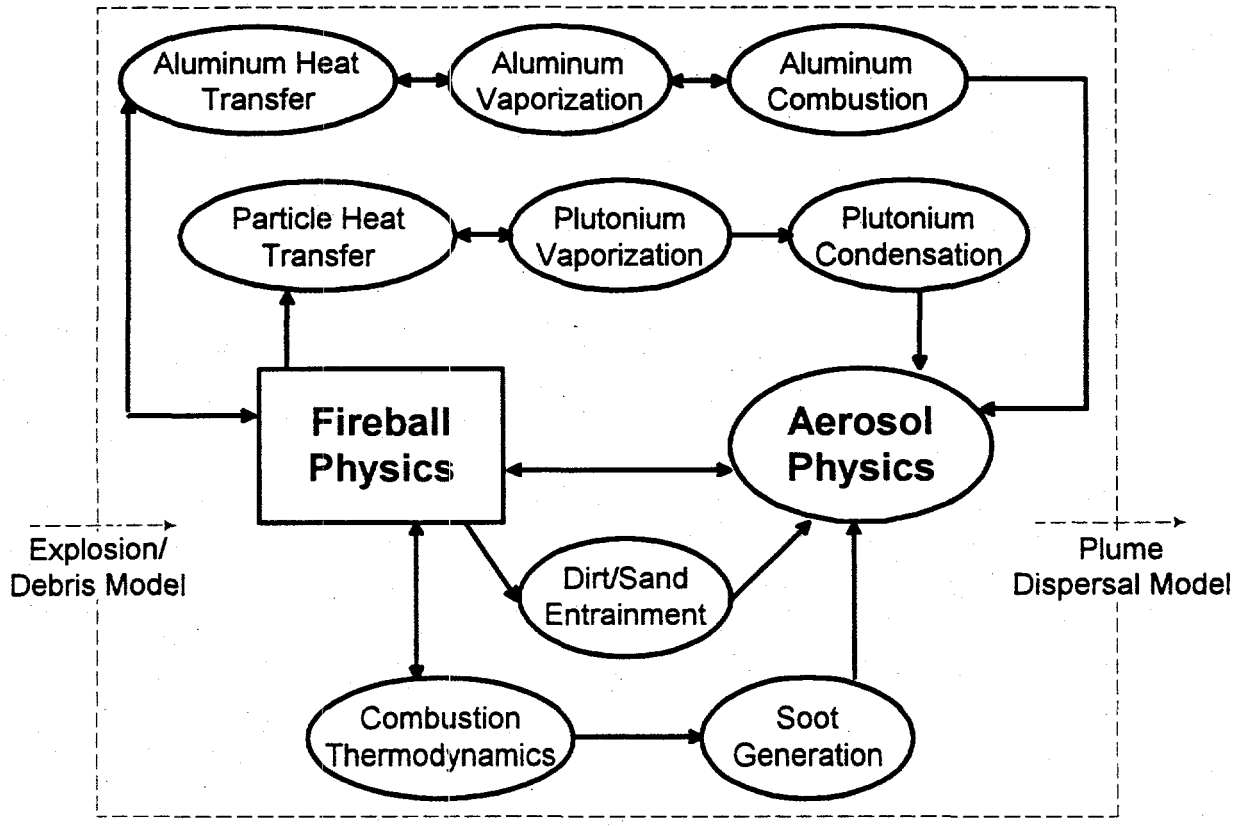

Figure 1. Schematic of the Fireball Model

A key feature of the Fireball code is that it provides a fully-integrated simulation capability involving thermodynamics, chemistry, heat and mass transfer, vaporization and condensation, and agglomeration. Thus all relevant processes are included in a single code and each process depends on the outcome of other processes. This fully-integrated feature significantly advances the state of the art for fireball simulations.

Of primary importance in the Fireball code is the fireball physics model. This model predicts the temperature, composition, size, and rise velocity of the fireball that develops after a hypothetical explosion of a launch vehicle. Although there is a wealth of experimental data on fireballs, this data provides only macroscopic features such as size, rise velocity, and luminosity. Because experimental data of flow structure details is lacking, and in light of the large uncertainties involved,

detailed multidimensional models do not seem warranted. The fireball physics model used in the Fireball code is based on a single uniformly-mixed control volume that changes size as combustion, air entrainment, and heat loss proceed. Solution of an energy equation for this control volume provides a first-order estimate of the fireball temperature.

For ground blasts, the fireball begins as a hemisphere and transitions to a full sphere upon liftoff. For air blasts, the fireball is treated as a sphere. The rise of the fireball is based on solution of a momentum equation including buoyancy, drag, and time-varying volume effects. Air entrainment into the fireball is coupled to this model and is based on the size and rise velocity of the fireball along with user-specified entrainment coefficients. Heat loss from the fireball is from radiation to the ambient environment, and from convection and radiation to any immersed structures. All gas properties are dependent on the fireball temperature. The fireball emissivity is based on the gas composition and particle inventory.

The quantity and composition of the products of combustion are calculated based on equilibrium thermodynamics. Because of the high reaction rates associated with the high temperatures involved in fireballs, the assumption of equilibrium is expected to be reasonable. Combustion thermodynamics is calculated using the CET89 code,[1,2] which has been converted to a callable subroutine. The thermophysical and transport properties of the combustion products are provided by the extensive property routines in the CET89 code. These properties are required in the solution of the fireball energy equation. The Fireball code package is configured to allow the introduction of any number of reactant mixes. These mixes can be specified to burn either sequentially or concurrently. In addition, the combustion rate and pressure for each mix can be specified, allowing different abort scenarios to be simulated. For example, a tail-down impact of the rocket would produce a different propellant-introduction timing sequence than a nose-first impact. Both of these abort scenarios can be simulated with the Fireball code by providing the appropriate reactant mix timing, combustion rate and pressure parameters.

Aerosol physics within the fireball is simulated using the Maeros2 code converted to a callable subroutine. The Maeros2 code is based on dividing the continuous distribution of particle sizes into a finite number of size sections. More sections increase accuracy but slow the calculation. The aerosol within the fireball is assumed to contain five components: (1) plutonium dioxide debris from the initial explosion, (2) condensed plutonium dioxide, (3) carbon (soot), (4) aluminum oxide, and (5) entrained dirt. Agglomeration of the various components is assumed to be due to three processes: (1) gravitational settling, (2) Brownian motion, and (3) turbulent diffusion. Particles can change size sections as agglomeration proceeds. The largest consumer of execution time in the fireball model is the generation of section coefficients used in the aerosol physics solution. To reduce this time, the section coefficients are evaluated based on user-specified time and

temperature intervals, as opposed to being evaluated every fireball time step. The transient agglomeration model maintains its own adaptive time step between section coefficient reevaluations. Linear interpolation of section coefficients and fireball property data is used at each agglomeration-model time step.

Heat transfer to particles immersed in the fireball is modeled for both agglomerated aerosol particles and plutonium "rock" particles. The larger rock particles are assumed to not behave as aerosol particles and do not agglomerate. Both aerosol and rock particle heat transfer models include the effects of the size change associated with plutonium vaporization and condensation. A quasi-static model is used for agglomerated aerosol particles and a full transient model is used for the larger rock particles which are assumed to not agglomerate. Both convection (forced and free) and radiation are included, with forced convection based on the particle terminal velocity in the fireball. The radiation model treats the fireball as a semitransparent medium such that the particle can exchange heat with both the fireball and the ambient environment depending on the fireball emissivity, which is based on the fireball gas composition and the particle inventory. Particles are assigned size sections consistent with those used for agglomeration. Particles can change size sections based on any vaporization or condensation occurring in that section.

The model for the vaporization of plutonium accounts for both the fireball temperature and its chemical composition. In addition, the model is coupled with the particle heat transfer models, which are in turn coupled with the aerosol physics model. The vaporization model also applies to heterogeneous condensation when the partial pressure driving potential is negative. Both heterogeneous and homogeneous condensation can occur simultaneously. Homogeneous condensation is initiated when the supersaturation ratio of plutonium dioxide vapor exceeds a user-specified critical limit. Condensed particles can agglomerate with other particles or vaporize depending on the evolution of the fireball.

To simulate the response of aluminum-alloy structures immersed in the fireball (such as rocket casings), models are included for structure heat transfer, vaporization, and combustion. The transient lumped-capacitance heat transfer model allows the specification of an effective heat transfer area to the fireball for multiple structures. Convection, radiation, melting, and appropriate mass loss terms are included. Any aluminum vaporized from a structure is assumed to immediately combust with the oxygen in the fireball, producing aluminum oxide particles. These particles are then allowed to agglomerate with other particles or to serve as condensation sites for plutonium vapor.

Because of the complexity and uncertainty associated with soot generation and dirt entrainment, only simple parametric models are included in the Fireball code package for these processes. Both soot and dirt particles affect the fireball emissivity and provide additional condensation and agglomeration sites. The soot

model allows the user-specified addition of supplemental soot, which is added to any soot predicted by the equilibrium chemistry solution. The dirt entrainment model allows the input of a dirt entrainment rate for both the combustion and air entrainment stages. These simple models allow the parametric investigation of soot and dirt particles in a fireball.

The following list is provided to summarize the key features of the Fireball code package:

- Fully-integrated thermodynamics, chemistry, heat and mass transfer, vaporization and condensation, and agglomeration models.
- Many user-selectable input parameters to facilitate parametric investigations.
- Adaptive time step control for the entire transient simulation.
- Sequential or concurrent combustion of multiple reactant mixes with a different combustion rate and pressure specified for each.
- Transient heat transfer solution for multiple aluminum-alloy structures, including melting, vaporization, and combustion of aluminum vapor.
- Quasi-static heat transfer solution for agglomerated aerosol particles with a coupled vaporization/condensation model.
- Transient heat transfer solution for non-aerosol particles (rocks) with a coupled vaporization/condensation model.
- Simultaneous heterogeneous and homogeneous condensation processes for plutonium based on both fireball temperature and chemical composition.
- Fireball emissivity based on the calculated composition of the combustion gases and on the concentration of all suspended particles.
- Fireball emissivity coupled to the structure and particle heat transfer models and to the fireball energy equation.
- Convection (based on the fireball properties) and radiation boundary conditions for all structure and particle heat transfer calculations, with the fireball treated as a semitransparent participating medium for radiation.
- Coupled aerosol physics model for the simulation of multicomponent particle agglomeration and gravitational settling.
- Five particle components considered for heat transfer and agglomeration: original plutonium, condensed plutonium, soot (equilibrium and supplemental), generated aluminum oxide, and entrained dirt.
- Non-spherical particles accounted for via user-specified shape factor that directly affects agglomeration, particle heat transfer, and fireball emissivity.
- Automatic update of agglomeration section coefficients based on user-specified time and temperature intervals.

- Time-varying control volume associated with fireball growth accounted for in agglomeration governing equations.
- Momentum equation for the fireball rise velocity accounts for buoyancy, drag, and time-varying volume effects.
- Calculation of entrained air for both the combustion and entrainment stages based on fireball size and velocity, and user-specified entrainment coefficients.
- Simple models of soot production and dirt entrainment allow parametric investigations of particle response in a fireball.

The governing equations for the fireball temperature, size, and rise velocity, along with the equations for the four particle-distribution-modifying mechanisms, and the aerosol physics equations are presented in the following sections. Suggested units are included in parentheses after each variable, providing a consistent set of units for numerical calculation.

Fireball Physics

The fireball is defined to include the products of combustion and entrained air. The combusting propellants are embedded within the fireball and are the source of the combustion products. This conceptual model of the fireball is shown schematically in Figure 2. Based on a single control volume, the time-dependent temperature of the fireball is determined by solving the following energy balance equation (assuming a constant-pressure combustion process):

$$\frac{d(n_f h_f)}{dt} = R - L + E \tag{1}$$

where n_f is the quantity of combustion products and entrained air that comprise the fireball (mol), h_f is the molar enthalpy of the fireball (J/mol), t is time (s), R is the reactant enthalpy inflow (W), L is the fireball energy loss rate (W), and E is the enthalpy inflow from air entrainment (W). Note that both n_f and h_f are dependent variables.

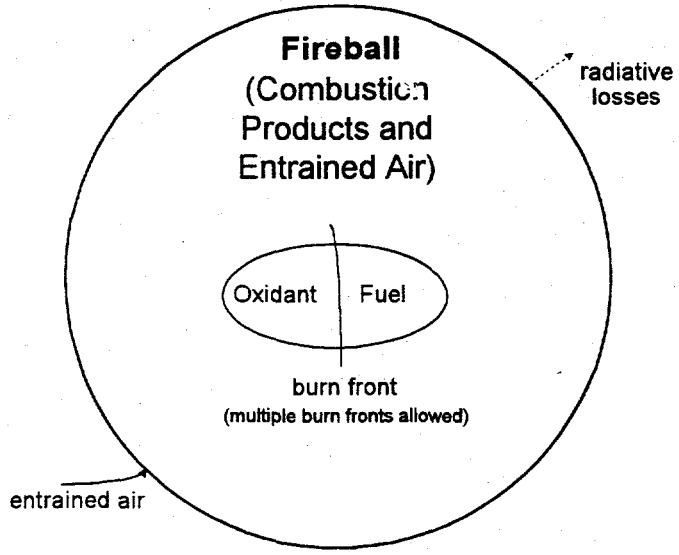

Figure 2. Schematic of the Fireball Control Volume

The molar gas quantity in the fireball is

$$n_f = n_p + n_a \tag{2}$$

where n_p is the quantity of combustion products (mol), and n_a is quantity of entrained air (mol). The reactant enthalpy inflow term, R, is given by

$$R = \dot{n}_r h_r \tag{3}$$

where $\dot{n}_r$ is the molar combustion rate of propellant reactants (mol/s), which is assumed known, and h_r is the specified enthalpy of the reactants (J/mol). Likewise, the air entrainment enthalpy inflow term is given by

$$E = \dot{n}_a h_a^\circ \tag{4}$$

where $\dot{n}_a$ is the molar rate of air entrainment (mol/s), and h_a° is the enthalpy of the ambient air (J/mol).

Equation (1) is expanded using the chain rule and rearranged to provide

$$\frac{dh_f}{dt} = \left[\dot{n}_r h_r - \dot{n}_p h_f - L + \dot{n}_a\left(h_a^\circ - h_f\right)\right] \Big/ n_f \tag{5}$$

where $\dot{n}_p \left(= \dfrac{dn_p}{dt}\right)$ is the molar product production rate (mol/s).

The product production rate, $\dot{n}_p$, is expressed in terms of the reactant combustion rate using

$$\dot{n}_p = y\frac{dn_r}{dt} = y\dot{n}_r \tag{6}$$

where y is the molar quantity of combustion products produced per mole of reactant, and $\dot{n}_r$ is the specified reactant combustion rate (mol/s). This equation is required for the solution of Equation (5). Based on equilibrium chemistry, the fraction y is determined using

$$y = \frac{n_p}{n_r} = \frac{W_r}{W_p} \tag{7}$$

where n_p is the quantity of products (mol), n_r is the quantity of reactants (mol), and W_r and W_p are the mean molecular weights of the reactants and products, respectively (g/mol). The mean molecular weights are given by

$$W_r = \sum_{j=1}^{N_r} y_r^j W_r^j \tag{8}$$

and

$$W_p = \sum_{i=1}^{N_p} y_p^i W_p^i \tag{9}$$

where N_r is the number of reactant species, N_p is the number of product species, y_r^j and y_p^i are the mole fractions of reactant species j and product species i, respectively, and W_r^j and W_p^i are the molecular weights of the reactant and product species, respectively (g/mol).

Equation (5) is now rearranged to provide

$$\frac{dh_f}{dt} = \left[\dot{n}_r\left(h_r - yh_f\right) - L + \dot{n}_a\left(h_a^\circ - h_f\right)\right]/n_f \tag{10}$$

This equation is based on the following definition of enthalpy:

$$h = h_F + \Delta h \tag{11}$$

where h_F is the enthalpy of formation (also known as the heat of formation) at the standard state (298.15 K, 1 atm), and Δh is the change in enthalpy from the standard state to some other state, including sensible heat and heats of transition when appropriate.

The loss term in Equation (5), L, is given by

$$L = \varepsilon\sigma A\left(T^4 - T_a^4\right) + \varepsilon_{Al}\varepsilon\sigma A_{Al}\left(T^4 - T_{Al}^4\right) + h_{Al}A_{Al}\left(T - T_{Al}\right) - q_{Al} \tag{12}$$

where ε is the effective emissivity of the fireball, σ is the Stefan-Boltzmann constant (5.67×10^{-12} W/cm^2·K^4), A is the surface area of the spherical fireball (cm^2), T is the temperature of the fireball (K), T_a is the ambient environment temperature (K), ε_{Al} is the surface emissivity of the aluminum structures within the fireball, T_{Al} is the surface temperature of the aluminum structures (K), h_{Al} is the heat transfer coefficient for convective heat transfer between the aluminum structures and the fireball (W/cm^2·K), and q_{Al} is the heat added to the fireball from aluminum combustion (W). Calculation of the aluminum surface temperature and the combustion source term are described in the Structure Heat Transfer and Aluminum Combustion Subsections.

Qualitatively, Equation (1) indicates that the time rate of change of the fireball energy equals the rate of energy inflow from reactants and air entrainment minus the rate of fireball energy loss. The loss term [Equation (12)] includes four contributions: (1) thermal radiation from the fireball to the ambient environment, (2) thermal radiation from the fireball interior (treated as a gray semitransparent participating medium) to the aluminum structures (the rocket) within the fireball, (3) convective heat transfer from the fireball interior to the aluminum structures, and (4) heat added to the fireball from combustion of aluminum structures.

Following liftoff, only the first loss term contribution is included because the structures are assumed to no longer be immersed in the rising fireball.

Using the calculated fireball enthalpy and product mole fractions, the fireball temperature is determined using

$$h_f = (1 - y_a)\sum_{i=1}^{N_p} y_p^i h_p^i + y_a h_a \tag{13}$$

where y_a is the molar air fraction defined as the molar quantity of entrained air in the fireball divided by the molar quantity of air and all combustion products in the fireball, y_p^i is the mole fraction of product species i, h_p^i is the enthalpy of product species i (J/mol), and h_a is the enthalpy of the air entrained into the fireball (J/mol). The molar air fraction is defined as

$$y_a = \frac{n_a}{n_f} \tag{14}$$

Because h_p^i and h_a are functions of fireball temperature T, Equation (13) must be solved iteratively for temperature. This is accomplished using Newton iteration, recognizing that the derivative of enthalpy with respect to temperature at constant pressure is equal to c_p, the constant-pressure specific heat (J/mol·K). Enthalpies are provided as fifth-order polynomials in temperature and account for heat of formation, sensible heat, phase transitions, and corrections for non-ideal gas behavior. Specific heats are provided as fourth-order polynomials in temperature.

The equilibrium product mole fractions are determined for a specified reactant mixture assuming a constant enthalpy-constant pressure thermodynamic state. This amounts to assuming that combustion occurs at a constant temperature associated with this state and not at the average fireball temperature. In other words, combustion occurs in one or more localized burn fronts within the fireball, depending on the number of reactant mixes specified. Entrained air is included with the fireball products but is assumed to not be available for combustion unless specified as a reactant. Calculation of the product mole fractions is provided by a propellant thermodynamic routine that incorporates thermodynamic data for all of the combustion species associated with the space vehicle. The product mole fractions are determined based on a minimization of the Gibb's free energy. The fireball code package is configured to allow the input of multiple reactant mixes, each with its own specified combustion rate. After consumption of a reactant mix, combustion proceeds with the next reactant mix until all available mixes are consumed.

Following completion of the combustion stage, the fireball lifts from the ground, rapidly entraining air. The molar rate of air entrainment, based on an assumed entrainment coefficient, is determined using

$$\dot{n}_a = \frac{\alpha u A p}{\bar{R} T} \tag{15}$$

where α is an entrainment coefficient, u is the rise velocity of the fireball (cm/s), A is the surface area of the fireball (cm^2), p is the pressure of the fireball (atm), which is assumed to equal the ambient pressure, $\bar{R}$ is the universal gas constant (82 cm^3·atm/mol·K), and T is the fireball temperature (K). The quantity of entrained air is added to the existing product species in the calculation of fireball temperature via Equation (13). Also, during the entrainment stage, the reactant enthalpy inflow term is zero.

The air entrainment model is based on the "macro-scale" process of a bubble (the fireball) rising through a medium (air), which is applicable after fireball liftoff. Such a model is common in bubble flow and atmospheric simulations. However, the model is also used before fireball liftoff when air entrainment is a "micro-scale" process in which turbulent eddies near the boundaries of the fireball bring in ambient air. Because these turbulent eddies are not captured in the fireball model, there is no reasonable way to predict this entrainment. The micro-scale entrainment is expected to be much smaller than the macro-scale entrainment. Different entrainment coefficients may be used during the combustion and entrainment stages to reflect the different processes. It is also possible to introduce entrained air by specifying it as a reactant; thus micro-scale entrainment calculated by some other means (such as a computational fluid dynamics code) can be incorporated in the fireball simulation if desired.

The rise velocity of the fireball is determined from solution of the following momentum balance:

$$\frac{d}{dt}(\rho V u) = gV\left(\rho_a^\circ - \rho\right) - \frac{C_d}{2}\rho_a^\circ A_P u^2 \tag{16}$$

where ρ is the density of the fireball (g/cm^3), V is the volume of the fireball (cm^3), g is the acceleration due to gravity (981 cm/s^2), C_d is the drag coefficient, ρ_a° is the density of the ambient air (g/cm^3), and A_P is the projected area of the fireball (cm^2). The first term to the right of the equal sign is the buoyant force due to the density difference of the ambient air and the fireball, and the second term is the drag force. Application of the chain rule and rearrangement of this equation provides the following equation for numerical solution:

$$\frac{du}{dt} = c_2 - c_1 u - c_3 u^{2+b} \tag{17}$$

with

$$c_1 = \frac{1}{\rho V}\frac{d(\rho V)}{dt} = \frac{d\ln(\rho V)}{dt} \approx \frac{\ln\left[\frac{(n_f W_f)^{k+1}}{(n_f W_f)^{k}}\right]}{\Delta t} \tag{18}$$

$$c_2 = g\left(\frac{\rho_a^\circ}{\rho} - 1\right) \tag{19}$$

and

$$c_3 = \frac{\pi}{n_f W_f} a(2)^{b-1}\left(\rho_a^\circ\right)^{1+b}\left(\mu_a^\circ\right)^{-b} r^{b+2} \tag{20}$$

where b is a constant that depends on the Reynolds number (defined later), n_f is the quantity of all fireball constituents (mol), which includes combustion products and entrained air, W_f is the mean molecular weight of the fireball mixture (g/mol), the superscript k indicates the time step number, Δt is the selected time step (s), ρ is the fireball density (g/cm^3), a is another constant that depends on the Reynolds number, ρ_a° is the density of the ambient air (g/cm^3), μ_a° is the dynamic viscosity of the ambient air (g/cm-s), and r is the fireball radius (cm). The product $n_f W_f$, which is the fireball mass, is calculated as

$$n_f W_f = n_p W_p + n_a W_a \tag{21}$$

where W_a is the molecular weight of air (28.97 g/mol).

The drag coefficient, C_d, is expressed as

$$C_d = a\,\mathrm{Re}^b \tag{22}$$

where Re is the Reynolds number of the rising fireball given as

$$\mathrm{Re} = \frac{\rho_a^\circ u 2r}{\mu_a^\circ} \tag{23}$$

where u is the rise velocity (cm/s) and r is the fireball radius (cm). The constants a and b are both functions of the Reynolds number, and for flow around a sphere are provided in Table 1, based on simple curve fits to graphical data.[4] Although the

fireball will deviate from a spherical shape, the errors introduced are considered insignificant for this application.

Table 1. Constants for Drag Coefficient

Range	*a*	*b*
$Re \leq 1.9$	24	−1
$500 > Re > 1.9$	18.5	−0.6
$Re \geq 500$	0.44	0

The height of the center of the fireball is determined by integrating the rise velocity over time with z equal to z_o as the initial condition. Thus

$$z = z_o + \int_0^t u dt \tag{24}$$

A hemispherical fireball is formed initially. The fireball grows in the shape of a truncated sphere as it rises, attaining a full spherical shape when it lifts from the ground. This growth is depicted schematically in Figure 3.

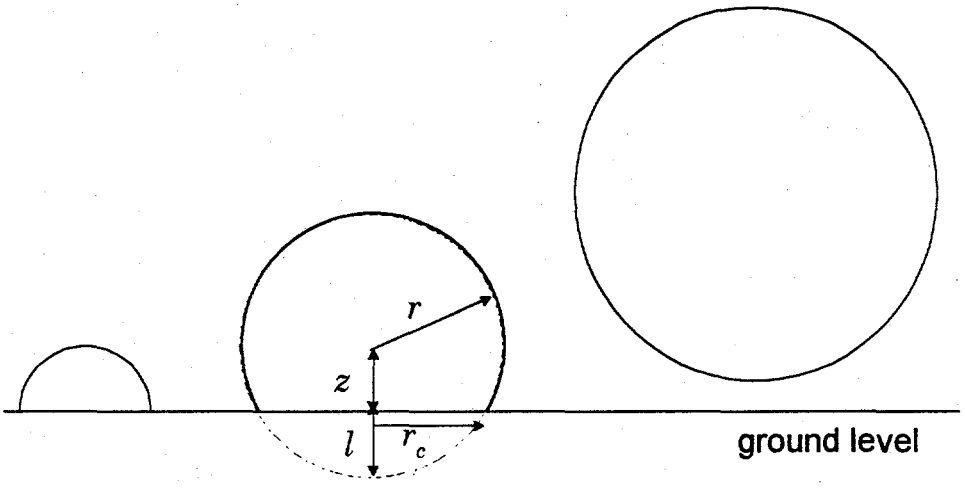

Figure 3. Geometry for Growth of the Fireball

It is possible for the initial fireball sphere to lift off before combustion is complete, depending on the calculated rise velocity and the selected combustion rates. In such cases, a second fireball hemisphere would begin to form, which would be attached to the first rising sphere. However, multiple attached spheres are not treated. Instead, the additional fireball products are added to the volume of the initial sphere and the fireball grows as a sphere. In the Fireball code package, liftoff is defined as the time of combustion completion. The entrainment stage begins at this time.

The volume and surface area of the fireball before liftoff are given by

$$V = \tfrac{4}{3}\pi r^3 - \tfrac{1}{6}\pi l\left(3r_c^2 + l^2\right) \tag{25}$$

and

$$A = 4\pi r^2 - 2\pi rl \tag{26}$$

with

$$l = r - z \tag{27}$$

and

$$r_c = \sqrt{r^2 - z^2} \tag{28}$$

where V is the volume (cm^3), r is the radius of the fireball (cm), r_c is the radius of the circle formed by the intersection of the fireball truncated sphere and the ground (cm), and z is the height of the fireball center (cm). Equations (25) through (28) are solved to determine r and A given V and z. Following liftoff, the volume and surface area of a full sphere are used.

The volume of the fireball is based on the ideal gas law:

$$V = \frac{n_f \overline{R} T}{p} \tag{29}$$

The quantity of all fireball constituents, n_f, is found by integrating the rate of fireball growth, $\dot{n}_f$, over time. Thus

$$n_f = \int_0^{t_{end}} \dot{n}_f dt = \int_o^{t_{end}} \left(y\dot{n}_r + \dot{n}_a\right) dt \tag{30}$$

where the fraction y [Equation (7)] is defined as the molar ratio of combustion products to reactants (determined by the equilibrium combustion solution), and $\dot{n}_a$ is the molar rate of air entrainment (mol/s).

The effective emissivity of the fireball, accounting for all particles within the fireball and assuming non-absorbing fireball gases and diffuse particle surfaces, is given by[5]

$$\varepsilon = 1 - \exp\left(-L_b \sum_{i=1}^{N_s} \varepsilon_p^i C^i A_p^i\right) \tag{31}$$

where L_b is an effective thickness of the fireball (cm), N_s is the number of particle sizes, ε_p^i is the emissivity of particle size i, C^i is the number concentration of particles of size i (cm^{-3}), and A_p^i is the effective projected area of particle size i (cm^2), which is given by

$$A_p^i = \frac{\pi}{4}\chi^i\left(d_e^i\right)^2 \tag{32}$$

where χ^i is the dynamic shape factor for particles of size i, and d_e^i is the diameter of the volume-equivalent sphere for particles of size i (cm), The effective fireball thickness, L_b, is usually referred to as the mean beam length, which for a sphere is given as [6]

$$L_b = 1.3r \tag{33}$$

where r is the fireball radius (cm). Before the fireball attains a full spherical shape, the mean beam length is approximated as

$$L_b = 3.9\frac{V}{A} \tag{34}$$

Equation (31) is easily modified to approximately account for absorbing gases (CO_2 and water vapor) within the fireball. Thus

$$\varepsilon = 1 - \left(1 - \varepsilon_g\right)\exp\left(-L_b\sum_{i=1}^{N_s}\varepsilon_p^i C^i A_p^i\right) \tag{35}$$

where ε_g is the effective gas emissivity based on the temperature, pressure, and mean beam length of the fireball product gases. The calculation of the gas emissivity is based on an engineering approach[6] assuming that water vapor and carbon dioxide are the dominant contributors to emissivity. Thus

$$\varepsilon_g = \varepsilon_{H_2O} f_{H_2O} + \varepsilon_{CO_2} f_{CO_2} - \Delta\varepsilon \tag{36}$$

where the H_2O and CO_2 subscripts refer to water vapor and carbon dioxide gas, respectively, and f and $\Delta\varepsilon$ are correction factors. The emissivities for the two dominant gases along with the correction factors are based on approximate curve fits to experimental data and are given as

$$\log_{10}\varepsilon_{H_2O} = -\left(0.88424 + 0.65524T^*\right) + \left(0.49502 + 0.294787T^*\right)\log_{10}\left(L_b y_{H_2O} p\right) - \left(0.061316 + 0.05272T^*\right)\left[\log_{10}\left(L_b y_{H_2O} p\right)\right]^2 \quad (37)$$

$$f_{H_2O} = 1 + \left\{0.897 - 0.2\left[\log_{10}\left(L_b y_{H_2O} p\right)\right]\right\}\left[p\left(1 + y_{H_2O}\right) - 1\right] \quad (38)$$

$$\log_{10}\varepsilon_{CO_2} = \left[-1.34561 + 0.0758127T^* - 0.122506\left(T^*\right)^2\right] + \left[0.35278 + 0.072651T^* + 8.4779\times10^{-3}\left(T^*\right)^2\right]\log_{10}\left(L_b y_{CO_2} p\right) + \left[-0.074333 + 0.0262193T^* - 9.8478\times10^{-3}\left(T^*\right)^2\right]\left[\log_{10}\left(L_b y_{CO_2} p\right)\right]^2 \quad (39)$$

$$f_{CO_2} = 1 - 0.768622\left[0.195377\log_{10}\left(L_b y_{CO_2} p\right) - 0.69448\right]\log_{10}\left(L_b y_{CO_2} p\right) \quad (40)$$

$$\Delta\varepsilon = \sin\left(\frac{y_{H_2O}}{y_{H_2O} + y_{CO_2}}\pi\right)\left(-4.2\times10^{-8}\eta^2 + 1.24\times10^{-4}\eta + 0.0361\right) \quad (41)$$

$$\eta = L_b p\left(y_{H_2O} + y_{CO_2}\right) \quad (42)$$

where T^* is equal to T divided by 1,000; T is the fireball temperature (K), L_b is the mean beam length (cm), y is the mole fraction, and p is the fireball pressure (atm). The data points chosen for the curve fits were selected to emphasize the high temperatures expected in a fireball.

Equation (35) for fireball emissivity couples the aerosol physics governing equations, which are used to determine the agglomerated particle concentrations, to the fireball temperature and size equations, and to the structure and particle heat transfer equations.

Both the fireball energy equation and the fireball rise velocity equation are solved using a Runge-Kutta Fehlberg[7] approach. An adaptive time step algorithm is incorporated to ensure both equations are solved accurately. This algorithm uses the difference between a fourth- and a fifth-order solution to control the truncation error as the solutions are advanced in time. Thus different combustion scenarios can be simulated without concern for time step selection.

It is necessary to define gas mixture properties for viscosity and conductivity in terms of the fireball constituent properties. The mixing model of Wilke as modified by Herning and Zipperer[8] is used for this averaging process:

$$\mu = \sum_{k=1}^{N_p} \left[y_k \mu_k / \sum_{j=1}^{N_p} y_j \left(\frac{W_j}{W_k} \right)^{1/2} \right] \tag{43}$$

where μ is the dynamic viscosity (g/cm·s), N_p is the number of gaseous product species in the fireball at the current time, y_k is the mole fraction for species k, and W_k is the molecular weight for species k. As suggested in Reference 8, the same equation is used for conductivity with μ replaced with k (W/cm·K).

The final equations presented here for fireball physics describe the calculation of the turbulent dissipation term, which follows the work of Turner.[9] This term is required in the aerosol physics solution of agglomeration due to turbulent diffusion. Although particle agglomeration due to Brownian motion is expected to dominate, the enhancement of agglomeration due to turbulence within the fireball ought not be neglected.

The local turbulent energy dissipation rate is approximated as the product of kinematic viscosity and the square of the vorticity:

$$\varepsilon_T = \frac{\mu}{\rho} |\nabla \times \vec{v}|^2 \tag{44}$$

where ε_T is the turbulent energy dissipation rate (cm²/s³), μ is the dynamic viscosity of the fireball gas mixture (g/cm·s), ρ is the fireball density (g/cm³), and $\vec{v}$ is the gas velocity vector (cm/s). The flow field within the fireball is assumed to be approximated by a spherical vortex, for which the stream function is

$$\Psi = \frac{u r^2 \sin^2 \theta}{4} \left(1 - \frac{r^2}{r_v^2} \right) \tag{45}$$

where u is the vortex (fireball) rise velocity, r is the radial position within the vortex, θ is the angle describing the azimuthal position within the fireball, and r_v is the radius of the vortex. The radial and angular components of the velocity vector, v_r and v_θ are given by

$$v_r = \frac{1}{r^2 \sin\theta} \frac{\partial \Psi}{\partial \theta} = \frac{u}{2} \cos\theta \left(1 - \frac{r^2}{r_v^2} \right) \tag{46}$$

and

$$v_\theta = \frac{-1}{r \sin\theta} \frac{\partial \Psi}{\partial r} = \frac{u}{2} \sin\theta \left(\frac{2r^2}{r_v^2} - 1 \right) \tag{47}$$

Now the vorticity can be evaluated as

$$\left|\nabla \times \vec{v}\right| = \frac{5ur\sin\theta}{2r_v^2} \tag{48}$$

The turbulent dissipation rate, assuming isotropic turbulence, can be expressed as

$$\varepsilon_T = \frac{25\mu u^2 r^2 \sin^2\theta}{4\rho r_v^4} \tag{49}$$

Because the fireball is modeled as a single uniform control volume, the spatial dependence of turbulent dissipation must be removed. A volumetrically-averaged dissipation can be derived as

$$\bar{\varepsilon}_T = \frac{3}{4\pi r_v^2}\int_0^{2\pi}\int_0^{r_v}\int_0^{\pi} \varepsilon_T r^2 \sin\theta d\theta dr d\phi = \frac{6\pi\xi}{4\pi r_v^3}\int_0^{r_v}\int_0^{\pi} r^4 \sin^3\theta d\theta dr \tag{50}$$

where

$$\xi = \frac{25}{4}\frac{u^2}{r_v^4}\frac{\mu}{\rho} \tag{51}$$

Now the average turbulent dissipation rate is

$$\bar{\varepsilon}_T = \frac{5}{2}\frac{u^2}{r_v^2}\frac{\mu}{\rho} \tag{52}$$

where the radius of the vortex is taken as the radius of the fireball. This quantity is evaluated based on the current state of the fireball and passed to the Maeros2 subroutine for calculation of agglomeration due to turbulent diffusion.

Combustion Chemistry and Thermodynamics

The fireball is created as a result of uncontrolled combustion of the propellants (fuel and oxidants) contained in the rocket. To determine the products of combustion and their relative amount, a calculation of the combustion thermodynamics is required. The thermodynamic properties of the fireball are necessary to determine the temperature and size of the fireball, and to assess the vaporization and agglomeration of the plutonium-bearing particles.

Some of the current launch vehicles in use today include the Titan, Atlas, Delta, Long March, and Ariane rockets. The propellant inventory of a Titan IV rocket with a Centaur upper stage is provided in Table 2 for demonstrative purposes. Fireballs occur when the fuel to be used for a mission are released and come in contact with oxidants in an uncontrolled manner. Three liquid-propellant fireball scenarios are considered for launch-abort analyses:

1. Ground/core fireballs – those occurring on the ground involving the "core" liquid propellants.
2. Air/core fireballs – those occurring in the air with the core propellant inventory reduced by the amount of propellant required to reach a specified altitude.
3. Space vehicle fireballs – those that involve the liquid propellants of the satellite and any upper stage.

Table 2. Propellant Inventory for a Titan IV Rocket

Rocket Stage	Fuel/Oxidant	Inventory (mol)
Titan IV Stage 1	Nitrous Oxide (N_2O_4)	1.086×10^6
	Hydrazine (N_2H_4)	0.836×10^6
	UDMH* ($C_2H_8N_2$)	0.446×10^6
Titan IV Stage 2	Nitrous Oxide (N_2O_4)	0.2418×10^6
	Hydrazine (N_2H_4)	0.1984×10^6
	UDMH ($C_2H_8N_2$)	0.1058×10^6
Centaur Upper Stage	Liquid Oxygen (O_2)	0.544×10^6
	Liquid Hydrogen (H_2)	1.726×10^6
Satellite (Final Stage)	Nitrous Oxide (N_2O_4)	0.01974×10^6
	MMH▲ (CH_6N_2)	0.0189×10^6

*Unsymmetrical Dimethyl Hydrazine, ▲Monomethyl Hydrazine

The full core fireballs could be the result of ground impact following a launch abort. The time it takes the liquid fuel to "find" the oxidizer depends on their relative location during impact. The Fireball code was designed so that any number of fuel and oxidant mixes can be "sourced" into the fireball at any time and at any specified combustion rate. Thus the effect of impact geometry can be accommodated by varying the timing in which the various fuels and oxidants are added to

the fireball. Such timing information could come from experiments or from hydrodynamic simulations. The rate of combustion therefore is intended to capture the bulk movement of fuel and oxidants as opposed to a kinetic-driven rate.

To simplify the combustion thermodynamics, two assumptions are made:

1. All combustion product gases are considered ideal although corrections are made to enthalpy for non-ideal behavior.
2. An equilibrium chemical solution describes the situation adequately, which is probably reasonable for the high temperatures and reaction rates involved.

The CET89 computer code developed by NASA was modified for use in the Fireball code to solve the chemical equilibrium problem. The code is based on the minimization of either Gibb's Free Energy or Helmholtz Free Energy as the criterion for chemical equilibrium. The minimization of the Gibb's Free Energy is used in this application.

The Gibb's free energy is a function of pressure, temperature, and chemical composition. For a mixture of N_p product species, the chemical contribution to the Gibb's free energy for the mixture is given by

$$g = \sum_{j=1}^{N_p} \mu_j n_j \tag{53}$$

where μ_j is the chemical potential for species j. If pressure and temperature are constant then

$$dg = \sum_{j=1}^{N_p} \mu_j dn_j \tag{54}$$

The condition for equilibrium is the minimization of free energy and is applied to this equation subject to mass balance and non-negativity constraints. The cited CET89 reference should be consulted for details of the minimization algorithm.

For use in the Fireball code package, the stand-alone version of CET89 was converted to a callable subroutine. The CET code was selected because it is a well-recognized and accepted code in the technical community. Most of the features in CET not applicable to fireball simulations were removed. A separate free-format input file contains the reactant data (such as reactant, enthalpy, and quantity) for as many reactant mixes as desired. Reactant mixes can be specified to burn concurrently or sequentially with other mixes. The combustion pressure for each mix can also be specified. Remaining input data required for CET are passed from the Fireball controlling subroutine based on the current state of the fireball. Likewise, relevant CET output data is passed back to Fireball for calculation of

fireball temperature, properties, and size. The extensive thermodynamic and transport libraries within CET are also incorporated into the Fireball code.

Aerosol Physics

Of principal interest for fireball simulations is the behavior of plutonium-bearing particles. The discipline of aerosol physics deals primarily with the agglomeration of aerosol particles, of the same or different size, in a gaseous suspension. Generally, particles of diameter less than 0.01 cm (100 μm) are considered to behave as aerosols. Larger particles, referred to here as "rocks," are assumed to not agglomerate and are discussed in the Particle Heat Transfer section. The objective here is to determine how the fireball environment modifies the size distribution of plutonium-bearing aerosol particles.

The 1995 version of Maeros2 was modified to perform the aerosol physics calculations in the Fireball code. Maeros2 differs slightly from that described in the Maeros users manual.[3] The principal differences are the inclusion of a better condensation model and improved data input/output procedures. The following description is based largely on the commentary provided with the latest version of Maeros2. Although many of the features in Maeros2 are not relevant to fireball applications, their descriptions are included here for completeness. In addition to the users manual, more details concerning Maeros2 can be found in the paper of Gelbard and Seinfeld.[10]

The Maeros2 code calculates aerosol composition and mass concentration as a function of particle size and time. The processes that are incorporated are (1) agglomeration due to Brownian motion, gravity and turbulence; (2) particle deposition due to gravitational settling, diffusion, thermophoresis and diffusiophoresis; (3) particle growth or shrinkage due to water vapor condensation or evaporation from the particle surface; and (4) time-varying sources of particles of different sizes and chemical compositions. Maeros2 was originally developed to address potential accidents in nuclear reactor operations and thus includes processes involving water. These processes are not involved in the fireball simulations and are simply not used. Also, water vapor condensation is not considered in the Fireball code because of the high temperatures involved.

The numerical method in Maeros2 is based on the assumption that the aerosols within a particular particle size section (bin) are homogeneous. That is, any subvolume of the fireball big enough to contain a representative sample of the aerosol will have aerosols distributed in exactly the same way as in any other subvolume. Because typical aerosol concentrations might be on the order of a million particles per cubic centimeter, the fireball can be considered homogeneous to a very fine level of spatial resolution. With the homogeneous aerosol assumption, the aerosol dynamic governing equation, which is the basis of Maeros2 and most other aerosol physics codes, is

$$\frac{\partial n(v,t)}{\partial t} = \frac{1}{2}\int_o^v K[U,v-U]n(U,t)n(v-U,t)dU - n(v,t)\int_o^\infty K[U,v]n(U,t)dU + \frac{S(v,t)}{V} - \frac{R(v,t)n(v,t)}{v} - \frac{\partial I(v,t)n(v,t)/V}{\partial v} \quad (55)$$

where $n(v,t)$ is the number concentration of particles having volumes of v to $v + dv$, $\int_o^v K[U,v-U]n(U,t)n(v-U,t)dU$ is the rate of formation of particles of volume v to $v + dv$ by agglomeration of smaller particles, $n(v,t)\int_o^v K[U,v]n(v,t)dU$ is the rate of agglomeration of particles of volume v to $v + dv$ to form larger particles, $K[U,v]$ is the agglomeration "kernel" for particles of volume v with particles of volume U, $S(v,t)$ is the rate at which particles of volume v to $v + dv$ are supplied (source term), V is the fireball volume, $R(v,t)\ n(v,t)$ is the rate of removal of particles from the fireball by any of a variety of mechanisms (such as gravitational settling), and $\frac{\partial I(v,t)n(v,t)}{\partial v}$ is the rate of growth by condensation of particles from the volume interval of v to $v + dv$. The agglomeration kernels are complex functions of the properties of both the particles and the encompassing gas (i.e., the fireball).

A second assumption made in the numerical approach in Maeros2 is that the particle size domain can be divided into sections (bins). Conservation of mass for the four processes given previously is then imposed for each chemical component. Therefore, the aerosol mass concentrations are grouped into size sections for which an average composition is determined. Aerosol particles in the Fireball code are assumed to consist of one or more of five components: (1) plutonium dioxide debris from the initial explosion, (2) condensed plutonium dioxide, (3) carbon (soot), (4) aluminum oxide from vaporized structures, and (5) entrained dirt. Each size section can have a different combination of the five components.

The code is restricted to agglomeration, deposition and condensation mechanisms, which are independent of chemical composition and dependent on particle mass. Only the source mechanisms may be both particle mass and composition dependent. Intra-particle chemical reactions and condensation of more than one component other than water vapor are not simulated. In the fireball code, water vapor condensation is not a factor because of the high temperatures involved. The condensation of plutonium and aluminum vapor is determined in new models within the Fireball code, outside the Maeros2 subroutine.

No assumptions are made regarding the distribution of chemical composition for a given particle size. If within a particle size section there are three chemical components a, b, and c, with mass concentrations of 10%, 40% and 50%, respectively, this may be the result of virtually an infinite number of possible composition

distributions. One often-used simplification is that all particles have the identical composition of the particle size section, and thus each particle is composed 10% of *a*, 40% of *b*, and 50% of *c*. Another equally-possible situation is that 10% of all the particles are composed purely of *a*, 40% of all the particles are composed purely of *b*, and 50% of all the particles are composed purely of *c*. For determining the evolution of mass concentration and composition in the Maeros2 code implementation, no assumptions as to the distribution of chemical composition within a particle size section are made. However, in the Fireball code implementation for agglomerated particle heat transfer, the often-used simplification that all particles in a size section have identical composition is adopted.

The integrodifferential general dynamic equation governing aerosol behavior is of considerable complexity. The Maeros2 code was selected for its solution because it is a well-recognized and accepted code in the aerosol physics community. Several changes were made to Maeros2 for incorporation into the Fireball code package. The stand-alone code was converted into a callable subroutine. Most features not relevant to fireball applications were removed. All input data required for Maeros2 are passed from the Fireball controlling subroutine based on the current state of the fireball. Likewise, all Maeros2 output data are passed back to Fireball for calculations of heat transfer, vaporization, condensation, and fireball properties. The dynamic volume term (the time-derivative of fireball volume) was added. Because Maeros2 was written for a fixed control volume, it was necessary to include the appropriate volume time-derivative term to account for the ever-changing volume of the fireball.

Maeros2 only supports the specification of a single component-averaged particle density and not an average density for each size section. Therefore, although an average density for each section is available from the particle heat transfer model, only a global average is passed to Maeros2. Preliminary indications are that this does not have a large impact on the agglomeration results.

The largest consumer of execution time in the Fireball code is the generation of section coefficients used in the aerosol physics solution. These section coefficients are complex double integrals involving particle and fireball properties. To reduce the execution time associated with these integrals, the section coefficients are not evaluated every fireball time step. Instead they are evaluated based on user-specified time and temperature intervals.

The mass of particles in one size section can move into another size section due to agglomeration, and this movement is handled by Maeros2. However, particles can also change size sections by the vaporization and condensation processes occurring within the fireball. These size section changes are handled by the algorithms for particle heat transfer and are discussed further in that section.

Particle Heat Transfer

Of primary concern in launch-abort fireball simulations is the response of the substoichiometric plutonium dioxide particles released during a hypothetical accident. Particles of dirt, soot, and aluminum oxide may also be present and can serve as condensation sites for plutonium vapor and as agglomeration sites. Two size classes of particles are modeled: agglomerated aerosol particles and plutonium "rock" particles. For the analyses considered here, aerosol particles are considered as those particles with volume-equivalent sphere diameters less than 0.01 cm (100 μm). This cutoff diameter, however, is an input parameter in the Fireball code package and can be modified if desired. Rock particles consist only of plutonium and are assumed to not agglomerate. The heat transfer response of particles in both size classes must be modeled to allow calculation of plutonium vaporization and condensation.

Particle heat transfer for both size classes is modeled using a lumped-capacitance approach in which spatial gradients are ignored. This approach is justified because the resistance to heat transfer at the surface of the particles is much greater than the internal conductive resistance, which can be demonstrated using a Biot number analysis. The Biot number for a sphere is defined as

$$\mathrm{Bi} = \frac{h_p d_p}{6k_p} \tag{56}$$

where h_p is the heat transfer coefficient of the particle (W/cm²·K), d_p is the particle diameter (cm), and k_p is the particle conductivity (W/cm·K). A common engineering practice is to treat particles with Biot numbers less than about 0.1 with a lumped-capacitance model. In such cases, insignificant errors in the calculated temperature response are incurred. Table 3 shows the range of Biot numbers for several different particle diameters.

Table 3. Biot Numbers for Selected Particle Diameters

Diameter (μm)	h_p (W/cm²·K)	Biot number
0.01	2500	0.021
100	0.65	0.055
500	0.25	0.042
1000	0.23	0.077
5000	0.06	0.367

The numbers in this table are based on a conductivity of 0.02 W/cm·K, which is the conductivity of PuO_2 at about 2000 K. Also, the heat transfer coefficients account for convective and radiative contributions. The convective contribution is

based on representative values of particle terminal velocity in the fireball and are discussed later. For the Biot number analysis, the radiative contribution is based on

$$h_c' = \sigma\varepsilon\left(T_f^2 + T^2\right)\left(T_f + T\right) \tag{57}$$

where h_c' is an effective heat transfer coefficient for radiation (W/cm²·K), σ is the Stefan-Boltzmann constant (5.67×10^{-12} J/s·cm²·K⁴), ε is the particle emissivity, T_f is the fireball temperature (K), and T is the particle temperature (K). For the approximate Biot number analysis presented here, an emissivity of 0.6, a fireball temperature of 2500 K, and a particle temperature of 2000 K were selected. This results in an effective heat transfer coefficient for radiation of 0.16 W/cm²·K, which is then added to the convective contribution.

This table shows that a lumped-capacitance model is justified for all aerosol particles and most rock particles. However, for the largest rock particle of diameter equal to 5000 μm, the assumption is questionable. The results from the lumped-capacitance model for this large rock particle were compared to the results from a one-dimensional model for a typical fireball scenario. The calculated surface temperature for the two models differed by less than 4%, which is much less than the error introduced by the heat transfer coefficient uncertainty. For errors less than 10%, the lumped-capacitance approach is reasonable for particles of up to about 8500 μm.

A quasi-static model is adopted for the aerosol particles and a full transient model is adopted for the rock particles. The models for both particle size classes are discussed in the following subsections. It should be noted that the aerosol particle heat transfer calculations are performed for each aerosol size section (bin) consistent with the size sections used for aerosol physics. Recall that aerosol particles change size sections due to agglomeration as determined in the aerosol physics solution. Particles also change size sections due to vaporization and condensation of plutonium, and these size-section changes are handled by the heat transfer algorithm within the fireball physics routine. Rock particles are also divided into various size sections for heat transfer calculations. If rock particles in any size section decrease in diameter sufficiently, the remaining mass in that section is moved into the appropriate aerosol section.

Agglomerated Aerosol Particles

Aerosol particles are those that are suspended in the fireball atmosphere and are free to agglomerate with other aerosol particles. This agglomeration, along with plutonium vaporization from or condensation onto the particles, complicates the heat transfer calculations. Fortunately, a quasi-static solution is applicable for these small particles because they have effective thermal time constants on the order of about ten milliseconds or less. (The 0.01-μm-diameter particles have a

time constant of about 20 μs.) Thus the aerosol particles reach thermal equilibrium with the fireball environment very quickly. This dispenses with the need to track the time history of a particle and its components as the particle changes in size due to vaporization, condensation, and agglomeration. Such a problem would be almost intractable.

A full transient governing equation is used as the starting point for the quasi-static model in order to properly introduce the mass loss term. Thus

$$\rho c \frac{d(VT)}{dt} = \alpha q''' V + q'' A - \dot{m}'' L_v A \tag{58}$$

where ρ is the average particle density (g/cm³), c is the average particle specific heat (J/g·K), V is the particle volume (cm³), T is the particle temperature (K), t is time (s), α is the plutonium volume fraction in the agglomerated particle, q''' is the volumetric heat generation rate due to the decay of plutonium (W/cm³), q'' is the heat flux at the particle surface (W/cm²), A is the effective particle surface area (cm²) accounting for irregular shape effects via the dynamic shape factor (χ), $\dot{m}''$ is the plutonium vaporization flux (g/cm²·s), and L_v is the latent heat of vaporization for plutonium (J/g). Both V and A can change with time. The vaporization flux, which is discussed in the Plutonium Vaporization Section, is defined as

$$\dot{m}'' = \frac{1}{A}\frac{dm}{dt} = \frac{\dot{m}}{A} \tag{59}$$

where $\dot{m}$ is the plutonium mass loss rate due to vaporization (g/s). Note that vaporization can occur from either the solid (sublimation) or liquid state.

Using the chain rule and after some rearrangement, the governing equation becomes

$$\frac{dT}{dt} = \frac{1}{\rho c}\left\{\alpha q''' + \frac{A}{V}\left[q'' - \beta \dot{m}''(L_v + cT)\right]\right\} \tag{60}$$

This equation accounts for the energy required to overcome the latent heat of vaporization and for the energy associated with plutonium mass loss (or gain). The correction factor β has been introduced to account for whether the vaporization rate is positive or negative (condensation). Condensation is assumed to occur over the entire surface of the agglomerated particle and the correction factor is set to one. However, vaporization occurs only from the fraction of the surface occupied by plutonium. For this case, the correction factor equals the plutonium surface area fraction and is approximated by

$$\beta = \alpha \tag{61}$$

where α is the plutonium volume fraction in the agglomerated particle. This approximation of the area fraction is common in the porous media modeling community. Because the plutonium can be dispersed anywhere within or on the agglomerated particle, a more sophisticated approach would require knowledge of the geometry of the agglomerated particle as it forms. Any model to determine the geometry would be very complex and is not warranted for the simulations considered here.

For a quasi-static model, the temperature time-derivative term is set to zero and the governing equation is

$$\alpha q''' + \frac{A}{V}\left[q'' - \beta \dot{m}''(L_v + cT)\right] = 0 \tag{62}$$

The heat flux at the particle surface, q'', consists of three terms: (1) convection to the fireball environment, (2) radiation to the ambient environment, and (3) radiation to the fireball. In equation form, the three terms are

$$q'' = h_c(T_f - T) + \sigma\varepsilon\tau_f\left(T_a^4 - T^4\right) + \sigma\varepsilon\varepsilon_f\left(T_f^4 - T^4\right) \tag{63}$$

where h_c is the convective heat transfer coefficient (W/cm^2·s), T_f is the fireball temperature (K), T is the particle temperature (K), σ is the Stefan-Boltzmann constant (5.67×10^{-12} W/cm^2·K^4), ε is an effective emissivity of the agglomerated particle, τ_f is the transmissivity of the fireball (one minus the fireball emissivity), T_a is the ambient temperature outside the fireball (K), and ε_f is the emissivity of the fireball.

The radiation flux model treats the fireball as a semitransparent participating medium between the particle and an ambient environment of infinite extent. The fireball emissivity is continually changing with time as the chemical composition, temperature, and particle content of the fireball change. Based on the fireball emissivity, the particle can exchange energy with both the fireball and the ambient environment.

Now the equation for heat flux is combined with the quasi-static governing equation and rearranged to yield

$$\sigma\varepsilon T^3 - \frac{a}{T} - \dot{m}''c - h_c = 0 \tag{64}$$

where the variable a is given by

$$a = T_f\left(h_c + \sigma\varepsilon\varepsilon_f T_f^3\right) + \alpha q'''\left(\frac{V}{A}\right) - \beta \dot{m}'' L_v + \sigma\varepsilon\tau_f T_a^4 \tag{65}$$

Equation (64) is solved for particle temperature, T, using Newton iteration. However, expressions for c, L_v, h_c, and ε are still required before this equation can be solved. The specific heat for plutonium (specifically for PuO_2) in units of J/g·K and with temperature in K is given by

$$c = 0.5324 - 2.1461 \times 10^{-4} T + 7.4467 \times 10^{-8} T^2 - 75.087 / T \tag{66}$$

The latent heat of vaporization for PuO_2 in units of J/g·K is given by

$$L_v = 2486.4 - 0.1262T \tag{67}$$

The heat transfer coefficient accounts for the motion of the particle through the fireball (neglecting the local turbulent motion of the fireball gases and any initial velocity that may be imparted to the particle by a launch-abort explosion) and is provided by the following correlation:[11]

$$h_c = \frac{k_f}{d}\left[2 + \underbrace{\left(0.4\,\mathrm{Re}^{1/2} + 0.06\,\mathrm{Re}^{2/3}\right)\mathrm{Pr}^{0.4}\left(\frac{T_f}{T}\right)^{0.175}}_{\text{forced convection}} + \underbrace{\frac{0.589\mathrm{Ra}^{1/4}}{\left[1 + \left(0.469/\mathrm{Pr}\right)^{9/16}\right]^{4/9}}}_{\text{free convection}}\right] \tag{68}$$

where k_f is the fireball thermal conductivity (W/cm·K), d is the particle volume-equivalent sphere diameter (cm), and Re, Pr, and Ra are the Reynolds, Prandtl, and Rayleigh numbers, respectively given by

$$\mathrm{Re} = \frac{\rho_f v_p d}{\mu_f} \tag{69}$$

$$\mathrm{Pr} = \frac{\mu_f c}{k_f} \tag{70}$$

and

$$\mathrm{Ra} = \frac{g c \rho_f^2 d^3 \left|T - T_f\right|}{T_f \mu_f k_f} \tag{71}$$

where v_p is the terminal velocity of the particle in the fireball environment (cm/s), g is the acceleration due to gravity (980 cm/s^2), and all properties for the fireball are evaluated at the bulk fireball temperature. This heat transfer coefficient correlation reflects heat transfer from diffusion, and forced and free convection. The forced-convection component of the correlation reflects the assumption that gas viscosity is proportional to gas temperature raised to the 0.7 power. Although

the convection terms are small for typical fireball simulations, they are included for completeness. Because c, L_v, and h_c are all a function of particle temperature, an iterative procedure is required for each. Successive substitution is used for this iteration with the Newton iteration for the governing equation embedded within the successive substitution iteration.

Before addressing the determination of the agglomerated particle average emissivity, calculation of the particle terminal velocity is described. The terminal velocity is used in the heat transfer coefficient correlation. This discussion is based primarily on the text of Hinds.[12] The terminal velocity represents a balance between gravity, buoyancy, and drag forces. The use of the terminal velocity (thereby neglecting inertia) for aerosol particle heat transfer is reasonable because the particles have very small mobility (inertial) relaxation times. A 100-μm-diameter particle in air at standard conditions reaches its terminal velocity in less than 0.1 s while a 10-μm-diameter particle requires less than 1 ms. These times decrease significantly as temperature increases. Another justification for using the terminal velocity is that particle heat transfer is dominated by radiation and is therefore relatively insensitive to the convection coefficient.

For the Stokes flow regime (Re < 1), the terminal velocity is

$$v_p = \frac{(\rho - \rho_f) d^2 g S}{18 \mu_f \chi} \tag{72}$$

where ρ is the average particle density (g/cm^3), g is the acceleration due to gravity (980 cm/s^2), S is the slip correction factor, which accounts for the fact that for very small particles, the mean free path of the gas molecules is not negligible, and χ is the dynamic shape factor. The slip correction factor is determined using[12]

$$S = 1 + \frac{\lambda}{d}\left[2.514 + 0.8 \exp\left(\frac{-0.55d}{\lambda}\right)\right] \tag{73}$$

where λ is the mean free path of gas molecules in the fireball (cm) approximated by

$$\lambda = \frac{2.7305 \times 10^{-10}}{\zeta} \tag{74}$$

where ζ is the particle concentration in the fireball (cm^{-3}). For particles not in the Stokes flow regime, the terminal velocity is given by

$$v_p = \left[\frac{4(\rho - \rho_f) d g}{3 C_D \rho_f \chi}\right]^{1/2} \tag{75}$$

where C_D is the drag coefficient for flow around a sphere given by the following curve fit of experimental data for $1 < \mathrm{Re} < 3.38 \times 10^5$:

$$C_D = 0.269159 - 1.113 \times 10^{-6}\,\mathrm{Re} + 9.908 \times 10^{-4}\sqrt{\mathrm{Re}} + \frac{5.835}{\sqrt{\mathrm{Re}}} + \frac{20.92}{\mathrm{Re}} \tag{76}$$

For $\mathrm{Re} > 3.38 \times 10^5$, the drag coefficient is set equal to 0.1. Because of the dependence of drag coefficient on the Reynolds number, a successive substitution iterative procedure is used to solve for terminal velocity.

Returning to the calculation of an average particle emissivity for agglomerated particles, the volume fractions of each of the five particle components (original PuO_2, condensed PuO_2, soot, Al_2O_3, and dirt) are determined using

$$\alpha_k = \frac{\dfrac{m_k}{\rho_k}}{\displaystyle\sum_{k=1}^{N_c} \frac{m_k}{\rho_k}} \tag{77}$$

where the k subscript indicates the particle component, and N_c is the number of particle components (five in this implementation). The average particle emissivity is assumed to be a volume average of the component emissivities. Thus

$$\varepsilon = \sum_{k=1}^{N_c} \varepsilon_k \alpha_k \tag{78}$$

It can be argued that because emissivity is a surface property, a surface area average should be used instead. However, this is not necessarily any better because any component can be positioned anywhere within the particle.

An average particle density is also required in the calculation of terminal velocity and is given as

$$\rho = \sum_{k=1}^{N_c} \rho_k \alpha_k \tag{79}$$

The properties, along with particle size, are updated every time step based on the current temperature. The vaporization and condensation rates also are updated every time step. The models for these processes are described in the Plutonium Vaporization and Condensation Sections.

Plutonium Rock Particles

Rock particles consist only of plutonium and are assumed to not agglomerate. Because of their larger size (and hence greater heat capacity) compared to aerosol particles, a quasi-static solution is not appropriate and the full transient governing heat transfer equation must be solved.

The same governing equation presented in the Agglomerated Aerosol Particle Subsection [Equation (60)] is used as a starting point and is repeated here for convenience:

$$\frac{dT}{dt} = \frac{1}{\rho c}\left\{q''' + \frac{A}{V}\left[q'' - \dot{m}''(L_v + cT)\right]\right\} \tag{80}$$

Note that the volume fraction correction terms are not needed now because the rock particles consist only of plutonium. The same expressions for the q'' terms used for aerosol particles are also used for rock particles [Equation (63)].

A fully-implicit solution of the governing equation is implemented to avoid any numerical problems associated with time step size. Using a finite-difference form of the time-derivative term, the transient governing equation becomes

$$\begin{aligned} &T^{n+1}\left\{1 + \frac{\Delta t}{\rho c}\frac{A}{V}\left[c\dot{m}'' + h_c + (a_1 + a_2)\overline{T}^3\right]\right\} = \\ &T^n + \frac{\Delta t}{\rho c}\frac{A}{V}\left\{q'''\frac{V}{A} - \dot{m}''L_v + h_c T_f + a_1 T_a^4 + a_2 T_f^4\right\} \end{aligned} \tag{81}$$

where the n+1 and n superscripts indicate new and old time steps, respectively, Δt is the current time step size (s), and $\overline{T}$ is an extrapolated particle temperature (K), which is determined by

$$\overline{T} = T^n + \frac{\Delta t}{2}\left(\frac{\Delta T}{\Delta t}\right)^n \tag{82}$$

where the n superscript again refers to the old time step.

This extrapolated-temperature procedure is used to address the problem introduced by the nonlinear radiative term. Thus the formulation is not strictly fully implicit. However, this procedure works quite well and avoids the necessity of iterating each time step. The vaporization fluxes, and the particle surface area and volume are updated each time step.

The transient heat transfer model also accommodates melting of PuO_2 in the event of a very hot fireball. To account for the latent heat of fusion, the specific

heat is appropriately modified in a narrow temperature interval about the PuO_2 melting temperature. Appropriate logic is included in the model to prevent skipping over this interval.

As with the aerosol particles, the terminal velocity is used in the determination of the heat transfer coefficient. For the larger rock particles, this may not be valid because of the longer time required to reach the terminal velocity, compared to aerosol particles. Also, the initial velocity, position, and direction of the rock particles (following the blast phase) is uncertain, as is the local velocity of the fireball gases in the rising vortex. Therefore, it does not seem worthwhile to calculate the ballistic trajectories of the rock particles through the fireball. Instead, a user-specified residence time is provided as a parametric variable available to the user. Analyses have shown that much of the particle heat transfer is due to radiation and that temperature results are not sensitive to the value of the heat transfer coefficient, which is not a strong function of velocity. Also, the larger rock particles heat very slowly and contribute very little to the plutonium vapor in the fireball. Use of the terminal velocity and an infinite residence time has negligible effect on the predicted quantity of vapor produced.

Plutonium Vaporization and Condensation

The hypothetical launch accident envisages the fragmentation of plutonium dioxide pellets in the General Purpose Heat Source (GPHS) and the dispersal of these fragments into the fireball atmosphere. The fragments will be suddenly exposed to a very high-temperature, chemically-reactive environment. In this environment it is possible for the plutonium dioxide to vaporize. The plutonium vapor will subsequently nucleate to form very fine aerosol particles or will condense and contaminate other aerosol particles in the fireball. Both the fine plutonium-rich particles nucleated from the vapor and the coarser particles contaminated with plutonium by condensation will have to be considered in the analyses of the consequences of a hypothetical launch accident. In this section, the extent of plutonium dioxide vaporization in a fireball is discussed.

A brief opportunity for the vaporization of plutonium dioxide arises when the particle temperature is high enough to create a thermodynamic driving force for substantial vaporization. The first step in the estimation of plutonium dioxide vaporization is the evaluation of this thermodynamic driving force. *The discussion of plutonium dioxide vaporization presented here emphasizes that the thermodynamic driving force is a function of both the temperature and the chemical composition of the fireball gases.*

The second step in the analysis of plutonium dioxide vaporization is the evaluation of the vaporization kinetics in response to the thermodynamic driving force. Here, arguments are made that the rate of plutonium dioxide vaporization depends on the plutonium dioxide fragment size, heat transport to the fragment, and mass transport away from the fragment.

Thermodynamics of PuO_2

Plutonium dioxide is not a stoichiometric compound. It is most accurately designated as $PuO_{2-x'}$, where x' assumes temperature-dependent values as large as about 0.35. The stoichiometry of plutonium dioxide in the GPHS is adjusted to minimize oxygen loss at the normal operating temperature. The fragments of plutonium dioxide dispersed into the fireball during an accident can be expected to have initial compositions ranging from $PuO_{1.96}$ to $PuO_{1.98}$.

In the fireball, the plutonium dioxide fragments will encounter an environment that is much hotter than the normal operating environment within the GPHS. The fireball atmosphere will also be chemically reactive. It would be expected, then, that the stoichiometry of plutonium dioxide will change in this environment. Thus

$$PuO_{2-x'} \Leftrightarrow PuO_{2-x} + \frac{(x - x')}{2} O_2 \qquad (83)$$

That is, the plutonium dioxide loses oxygen to the fireball atmosphere and this oxygen loss reduces the chemical potential of oxygen in the plutonium dioxide. This transformation of plutonium dioxide will proceed to larger values of x until the ambient chemical potential of oxygen is equal to the chemical potential of oxygen in the nonstoichiometric plutonium dioxide. The changes in the stoichiometry of the plutonium dioxide can be expected to affect the vapor pressure which is the thermodynamic driving force for vaporization.

The chemical potential of oxygen in the fireball atmosphere is determined by the details of the combustion process and the extent to which air is entrained as the fireball rises. The chemical potential of oxygen can be defined as

$$\mu(O_2) = \Delta\overline{G}(O_2) = RT \ln P(O_2) \tag{84}$$

where $\mu(O_2)$ is the oxygen chemical potential, $\Delta\overline{G}(O_2)$ is the partial Gibb's free-energy of oxygen, R is the gas constant, T is the absolute temperature, and $P(O_2)$ is the partial pressure of oxygen in the fireball atmosphere. This definition of the chemical potential of oxygen assumes that oxygen in the fireball behaves like an ideal gas. Such an assumption is expected to be adequate for the purposes of this work.

To evaluate the stoichiometry of the plutonium dioxide in equilibrium with the fireball oxygen potential, the suggestion by Green[13] has been adopted and a model similar to that devised by Blackburn[14] for nonstoichiometric uranium dioxide has been devised. Substoichiometric plutonium dioxide is hypothesized to be composed of Pu^{6+}, Pu^{4+},Pu^{3+}, $Pu^{2+}$and O^{2-} ions. From consideration of the mass balance among plutonium ions, charge balance among ions, and vapor pressure data for substoichiometric plutonium dioxide:

$$P(O_2)^{1/4} = \frac{(2-x)^{3/2}\left[0.5K_4 + K_5(2-x)^{1/2} / P(O_2)^{1/4}\right]}{P(O_2)^{1/2} K_3 + x(2-x)\Phi} \tag{85}$$

where

$$\Phi = 1 + \frac{K_3 P(O_2)^{1/2}}{2-x} + \frac{K_4(2-x)^{1/2}}{P(O_2)^{1/4}} + \frac{K_5(2-x)}{P(O_2)^{1/2}} \tag{86}$$

$$\ln(K_3) = -11.26 - 2037/T \tag{87}$$

$$\ln(K_4) = 5.2 - 25400/T \tag{88}$$

$$\ln(K_5) = 15.9 - 71700/T \tag{89}$$

where $P(O_2)$ is the partial pressure of O_2 (atm), and T is the particle surface temperature in units of K for these expressions.

Vaporization of plutonium dioxide is complicated by the existence of multiple plutonium-bearing species. Widely recognized are gaseous PuO_2, PuO, and Pu. It has been common to assume that the vaporization of plutonium occurs at the "congruently-vaporizing" composition.[15,16] That is, the vapor composition with respect to plutonium and oxygen is the same as the composition of the vaporizing solid. Then, the vapor pressure is just a function of temperature:

$$\log_{10} P_t = 7.5 - 29260 / T \tag{90}$$

where P_t is the total partial pressure of plutonium-bearing species in the fireball atmosphere (atm). This approach is the basis for previous fireball modeling efforts. The congruently-vaporizing assumption is <u>not</u> made in the Fireball code.

The assumption of congruent vaporization is neither realistic nor necessarily conservative for the conditions of a fireball. These conditions are such that the nonstoichiometry of the plutonium dioxide can be well below the congruent vaporization composition. A more realistic estimate of the vapor pressure, which is the thermodynamic driving force for vaporization, explicitly recognizes the effects of both temperature and the ambient chemical potential of oxygen:

$$PuO_{2-x}(solid) + \frac{x}{2}O_2 \Leftrightarrow PuO_2(gas) \tag{91}$$

$$PuO_{2-x}(solid) \Leftrightarrow PuO(gas) + \frac{(1-x)}{2}O_2 \tag{92}$$

$$PuO_{2-x}(solid) \Leftrightarrow Pu(gas) + \frac{(2-x)}{2}O_2 \tag{93}$$

$$2PuO_{2-x}(solid) \Leftrightarrow Pu_2(gas) + (2-x)O_2 \tag{94}$$

Thus the low oxygen partial pressures expected in a fireball promote vaporization of plutonium dioxide as gaseous PuO and Pu. Vapor pressures can then be higher than what would be predicted by simply considering the temperature-dependent congruent vaporization pressure. [The reaction presented in Equation (94) is not considered in the Fireball model because the concentration of Pu_2 over any oxide is assumed to be minuscule.]

As implemented in the Fireball code, the steps in the calculation of the plutonium dioxide vapor pressure are

1. Determine the particle surface temperature, T, from the particle heat transfer equations. Determine the oxygen (O_2) partial pressure from the fireball physics and combustion chemistry equations. Note that these quantities vary with time.

2. Assuming the stoichiometry of the surfaces of plutonium fragments instantly adjusts to be in equilibrium with the fireball atmosphere, calculate x in PuO_{2-x} using Newton iteration via

$$x = \left\{ \frac{\left[\exp(c_1 + c_2 / T)\right]^{1/2} (2-x)(1-2x)^2}{4P(O_2)^{1/2}} \right\}^{1/2} \tag{95}$$

where c_1 equals 20.8, and c_2 equals −101,600.

3. Calculate the partial pressures of PuO_2, PuO, and Pu from

$$P(PuO_2) = P(O_2)^{x/2} \exp[-\Delta G(PuO_2) / RT] \tag{96}$$

$$P(PuO) = P(O_2)^{(x-1)/2} \exp[-\Delta G(PuO) / RT] \tag{97}$$

$$P(Pu) = P(O_2)^{(x-2)/2} \exp[-\Delta G(Pu) / RT] \tag{98}$$

where

$$\Delta G(PuO_2) = G(PuO_2) - \frac{x}{2} G(O_2) - G(PuO_{2-x}) \tag{99}$$

$$\Delta G(PuO) = G(PuO) + \frac{(1-x)}{2} G(O_2) - G(PuO_{2-x}) \tag{100}$$

$$\Delta G(Pu) = G(Pu) + \frac{(2-x)}{2} G(O_2) - G(PuO_{2-x}) \tag{101}$$

and

$$G(PuO_{2-x}) = G(PuO_2)(solid) - \frac{x}{2} G(O_2) - \frac{RT}{2}\left[x(c_1 + c_2 / T) - 2I\right] \tag{102}$$

$$I = (1-2x)\ln(1-2x) + 2x(2x) + (2-x)\ln(2-x) + x - 1.3268335 \tag{103}$$

$$G(\Psi) = h_F(\Psi) - Tf(\Psi) \tag{104}$$

$$f(\Psi) = \sum_{i=1}^{4} a_i(\Psi)\left[T^*\right]^{i-1} + a_5(\Psi)\ln T^* + a_6(\Psi)/T^* + a_7(\Psi)T^*\ln T^* \qquad (105)$$

where Ψ represents solid and liquid PuO_2, or gaseous PuO_2, PuO, and Pu, h_F is the enthalpy of formation (J/mol), f is the free energy of formation (J/mol·K), a_i are the free-energy-of-formation coefficients, and T^* is T divided by 10,000.

4. Sum the partial pressures of plutonium-bearing species to get the total plutonium vapor pressure, P_t (also known as the equilibrium pressure):

$$P_t = P(PuO_2) + P(PuO) + P(Pu) \qquad (106)$$

There are unresolved issues that could affect the predictions of the vapor pressure of plutonium dioxide. The first of these is that the fireball atmosphere may react with the surfaces of plutonium dioxide fragments to form chemical species other than the hypo-stoichiometric oxide. Nitrogen partial pressures in the fireball atmosphere may be high enough to form plutonium nitride (PuN) on the fragment surfaces. Similarly, the chemical potentials of carbon in the fireball atmosphere may be high enough in oxidant-poor fireballs to cause the formation of carbides or oxycarbides (PuOC). Formation of nitrides or carbides on the fragment surfaces would, undoubtedly, affect the vapor pressure and the thermodynamic driving force for plutonium vaporization. These surface species could suppress the vapor pressure from values calculated by the method described here. Though the effects of carbide and nitride formation have not been investigated in detail, it appears the suppression will not be to values lower than those calculated assuming congruent vaporization.

The second issue that could affect the prediction of plutonium dioxide vapor pressures is the possible neglect of important vapor species. Additional vapor species will, of course, enhance the vapor pressure of plutonium dioxide and the driving force for vaporization. The vapor species PuN is known.[17] It is, however, not especially stable and probably will not greatly enhance the apparent vapor pressure of plutonium dioxide in a fireball. Of more concern is the possibility that water vapor in the fireball could lead to the formation of vapor phase oxyhydroxide species. Krikorian[18] has estimated the thermodynamic properties of several possible oxyhydroxide species including: PuOH, PuO(OH), $PuO_2(OH)$, $Pu(OH)_2$, $PuO(OH)_2$, $PuO_2(OH)_2$, $Pu(OH)_3$, and $PuO(OH)_3$. He argues that these species could enhance the high-temperature vapor pressure of plutonium dioxide. Recent experimental evidence suggests that, indeed, the vapor pressure of plutonium dioxide is increased when water vapor is present in the ambient atmosphere. The enhancement is not as great as would be derived from the estimated thermodynamic properties of the various oxyhydroxide species considered by Krikorian.

Kinetics of PuO_2 Vaporization

Vaporization of plutonium dioxide from fragments dispersed in the fireball requires that there be some mass transport of vapor from the fragment surface. This mass transport comes about because of vapor diffusion enhanced by the relative motions of fragments and the fireball gases. Fragment sizes produced by the impact of a GPHS in a hypothetical accident are expected to vary over a very broad range.[19] The convective enhancement of diffusion can then be brought on by the ballistic motions of very large fragments falling through the fireball or the natural convection of gas around small fragments suspended in the fireball gas.

Vaporization is an endothermic process. For example, the vaporization of PuO_2 requires 2234 J/g at 2000 K. Consequently, sustained vaporization requires that there be heat transport to the fragment. Even with this heat transfer to the fragment, there will always be a temperature difference between the fragment and the surrounding gas due to vaporization. This temperature difference can affect the diffusive mass transport from the fragment surface.

Either mass transport of vapor or heat transport to the fragment can limit the extent of vaporization from plutonium-dioxide fragments dispersed in the fireball. In this section, the estimation of the rate of plutonium dioxide vaporization from fragments is discussed. It is assumed for the purposes of estimating the vaporization rate that the fragments can be considered spheres and that a quasi-steady vaporization rate instantly develops when the fragments are dispersed in the fireball.

The formation of vapor at the surface of the fragment is assumed to be controlled by surface processes approximated by Hertz-Knudsen vaporization (the vaporization in a vacuum) to an interfacial boundary a vanishingly-small distance from the geometrical surface of the fragment. Vapor diffuses from this interface across a boundary layer that is of thickness δ and into the bulk fireball atmosphere. With the quasi-static assumption, the vapor flux from the surface due to Hertz-Knudsen vaporization is equal to the vapor flux away from the fragment by convection-enhanced diffusion. A serial resistance to vaporization is thus hypothesized to exist. Inclusion of the Hertz-Knudsen resistance assures that at the very high temperatures possible in fireballs, physically unrealistic vaporization rates will not be calculated.

The Hertz-Knudsen (HK) vaporization flux rate is given by [20,21]

$$\left.\frac{1}{A}\frac{dn}{dt}\right|_{HK} = \dot{n}''_{HK} = \frac{44.84}{\sqrt{WT}}(P_t - P_I)f(\alpha) \qquad (107)$$

where A is the fragment surface area, n is the quantity of plutonium vaporized, $\dot{n}''_{HK}$ is the molar vaporization flux (mol/cm^2·s), W is the molecular weight of the

vaporizing species (g/mol), T is the absolute temperature of the fragment surface (K), P_t is the total plutonium vapor pressure at the surface temperature and surface composition in equilibrium with the fireball atmosphere (atm), P_I is the total plutonium partial pressure at an interfacial plane a vanishingly-small distance from the particle surface (atm), and

$$f(\alpha) = 8\alpha(\alpha + 1)/(5\alpha^2 - 4\alpha + 8) \tag{108}$$

where α is the condensation coefficient (assumed to equal unity).

The vapor diffuses from the interfacial plane across a boundary layer. The thickness of this boundary layer is found from

$$\delta = \text{Đ} / k_m \tag{109}$$

where δ is the boundary layer thickness (cm), Đ is the diffusion coefficient of the vapor in the fireball gas (cm²/s), and k_m is the mass transport coefficient (cm/s).

The mass transport coefficient is found from the following analogy between heat and mass transfer:

$$k_m = \frac{h_c}{\rho_f c_f}\left(\frac{\rho_f c_f \text{Đ}}{k_f}\right)^{2/3} \tag{110}$$

where h_c is the heat transfer coefficient as described in the Particle Heat Transfer Section, ρ_f, c_f, and k_f are the density, specific heat, and conductivity of the fireball, respectively, and Đ is the diffusion coefficient of the vaporizing PuO_{2-x} at the fireball temperature.

The particle surface is necessarily at lower temperature than the bulk gas. There is, consequently, a temperature gradient across the boundary layer. To describe the diffusion in this thermal gradient, the approximations developed by Kumala and Vesala[22] are adopted and thermal diffusion is neglected.

The variation in temperature with radial distance from the fragment is taken as

$$T(r) = T_f + \frac{\Delta T d}{2\delta} - \frac{\Delta T d(d + 2\delta)}{4r\delta} \tag{111}$$

where ΔT is temperature difference between the fireball and the particle surface ($T_f - T$), d is the particle diameter, and r is the radial position in the boundary layer.

Similarly, the radial variation in the mole fraction of plutonium vapor is taken as

$$y(r) = y_f - \frac{\Delta y d}{2\delta} + \frac{\Delta y d(d+2\delta)}{4r\delta} \tag{112}$$

where Δy is the mole fraction difference between the particle surface and the fireball ($y - y_f$). Now, the convection-enhanced diffusive flux from the interfacial plane to the bulk fireball is given by

$$\frac{1}{A}\frac{dn}{dt}\bigg|_c = \dot{n}_c'' = \frac{\mathcal{D}}{2RT_f^{3/2}}\left(T_f^{1/2} + T^{1/2}\right)\frac{(d+2\delta)}{d\delta}\left[P_I - P_b\right] \tag{113}$$

where $\dot{n}_c''$ is the convection-enhanced molar vaporization flux (mol/cm²·s), and P_b is the partial pressure of plutonium vapor in the bulk fireball (atm). At steady-state conditions

$$\dot{n}_{HK}'' = \dot{n}_c'' = \dot{n}'' \tag{114}$$

The governing equation for the plutonium vaporization model in the Fireball code is obtained by adding the Hertz-Knudsen and convection-enhanced fluxes and rearranging to yield:

$$\dot{n}''\left\{\frac{dRT_f^{3/2}}{\left(\mathcal{D}+k_m d/2\right)\left(T_f^{1/2}+T^{1/2}\right)} + \frac{\sqrt{WT}}{44.84f(\alpha)}\right\} = P_t - yp \tag{115}$$

where y is the mole fraction of plutonium vapor in the fireball, and p is the fireball pressure, which is assumed equal to the ambient atmospheric pressure (atm). The molar vaporization flux is related to the mass vaporization flux, which is used in the particle heat transfer calculations, by

$$\dot{m}'' = W_{PuO_2}\dot{n}'' \tag{116}$$

where W_{PuO_2} is the molecular weight of PuO_2 (g/mol).

The dif fusion coefficient of the vaporizing species at the fireball temperature is assumed to vary with temperature according to

$$\mathcal{D} = \mathcal{D}_{ref}\left(T_f / T_{ref}\right)^{3/2} \tag{117}$$

where $\mathcal{D}$ is the diffusion coefficient (cm²/s), the subscript *ref* refers to the reference temperature of 300 K, and T_f is the fireball temperature (K).

To determine the reference value of the diffusion coefficient as a function of the current fireball composition, a conventional Wilke-Lee[8] estimate of the binary diffusion coefficient at the reference temperature is adopted. Thus

$$\mathcal{D}_{AB} = \frac{\left(3.03 - 0.98/W_{AB}^{1/2}\right) T_{ref}^{3/2}}{1.0132 \times 10^3 \, p W_{AB}^{1/2} \sigma_{AB}^2 \Omega} \tag{118}$$

where p is the fireball pressure (atm), W_A is the molecular weight of species A (i.e. the plutonium vapor) (g/mol), W_B is the molecular weight of species B (i.e. all fireball combustion gases) (g/mol), and W_{AB} is the binary molecular weight given by

$$W_{AB} = \frac{2}{1/W_A + 1/W_B} \tag{119}$$

and σ_{AB} is the binary collision cross section given by

$$\sigma_{AB} = \frac{\sigma_A + \sigma_B}{2} \tag{120}$$

where σ_A is the collision cross section of species A, and σ_B is the collision cross section of species B (Angstroms). Also, Ω is the collision integral given by

$$\Omega = \frac{1.06036}{\left(T^*\right)^{0.1561}} + \frac{0.1930}{\exp\left(0.47635 T^*\right)} + \frac{1.03587}{\exp\left(1.52996 T^*\right)} + \frac{1.76474}{\exp\left(3.89411 T^*\right)} \tag{121}$$

where T^* is given by

$$T^* = \frac{kT}{\varepsilon_{AB}} = \frac{T}{\sqrt{\frac{\varepsilon_A}{k}\frac{\varepsilon_B}{k}}} \tag{122}$$

where $\frac{\varepsilon}{k}$ is the energy parameter (K).

In the gas mixture of the fireball, the diffusion coefficient of the plutonium species is found from the binary diffusion coefficients using

$$\frac{1-y}{\mathcal{D}} = \sum_{i=1}^{N_p} \frac{y_i}{\mathcal{D}_{AB_i}} \tag{123}$$

where y is the PuO_{2-x} mole fraction in the fireball, N_p is the number of gaseous product species, y_i is the mole fraction for species i, and B_i represents the i^{th} product species in the fireball.

Homogeneous Condensation

Both heterogeneous and homogeneous condensation are modeled in the Fireball code. The model for heterogeneous condensation uses the same rate expression developed for plutonium dioxide vaporization. Condensation does, of course, release heat at the particle surface so that the surface becomes hotter than the ambient gas. When the partial pressure of the vapor species is greater than the surrounding equilibrium partial pressure of the vapor species evaluated at the surface temperature, the rate expression describes condensation rather than vaporization. Thus Equation (115) is used to predict heterogeneous condensation when the driving potential is negative. Condensation is assumed to occur over the entire surface of the agglomerated particle whereas vaporization occurs only from the area occupied by plutonium.

The homogeneous-condensation model is based on the supersaturation ratio, s. This is the ratio of the actual plutonium partial pressure to the equilibrium partial pressure at the fireball temperature. Thus

$$s = \frac{yp}{P_t} \tag{124}$$

where y is the mole fraction of plutonium vapor in the fireball at the current time, p is the fireball pressure (atm), and P_t is the equilibrium plutonium vapor pressure evaluated at the current fireball temperature (atm).

When the supersaturation ratio exceeds a user-specified critical supersaturation ratio, the plutonium vapor mass is reduced by the amount required to restore the supersaturation ratio to the critical value. This mass is assumed to condense homogeneously, with rate considerations ignored. An alternate approach is to restore the ratio to unity. Because the equilibrium vapor pressure drops precipitously at the end of the combustion stage, both approaches yield results that are essentially indistinguishable. The first approach is implemented in Fireball because it introduces somewhat less of a discontinuity into the code numerics. These approaches are consistent with the approach taken in reactor safety codes such as VICTORIA[23] and CONTAIN.[24] Experience with these codes indicates that more sophisticated models are not warranted.

The size of the homogeneously-condensed plutonium particles is given by

$$d^* = \frac{4\sigma_{PuO_2} W_{PuO_2}}{\rho R T \ln s} \tag{125}$$

where d^* is the minimum-stable particle diameter for homogeneous condensation (cm), σ and W are the surface tension (J/cm^2) and molecular weight (g/mol), respectively, of PuO_2, ρ is the PuO_2 density (g/cm^3), R is the gas constant (8.314 J/mol·K), and T is the fireball temperature (K). The condensed plutonium mass is then placed in the appropriate size section based on this diameter.

Aluminum Structure Response

Rockets consist mainly of aluminum alloy structures which have the potential of being vaporized by a fireball. The combustion of the vaporized aluminum would then lead to the formation of aluminum-oxide (Al_2O_3) particles. These particles would provide additional agglomeration and condensation sites in the fireball. It is therefore desirable to have models of aluminum heat transfer, vaporization, and combustion in the Fireball code package.

As with the particle heat transfer models, a lumped-capacitance model is adequate to capture the transient temperature response of the aluminum-alloy structures. This is indicated by a Biot number analysis where, for thin-walled hollow cylinders and for flat plates, the Biot number (Bi) is given as

$$\mathrm{Bi} = \frac{h_s \delta_s}{2k_s} \tag{126}$$

where h_s is the heat transfer coefficient for the structure (W/cm²·K), δ_s is the structure wall thickness (cm), and k_s is the structure thermal conductivity (W/cm·K). The results of the Biot number analysis are provided in the following table for each of the structures in a Titan IV rocket with a Centaur upper stage. This rocket configuration was selected for example purposes only.

Table 4. Biot Numbers for Titan IV Structures

Structure	Thickness (cm)	Biot number
Centaur Attachment	1.6765	0.048
Payload Fairing	0.5715	0.016
Space Vehicle	0.9871	0.028
Stage 1	0.8439	0.024
Stage 2	1.4027	0.040

These results are based on a conductivity of 1.8 W/cm·K and on a heat transfer coefficient of 0.1032 W/cm²·K. The heat transfer coefficient consists of a convective component (0.02 W/cm²·K) and a radiative component (0.0832 W/cm²·K). The radiative component is based on an emissivity of 0.6, a structure temperature of 933 K, and a fireball temperature of 2500 K. A Biot number less than about 0.1 is generally accepted as the cutoff for neglecting spatial gradients. The low Biot numbers for all structures is a result of the high conductivity of aluminum alloys.

If the temperature of an aluminum-alloy structure is sufficiently high (greater than about 1300 K), aluminum vaporization from the surface into the fireball will occur with subsequent combustion of the vapor to form aluminum oxide particles.

The heat transfer, vaporization, and combustion models for aluminum-alloy structures in the fireball are described in the following subsections.

Structure Heat Transfer

The heat transfer model for aluminum-alloy structures is similar to that for rock particles and begins with the following governing equation:

$$\rho_s c_s \frac{d(V_s T_s)}{dt} = q_s'' A_s - \dot{m}_s'' L_v^s A_s \tag{127}$$

where ρ_s is the structure density (g/cm^3), c_s is the structure specific heat (J/g·K), V_s is the structure volume (cm^3), T_s is the structure temperature (K), t is time (s), q_s'' is the heat flux at the structure surface (W/cm^2), A_s is the surface area of the structure exposed to the fireball (cm^2), $\dot{m}_s''$ is the mass vaporization flux (g/cm^2·s), and L_v^s is the latent heat of vaporization (J/g). This equation is then expanded and rearranged to yield:

$$\frac{dT_s}{dt} = \frac{A_s}{c_s m_s}\left[q_s'' - \dot{m}_s''\left(L_v^s + c_s T_s\right)\right] \tag{128}$$

where m_s is the mass of the aluminum-alloy structure (g), which can vary with time depending on the vaporization rate. The structure surface area represents the area exposed to the fireball. Thus both the inside and outside surfaces of a structure can be included if it is assumed that the structure fragments during the hypothetical explosion. Although the structure may melt, the very high surface tension of aluminum should prevent the melt from being entrained into the fireball or from dripping from the surface during the short duration of the fireball. Thus, the surface area is assumed to remain constant throughout the transient. Heat transfer to structures occurs only during the combustion stage, which is the period before the fireball lifts from the ground. For those fireballs occurring in the air, a residence time for structures can be specified, which then determines the time period for structure heat transfer.

Properties for 7075-T6 aluminum alloy (a common alloy used in rocket structures) are used for all structures, with the specific heat given by

$$c_s = 0.39 + 0.014\,T_s^{0.6076} \tag{129}$$

The heat flux boundary condition is given by

$$q_s'' = h_s\left(T_f - T_s\right) + \sigma\varepsilon\tau_f\left(T_a^4 - T_s^4\right) + \sigma\varepsilon\varepsilon_f\left(T_f^4 - T_s^4\right) \tag{130}$$

where h_s is the convection heat transfer coefficient (W/cm^2·s), T_f is the fireball temperature (K), T_s is the structure temperature (K), σ is the Stefan-Boltzmann constant (5.67 × 10^{-12} W/cm^2·K^4), ε is the emissivity of the surface, τ_f is the transmissivity of the fireball (one minus the fireball emissivity), T_a is the ambient temperature outside the fireball (K), and ε_f is the emissivity of the fireball. The radiation flux model treats the fireball as a semitransparent participating medium between the structure and an ambient environment of infinite extent.

In addition to convection, this heat flux consists of radiative contributions between the surface and the fireball and between the surface and the ambient air outside the fireball. Presently, the convection heat transfer coefficient is a user-specified parameter as opposed to being calculated by the code. Introduction of this parameter avoids the difficulty associated with determining the appropriate velocity to use for a structure fragment careening through a turbulent fireball. The uncertainty associated with this difficulty can best be investigated parametrically.

The latent heat of fusion effects associated with melting are accommodated by modifying the specific heat according to

$$\hat{c}_s = c_s + \frac{L_f^s}{T_{liq} - T_{sol}} \tag{131}$$

where $\hat{c}_s$ is the modified specific heat (J/g·K), L_f^s is the latent heat of fusion (J/g), T_{liq} and T_{sol} are the liquidus and solidus temperatures (K) of aluminum alloy, respectively, given by

$$T_{liq} = T_{melt}^s + 2.5 \tag{132}$$

and

$$T_{sol} = T_{melt}^s - 2.5 \tag{133}$$

where T_{melt}^s is the melt temperature of the alloy (933 K). The augmented specific heat is used only when the structure temperature is between the liquidus and solidus temperatures. Logic is included to preclude skipping over this arbitrarily-selected phase-change zone.

An explicit time-integration scheme is used to solve the transient heat transfer equation for each structure, with the time step determined by the fireball energy and rise velocity equations. The very small time step dictated by the fireball energy equation ensures that the explicit integration approach is sufficient for these large heat capacity structures. However, if a structure vaporizes significantly, the explicit approach may cause numerical problems. Currently this is

avoided by terminating the structure heat transfer solution when the mass falls below an arbitrarily-selected cutoff. The small remaining mass is then simply added to the aluminum vapor inventory.

The exposed surface area and the mass of all the aluminum-alloy structures are provided in the following table for a Titan IV rocket/Centaur upper stage configuration. The surface area represents both inside and outside surfaces.

Table 5. Titan IV Aluminum-Alloy Structures

Structure	Area (cm^2)	Mass (g)
Centaur Attachment	3.3626×10^5	7.8926×10^5
Payload Fairing	5.6685×10^6	4.5360×10^6
Space Vehicle	9.6961×10^5	1.3399×10^6
Stage 1	5.0347×10^6	5.9481×10^6
Stage 2	1.6266×10^6	3.1943×10^6

Aluminum Vaporization

The thermodynamic driving force for aluminum vaporization is the difference between the aluminum vapor pressure, evaluated at the surface temperature, and the aluminum partial pressure in the fireball (which is essentially zero). The equilibrium vapor pressure for pure aluminum is determined by a curve fit of the appropriate JANAF table.[25] Thus

$$\log_{10} P_{Al} = 7.9462378 - 1.03948 \times 10^{-3} T_s + 1.52468 \times 10^{-7} T_s^2 - \frac{17{,}389}{T_s} \qquad (134)$$

where P_{Al} is the equilibrium vapor pressure of aluminum (atm), and T_s is the aluminum-structure surface temperature (K).

Aluminum vapor is quite reactive and can extract oxygen from any of the oxygen-bearing fireball gases, including H_2O, CO, and CO_2. This extreme reactivity of aluminum vapor affects the mass transport away from the structure by greatly increasing the concentration gradient adjacent to the vaporizing surface. The increased concentration gradient, which is the driving force for mass transport, accentuates aluminum vaporization. Within the metallurgical field this is known as "fog-line" formation.[26] It can increase the vaporization rate to the physical maximum of free molecular vaporization.

To estimate the rate of vaporization of aluminum from structures, it is assumed that the flow of fireball gases over the structures gives rise to a boundary layer of thickness δ. Oxygen diffuses from the fireball across this boundary layer toward the aluminum surface while aluminum vapor from the surface diffuses toward the fireball. As the diffusing species encounter each other they can react.

It is assumed that a quasi-steady vaporization rate is established instantaneously at the current structure temperature and that the structure surface is a flat plate. The flux of aluminum vapor across the boundary layer is

$$\dot{n}''_{Al} = -c_g \mathcal{D}_{Al} \frac{\partial y_{Al}}{\partial x} + y_{Al}(\dot{n}''_{Al} + \dot{n}''_O) \tag{135}$$

where $\dot{n}''_{Al}$ is the molar flux of aluminum vapor (mol/cm²·s), c_g is the molar concentration of fireball gases (mol/cm³), $\mathcal{D}_{Al}$ is the diffusion coefficient of aluminum vapor in the fireball (cm²/s), y_{Al} is the mole fraction of aluminum at the surface (equal to P_{Al}/p), p is the fireball pressure (atm), x is the boundary layer position coordinate normal to the surface (cm), and $\dot{n}''_O$ is the molar flux of oxygen (mol/cm²·s). Similarly, the oxidant mass flux is

$$\dot{n}''_O = -c_g \mathcal{D}_O \frac{\partial y_O}{\partial x} + y_O(\dot{n}''_{Al} + \dot{n}''_O) \tag{136}$$

where $\mathcal{D}_O$ is the diffusion coefficient of oxidant (oxygen) in the fireball (cm²/s), and y_O is the effective mole fraction of oxygen in the fireball (i.e., at $x = \delta$). At steady state, the molar fluxes will be in a stoichiometric proportion given by

$$\frac{3}{2}\dot{n}''_{Al} = -\dot{n}''_O \tag{137}$$

where the minus sign arises because the fluxes are in opposite directions.

There is a temperature gradient across the boundary layer which is assumed linear for simplicity. Thus

$$T(x) = T_s + \frac{T_f - T_s}{\delta} x \tag{138}$$

The diffusion coefficients are assumed to have a temperature dependence given by

$$\mathcal{D}(T) = \mathcal{D}_{ref}\left(\frac{T}{T_{ref}}\right)^{3/2} \tag{139}$$

where the *ref* subscript refers to the reference condition, taken here to be 300 K.

Now making use of Equations (137) through (139), the equation for the aluminum vapor flux can be integrated from the surface ($x = 0$) to an arbitrary position within the boundary layer ($x = X$). Also, the equation for the oxidant flux

can be integrated from the outer edge of the boundary layer ($x = \delta$) to the arbitrary position within the boundary layer ($x = X$). For brevity, the details of the rather lengthy integrations and subsequent equation manipulations are omitted. The results are given by

$$\dot{n}''_{Al} = \frac{-\ln\left(1+\frac{y_{Al}}{2}\right) c_g \, \mathcal{D}_{Al}^{ref} (T_f - T_s)}{34.64\left(\frac{1}{\sqrt{T_X}} - \frac{1}{\sqrt{T_s}}\right)} \tag{140}$$

where

$$T_X = T_s + (T_f - T_s)\frac{X}{\delta} \tag{141}$$

and

$$\frac{X}{\delta} = \frac{\dfrac{(\beta-\alpha)^2 T_f T_s}{\left(\beta\sqrt{T_f} - \alpha\sqrt{T_s}\right)^2} - T_s}{T_f - T_s} \tag{142}$$

where

$$\beta = \mathcal{D}_O^{ref} \ln\left(1 - \frac{y_O}{3}\right) \tag{143}$$

and

$$\alpha = \mathcal{D}_{Al}^{ref} \ln\left(1 + \frac{y_{Al}}{2}\right) \tag{144}$$

The effective mole fraction of oxygen in the fireball is based on the current composition of the fireball using

$$y_O = \sum_{i=1}^{N_O} y_i^O a_i \frac{W_O}{W_i^O} \tag{145}$$

where N_O is the number of oxygen-bearing gas species in the fireball, y_i^O is the mole fraction of oxygen-bearing species i, a_i is the number of oxygen atoms per mole of oxygen-bearing species i, W_O is the molecular weight of oxygen (g/mol), and W_i^O is the molecular weight of oxygen-bearing species i (g/mol).

The molar vaporization flux is related to the mass vaporization flux, which is used in the heat transfer calculation, by

$$\dot{m}''_{Al} = W_{Al}\dot{n}''_{Al} \tag{146}$$

The diffusion coefficients at the reference temperature are determined as a function of fireball composition using the method of Wilke-Lee. This method is outlined in the Kinetics of Plutonium Vaporization Subsection and is not repeated here. The equation for the Hertz-Knudsen limit is also described in that subsection. This limit is imposed on the aluminum vaporization rate calculated here.

Aluminum Combustion

The combustion of aluminum vapor is highly exothermic. The energy associated with this combustion is added directly to the fireball assuming that enough oxygen is available to burn stoichiometrically. The chemical process for this combustion is given as

$$4Al + 3O_2 \Rightarrow 2Al_2O_3 \tag{147}$$

The aluminum combustion power added to the fireball can be calculated as

$$q_{Al} = \dot{n}_r h_r - \dot{n}_p h_p \tag{148}$$

where q_{Al} is the rate of energy production (W), $\dot{n}_r$ is the molar combustion rate of the aluminum vapor and O_2 reactants (mol/s), h_r is the enthalpy of the reactants (J/mol), $\dot{n}_p$ is the molar rate of product formation (mol/s), and h_p is the enthalpy of the Al_2O_3 product (J/mol). Assuming the aluminum vapor burns at the same rate it is formed yields

$$q_{Al} = \dot{n}_{Al}\left(h_{Al} + \tfrac{3}{4}h_{O_2} - \tfrac{1}{2}h_{Al_2O_3}\right) \tag{149}$$

where $\dot{n}_{Al}$ is the vaporization rate of aluminum from all structures (mol/s), h_{Al} is the enthalpy of aluminum vapor (J/mol), h_{O_2} is the enthalpy of O_2 gas (J/mol), and $h_{Al_2O_3}$ is the enthalpy of solid aluminum oxide (J/mol). This quantity is subtracted from the loss term, L [Equation (12)], that appears in the fireball energy equation.

Based on the stoichiometric reaction of aluminum and oxygen, the mass of aluminum oxide formed equals 1.89 times the mass of aluminum vapor produced. The particles of aluminum oxide associated with this mass are free to agglomerate with other particles or to serve as condensation sites for plutonium vapor. The diameter of the aluminum oxide particles is specified by user input.

Soot Generation

The presence of soot in the fireball provides additional sites for condensation and agglomeration and thus can alter the final plutonium size distribution. The amount of soot generated from large-scale combustion almost always exceeds the theoretical amount of soot. Thermodynamically, soot should only form when the carbon-to-oxygen (C/O) ratio is greater than one. Experimentally, the limits of soot formation are usually equated with the onset of luminosity and this usually occurs when the C/O ratio is about 0.5.[27] This limit is called the critical C/O ratio. There are many factors that affect the generation of soot such as localized non-stoichiometric regions due to hydrodynamic effects, localized pressure and temperature regions, the presence of diluents, the presence of nitrogenous species, and the presence of metals.

The effects of several factors affecting soot generation are summarized in Table 6, which is based mostly on the work of Haynes et al[27] and Walton.[28] The table is applicable primarily to the combustion of oil and conventional fuels. Effects associated with the different carbon chemistry of rocket propellants are not addressed.

Table 6. Factors Affecting Soot Generation

Factor	Effect	Comments
Localized oxygen depletion due to fluid flow effects	Increases soot generation.	Decomposition of soot to basic elements is enhanced by stoichiometric conditions.
Increased pressure	Increases soot generation in some cases.	Strong effect for hexane and hexene, but weak effect for benzene. Weak influence on critical C/O ratio, but may cause shifting of gas-solid absorption balances to favor more condensation.
Increased temperature	Decreases soot generation near critical C/O ratio. Increases soot generation in fuel rich flames.	Appearance of cellular structure changes the influence of increasing temperature from anti-soot to pro-soot.
Addition of inert diluents	Decreases soot generation at constant temperature.	If diluent reduces the temperature, promotion of soot may occur. High concentration (>5%) required to produce significant changes in generation of soot.

Factor	Effect	Comments
Addition of nitrogenous species such as NH_3, NO and NO_2	Decreases soot generation.	Directly applicable to rocket propellants.
Addition of sulfur compounds such as H_2S and SO_2	Decreases soot generation.	Seems to be more effective than other species in reducing soot yield.
Addition of H_2 or CO	Increases soot generation.	Weak effect. These species act as oxygen sinks causing richer flames.
Addition of hydrocarbons	Increases soot generation.	Increases carbon content of mixture.
Addition of CO_2 or H_2O	Decreases soot generation.	Suppresses luminosity.
Addition of halogens	Increases soot generation.	Catalyzes radical recombination neutralizing OH radicals which would otherwise oxidize soot.
Addition of O_2	Increases or decreases soot generation.	Depends on structure of flame and flow conditions.
Addition of metals	Decreases soot generation.	Used as soot suppressant, but can promote soot generation in parts of flame.

Considering the uncertainty in the state-of-the-art soot models, a complicated soot treatment is not justified for the fireball model. Instead, a parametric approach is used to explore the impact of generated soot based on the following equation:

$$m_t^{soot} = m_i^{soot} + m_{eq}^{soot} + f_s m_c \tag{150}$$

where m_t^{soot} is the total mass of soot in the fireball at any given time (g), m_i^{soot} is the initial mass of soot in the fireball (a specified input parameter), m_{eq}^{soot} is the mass of soot (solid carbon) calculated by the chemical equilibrium solver, f_s is the supplemental soot fraction which is defined as the fraction of available gaseous carbon to be added as supplemental soot, and m_c is the mass of available gaseous carbon. Thus the quantity of soot in the fireball is the sum of initial, equilibrium, and supplemental soot. The supplemental soot fraction, f_s, is a specified input parameter that can be different for every reactant mix involved in the fireball.

Dirt Entrainment

The entrainment of dirt and sand into the fireball directly affects the fireball emissivity, particle agglomeration, particle heat transfer, and plutonium condensation processes. Thus dirt entrainment can significantly alter the size distribution of plutonium-bearing particles.

There is a large body of literature dealing with dirt entrainment models. Such models consider adhesive and cohesive forces between the particles and the ground. These forces are functions of many variables such as humidity, particle size and roughness, chemical composition, surface tension, intermolecular and electrostatic attractions, and local flow velocity vectors. Even whether or not the sun is shining has an effect on entrainment! Experimental measurements show adhesive forces that vary over eight orders of magnitude for particles in the 10- to 100-μm-diameter size range for various surface conditions, materials, and humidity levels.[29] In general, the models have many adjustable parameters and do not have reliable predictive capability. Complicating the problem is the potential for crater formation for several launch-abort scenarios. Therefore, the issue of dirt entrainment is handled parametrically in the Fireball code using the following equation:

$$m_d = m_d^i + \underbrace{\int_{t_0}^{t_1} \dot{m}_d^{(1)} dt}_{\text{combustion stage}} + \underbrace{\int_{t_1}^{t_2} \dot{m}_d^{(2)} dt}_{\text{entrainment stage}} \tag{151}$$

where m_d is the mass of dirt in the fireball, which can vary with time (g), m_d^i is the initial mass of dirt inserted into the fireball from crater formation (g), $\dot{m}_d^{(1)}$ is the rate of dirt entrainment into the fireball during the combustion stage (g/s), $\dot{m}_d^{(2)}$ is the rate of dirt entrainment into the fireball during the air entrainment stage (g/s), t_0 is the time at the beginning of the fireball simulation (0 s), t_1 is the time at the end of the combustion stage (s), and t_2 is the end of the entrainment stage (s), which is also the end of the simulation.

By varying the two entrainment rates and the initial mass parameters, the effect of dirt entrainment on the fireball simulation can be explored parametrically. The diameter, emissivity, and density of entrained dirt can also be varied via the input file. Also, the dirt parameters can be used to simulate solid propellant rocket exhaust particles if desired. The diameter and distribution of dirt particles depends on the location of rocket impact. Currently, only a single diameter can be specified for dirt particles. The mass of dirt is assigned to the appropriate aerosol bin based on this diameter.

Model Integration

As mentioned previously, all of the models in the Fireball code package are integrated (i.e., the results of each model depend on the results of other models). Throughout this report, the relationships between variables in the different models are discussed in the appropriate sections. This section is included to summarize and elucidate these relationships and to outline the sequence of steps in a fireball simulation. This description includes the major steps but omits many of the peripheral steps required to produce a working computer code. No attempt is made to describe the complicated "bookkeeping" associated with the code package.

After processing the input files, appropriate variables are initialized. Next, a thermodynamic equilibrium calculation is performed for the first reactant mix to determine the products of combustion and their respective mole fractions. A reactant mix may consist of a single mix or of submixes burning concurrently. This information is used to solve the fireball energy equation for enthalpy. A Runge-Kutta Fehlberg (RKF) algorithm is used to integrate the energy equation over time. However, an Euler solution is used for the first time step to avoid the singularity that occurs at time zero in the RKF algorithm. Initialization of variables dependent on combustion occurs after the Euler time step. Next, using the computed enthalpy and Newton iteration, the fireball temperature is determined.

Based on the specified combustion rates for the current reactant mix, the quantity of combustion products comprising the fireball is determined for the current time step. Based on the current temperature, the fireball specific heat, viscosity, and conductivity are calculated. The transient equation for structure heat transfer is calculated next, followed by calculation of the aluminum vaporization rates. All properties are based on the current state of the fireball. Combustion energy associated with any aluminum vaporization is then determined and added to the fireball energy equation.

The quantity of aluminum oxide particles formed as a result of any aluminum combustion is determined next. Based on user-specified dirt entrainment rates, the current quantity of dirt particles in the fireball is also calculated. Likewise, the quantity of soot particles, based on equilibrium and supplement soot, is calculated. Based on the current inventory of these particles, along with the current inventory of plutonium particles (original and condensed), the fireball emissivity is determined. This calculation also depends on the temperature and chemical composition of the fireball. Also, the average properties of agglomerated particles are determined at this time.

The temperature of the plutonium rock particles and of the agglomerated aerosol particles is determined next, for all particle size sections (bins). Heat and mass transfer coefficients, terminal velocities, and particle properties are based on

the current fireball and particle conditions. The particle temperature calculations are followed by a check of the plutonium vapor supersaturation ratio. If this ratio exceeds a user-specified critical value, homogeneous condensation is initiated. Now the vaporization (or condensation) rate of plutonium is determined. Based on the calculated rates, particle sizes are updated and the resulting particles assigned to appropriate new size bins.

Based on the quantity of all combustion products and the fireball temperature, the size of the fireball is determined. This is used in turn to calculate the fireball rise velocity and height. The rise velocity calculation includes buoyant and drag force effects, and is solved using an RKF algorithm. With the fireball rise velocity and size available, the quantity of entrained air is determined and added to the fireball inventory.

The aerosol physics equations are solved next based on the current inventory of plutonium, soot, dirt, and aluminum oxide. Original and condensed plutonium are treated separately so they may be tracked separately for output purposes. Agglomeration may move particles into different size bins. Also, particles may leave the fireball due to gravitational settling. The aerosol physics calculations are not performed every fireball time step but instead are performed based on user-specified time or temperature intervals. This is illustrated in the following figure, which schematically shows the fireball and aerosol physics time steps.

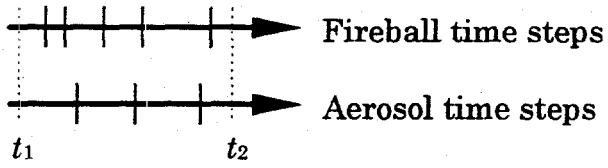

Figure 4. Fireball and Aerosol Physics Time Steps

In this example, the time interval for updating the aerosol physics solution is just $t_2 - t_1$. Time step boundaries are indicated by solid vertical lines. The fireball physics solution proceeds from t_1 to t_2, using an adaptive time step dictated by the fireball energy and rise velocity equations. The aerosol physics solution proceeds with its own adaptively-controlled time step dictated by the agglomeration equations. The fireball parameters to be passed to the aerosol physics routine are saved at times t_1 and t_2. The aerosol physics routine uses these parameters to linearly interpolate appropriate values at the aerosol physics time steps. Fireball parameters passed to the aerosol physics routine include: temperature, pressure, density, viscosity, molecular weight, turbulent energy dissipation rate, radius, and volume, along with component masses for each bin and average particle density. Section coefficients are also linearly interpolated between t_1 and t_2. Section coefficients are used in the agglomeration solution and are very time consuming to compute. Thus, updating section coefficients only at t_1 and t_2 saves considerable execution time. If desired, the time interval can be decreased sufficiently such that

the aerosol physics equations are solved every fireball time step; however, this has been found to be unnecessary.

A temperature interval can also be specified to control updating of the aerosol physics solution. The solution is updated whenever the fireball temperature changes by the selected temperature interval. Also, if more than 1 μg of plutonium vapor is available in the fireball and more than 5% of this vapor is homogeneously condensed in a single time step, the aerosol physics solution is automatically updated. This ensures that large "dumps" of plutonium particles into the fireball are captured immediately in the agglomeration solution.

Time steps are continued until all reactants for the current mix are combusted. Once complete, a check is made for any additional mixes, and the procedure is repeated accordingly. All combustion products from all mixes and submixes are tracked for subsequent calculation of fireball properties. After all reactant mixes are depleted, the combustion stage is terminated and the calculation proceeds with the air entrainment stage. The sequence of steps for this stage is the same as for the combustion stage except no additional calls to the chemical equilibrium solver are required and the combustion term is absent from the fireball energy equation. Also, for ground-blast scenarios, heat transfer to aluminum structures is terminated as the fireball lifts from the ground. The air entrainment rate is a function of fireball size, which in turn is a function of how much air has been entrained. Because the prediction of air entrainment is of primary concern during this stage, a successive-substitution procedure is used to resolve this dependency, as opposed to simply using the most current value of entrainment rate. Time steps continue until the end of the simulation is indicated.

As mentioned previously, particles are assigned size sections (bins), based on diameter, for both the aerosol physics calculations and particle heat transfer calculations. A restriction of Maeros2 is that the diameter at each bin boundary must be at least twice that of the preceding bin boundary. This is known as the geometric constraint. A uniform logarithmic spacing in volume satisfies this constraint, which can be expressed in terms of diameters at the bin boundaries according to

$$d_i = d_0^{1-i/N_b} d_{N_b}^{i/N_b} \tag{152}$$

where d_i is the diameter of the i^{th} bin boundary (cm), i is the bin boundary index, which increments from 1 to $N_b - 1$, N_b is the number of bins, d_0 is the diameter of the lower boundary of the smallest bin, and d_{N_b} is the diameter of the upper boundary of the largest bin. The same equation is used separately for both aerosol and rock bins. Because rock particles are not part of the aerosol physics solution, the geometric constraint does not apply. However, it is enforced for consistency with the aerosol particle diameter assignments.

Particles can change bins by agglomeration and by vaporization or condensation. For heat transfer calculations, all the particles in a bin are initially assigned the geometric-mean diameter of the bin, which is given by

$$d_i = \sqrt{d_{i-1} d_i} \tag{153}$$

where i increments from 1 to N_b. The particle bin diameters change as vaporization and condensation proceed.

If the particles in a bin decrease in diameter (from mass loss by vaporization) to a value below the lower-boundary diameter, all the mass in the bin is moved into the next lower bin and assigned the current diameter of that bin. Likewise, if particles in a bin increase in diameter (from mass gain by condensation) to a value above the upper-boundary diameter, all the mass in the bin is moved into the next higher bin and assigned the current diameter of that bin. If a bin is left empty of particles, any particles subsequently entering the bin are assigned the associated geometric-mean diameter for heat transfer calculations. Other strategies for managing particle bin changes due to vaporization and condensation are possible but have not been explored. Recall that particle bin changes due to agglomeration are managed by the Maeros2 subroutine.

Code Input and Use

The input for a fireball simulation is contained in three files: "fireball.in," "cetsub.in," and "maeros2s.in." This section contains a description of the input parameters contained in these three files. Information concerning the procedures for compiling and running the code is also included, along with a description of the code output.

The parameters for the three input files are described in the following three tables, starting with the "fireball.in" file. Additional comments follow each table. Included in the tables is a default value, which is used by the code if the corresponding data field is left blank. These are not necessarily the recommended values, which are dependent on the particulars of the desired simulation. Review of these input parameters provides an overview of the versatility provided by the Fireball code package.

Table 7. Input Parameter Descriptions for "fireball.in"

Parameter	Description and Units	Default
title	problem title of up to 132 characters	none
timestep	initial time step for solution of fireball physics (s)	1×10^{-5}
tstop	problem end time (s)	100.0
iprint	print frequency (*timesteps*)	50
nmax	maximum number of time steps allowed (*timesteps*)	10000
nnmax	maximum number of Newton iterations allowed	25
drelerr	desired relative error for Newton iteration convergence	1×10^{-3}
dtrerr	desired truncation error for adaptive time step control	1×10^{-2}
tsmax	maximum-allowed time step (s)	1.0
tsmin	minimum-allowed time step (s)	1×10^{-6}
tamb	ambient temperature (K)	300.0
press	fireball combustion-product pressure (atm)	1.0
zfbi	initial elevation of the center of the fireball (cm)	0.0
vrisei	initial rise velocity of the fireball (cm/s)	0.0
sootmi	initial mass of soot added to the fireball (g)	0.0
ecoef1	air entrainment coefficient during the combustion stage	0.025
ecoef2	air entrainment coefficient during the entrainment stage	0.25
dirtmi	initial mass of dirt injected into the fireball (g)	0.0
dirter1	dirt entrainment rate during the combustion stage (g/s)	100.0
dirter2	dirt entrainment rate during the entrainment stage (g/s)	0.0
dirtden	density of entrained dirt particles (g/cm^3)	2.0
sootdp	diameter of generated soot particles (cm)	2.2×10^{-5}
aodp	diameter of generated aluminum oxide particles (cm)	5×10^{-6}

Parameter	Description and Units	Default
dirtdp	diameter of entrained dirt particles (cm)	5×10^{-5}
puo2emis	emissivity of PuO_2 particles	0.5
sootemis	emissivity of soot particles	0.9
aoemis	emissivity of aluminum oxide particles	0.6
dirtemis	emissivity of dirt particles	0.6
puo2ti	initial PuO_2 rock particle temperature (K)	1520.0
puo2qppp	volumetric heat generation rate in PuO_2 (W/cm^3)	2.64
puo2melt	melt temperature of PuO_2 (K)	2698.0
critssr	critical supersaturation ratio of PuO_2 vapor	4.0
surften	surface tension of PuO_2 (J/cm^2)	6.2×10^{-5}
delay	delay time for injection of PuO_2 particles into the fireball (s)	0.0
dshapef	dynamic shape factor for all particles	1.2
dcutoff	diameter cutoff for quasi-steady treatment of rock particle heat transfer (cm)	1×10^{-3}
residnct	residence time in the fireball for PuO_2 rock particles (s)	50.0
nstruct	number of aluminum-alloy structures exposed to fireball	1
strrest	structure residence time in the fireball (s)	100.0
semis	emissivity of all structures	0.6
shtc	convection heat transfer coefficient for all structures ($W/cm^2 \cdot K$)	0.02
sarea	exposed surface area of each structure (cm^2)	100.0
smass	mass of each structure (g)	100.0
sname	name for each structure up to 24 characters	none
aerostrt	start time for aerosol physics solution (s)	0.0
aerodt	time interval for updating of aerosol physics solution (s)	2.0
adtemp	temperature interval for updating of aerosol physics solution (K)	50.0
nabins	number of aerosol particle size bins	10
nrbins	number of rock particle size bins	5
adiam0	minimum aerosol particle diameter (cm)	1×10^{-6}
adiamna	maximum aerosol particle diameter or minimum rock particle diameter (cm)	1×10^{-2}
adiamnr	maximum rock particle diameter (cm)	1.0
readmass	if .true., the initial PuO_2 mass distribution for all bins is read from input file "massdist.in"	.false.
puo2mass	mass of PuO_2 injected into the fireball (g)	1.0
rupture	diameter of the rupture (cm)	1.0
escfrac	fraction of PuO_2 particles with diameter less than *rupture* that escape from the rupture	1.0

Comments:

- The simulation is terminated if the maximum number of Newton iterations allowed (*nnmax*) is exceeded. Newton iteration is used to find the fireball temperature, the area of a truncated sphere (representing the rising fireball), the temperature of aerosol particles, and the value of x used to specify the stoichiometry of PuO_{2-x}.
- The desired truncation relative error (*dtrerr*) is used to control the time step for the fireball energy and rise velocity calculations. The smaller this value, the smaller will be the resulting time steps.
- The initial fireball elevation (*zfbi*) and rise velocity (*vrisei*) allow the simulation of either ground blasts or air blasts. An elevation of zero indicates a ground blast and the fireball begins as a hemisphere. Otherwise, it begins as a sphere. The initial rise velocity is used for the initial condition in the fireball momentum equation. For air blasts, it would be set to the rocket velocity at the time of the blast. A negative value indicates downward travel.
- Zero values of entrainment coefficients (*ecoef1* or *ecoef2*) indicate no air will be entrained by the rising fireball. Entrained air can also be added as a combustion reactant via the "cetsub.in" file.
- The initial mass of dirt injected into the fireball (*dirtmi*) can be used to account for dirt from crater formation in the event of a ground-impact scenario. However, if too much dirt is added via this parameter, the aerosol physics routine will terminate with an error. This can occur if the corresponding volume of dirt is large compared to the volume of the fireball after the first time step. This can be accommodated by appropriately modifying the dirt entrainment rate for the combustion stage. This problem can also arise if excessive values of *sootmi* are selected.
- The parameters used to specify particle diameters (*sootdp*, *aodp*, and *dirtdp*) are used to determine the appropriate bin number for assignment of the mass associated with these particles. Thus the particle diameter assumes a range of values dictated by the width of the bin.
- The dynamic shape factor (*dshapef*) is used in the agglomeration solution, the particle heat transfer solution (both aerosol and rock), and the fireball emissivity solution.
- The cutoff diameter (*dcutoff*) is used to force a quasi-static heat transfer solution for rock particles with diameters less than this value. In general, a full transient solution should be selected for rock particles.
- The residence time for rock particles (*residnct*) is used to account for the lack of a ballistic trajectory model in the Fireball code. Rock particles are assumed to leave the fireball (thus terminating heat transfer and vaporization calculations) when the residence time is exceeded.
- Multiple aluminum-alloy structures can be specified using the value of *nstruct*, with a maximum-allowed value of 8. All structures are assumed to be composed of 7075 T-6 aluminum alloy. The temperature of a structure is used to determine aluminum vaporization rates and to determine heat loss from the

fireball. Thus large non-aluminum structures that are not expected to vaporize (such as the solid rocket motors), but that may serve as a significant heat sink, can be included in the model. In general, however, heat loss to structures is a tertiary effect for large fireballs.

- The structure residence time (*strrest*) dictates how long heat transfer to aluminum-alloy structures continues. Heat transfer is also terminated at the end of the combustion stage for ground-blast fireballs.
- The convection coefficient (*shtc*) for structure heat transfer can be determined using correlations for forced flow over a flat plate or cylinder. However, the appropriate velocity for a structure fragment careening through a turbulent fireball is not obvious!
- The exposed surface area for a structure depends on whether the structure is assumed to stay intact or to fragment during the blast, in which case both sides of the structure would be exposed.
- The aerosol physics solution start time (*aerostrt*) is intended to allow the user to disable agglomeration for parametric investigations.
- The maximum-allowed value for the number of aerosol bins (*nabins*) is dictated by the Maeros2 subroutine, which sets this maximum at 40. Also, the total number of aerosol and rock particles bins together is limited to 55.
- If the initial mass of PuO_2 for each of the aerosol and rock bins is not supplied via the "massdist.in" file, it is automatically calculated using a Weibull distribution. If *readmass* is set to .false. then, values for *puo2mass*, *rupture*, and *escfrac* must be specified. In this case the mass distribution is determined using

$$F_i = \exp\left[-\left(\frac{d_{i-1}}{c_1 \varepsilon_f d_r}\right)^{c_2}\right] - \exp\left[-\left(\frac{d_i}{c_1 \varepsilon_f d_r}\right)^{c_2}\right] \tag{154}$$

where F_i is the fraction of mass in bin i, d is the particle diameter at a bin boundary (cm), ε_f is the escape fraction (*escfrac*), d_r is the rupture diameter (*rupture*) (cm), and c_1 and c_2 are constants equal to 0.32297 and 0.9976, respectively. The constants were chosen to provide reasonable agreement with experimental data.

The next table provides a description of the input parameters used by the thermodynamic equilibrium solver, which is a subroutine version of the CET89 code. The standard CET input file has been replaced with an easier-to-read and simpler free-format file. Additional parameters particular to fireball simulations were also added and comment lines can now be included. Some of the regular input parameters of CET have been removed and are instead passed to CET from the main Fireball calling subroutine.

Table 8. Input Parameter Description for "cetsub.in"

Parameter	Description and Units	Default
pressure	combustion pressure for a reactant mix (atm)	1.0
trace	combustion products with calculated mole fractions less than *trace* are omitted	1×10^{-7}
deltmix	burn duration for the reactant mix (s)	data
sootfrac	fraction of available gaseous carbon to be added to equilibrium carbon as supplemental soot	1×10^{-6}
moles	number of moles of a reactant	none
h	assigned enthalpy of reactant (J/mol)	none
phz	phase of reactant (S for solid, L for liquid, G for gas)	none
T	temperature of reactant (K)	none
Units	energy unit of assigned enthalpy (J for Joules/mol or C for calories/mol)	none
F/O	reactant type (F for fuel, O for oxidant)	none
REACTANT	keyword indicating the start of a reactant mix	-
PLUS	keyword indicating that the next reactant mix burns concurrently with the previous	-
END	keyword indicating the end of a reactant mix	-
STOP	keyword indicating the end of all mixes	-

Comments:

- Reactants are indicated by entering their chemical composition. For example, N, 2.0, O, 4.0 would be entered to specify N_2O_4. A total of up to 72 reactant mixes and submixes can be included. A mix can consist of up to 7 submixes.
- The combustion pressure (*pressure*) indicates the local pressure at which combustion of the reactants occurs. This differs from the combustion-product pressure (*press*) entered in the "fireball.in" file, which is the global pressure of the fireball.
- The burn duration (*deltmix*) specifies how long the reactants take to combust. Thus the number of reactant moles divided by *deltmix* produces the molar combustion rate. This is used in the fireball physics routines but not by the chemical equilibrium solver. For mixes with more than one concurrently burning submix, the burn duration is the maximum value of *deltmix* for all submixes. If only a single mix is included and the value of *deltmix* is left blank, the default value is calculated from a curve fit of experimental fireball data given by

$$\Delta t_{mix} = 0.20636 m_{mix}^{1/6} \tag{155}$$

where Δt_{mix} is the mix burn duration (*deltmix*) (s), and m_{mix} is the mass of the reactant mix (g). Hydrodynamic simulations may be required to determine the

burn duration for complicated launch-abort scenarios. In such scenarios, burn duration defines the time it takes for fuel and oxidant to come together.

- The value of *sootfrac* is used only in the fireball physics routines to supplement the amount of solid carbon predicted by the equilibrium solver, which is usually zero for typical fireball reactants.
- The parameters *phz*, *T*, and *F/O* are not required to determine the products of combustion for fireball simulations but are included to allow quantities of interest to be determined and printed.

The final table provides a description of the input parameters used by the aerosol physics routine, which is a subroutine version of the Maeros2 code. Much of the regular Maeros2 input has been removed and is instead passed to the Maeros2 subroutine from the main fireball subroutine. The output frequency parameters have been added to accommodate multiple calls of the Maeros2 subroutine.

Table 9. Input Parameter Description for "maeros2s.in"

Parameter	Description and Units	Default
mesgfrq	output frequency for message output file (message results are printed every *mesgfrq calls* to the Maeros2 subroutine)	1
moutfrq	output frequency for Maeros2 text output (*calls*)	1
mpltfrq	output frequency for Maeros2 bar plot output (*calls*)	1
idebug	status report flag: 0 for none, 1 for minimal, 2 for normal, and 3 for maximum	0
iscal	plot scaling flag: –3 for user-defined limits for a log scale, –2 for user-defined limits but will be overridden if beyond range, –1 for automatic log scaling, 0 for no plots, 1 for automatic linear scaling, 2 for user-defined limits but will be overridden if beyond range, 3 for user-defined linear scale	1
ifkplt	component plot flag: 0 for no plot of component mass concentrations, 1 to include individual component mass concentrations along with stacked plots	0
nrow	number of rows used to produce plots, ranging from 13 to 50	none
ncol	number of columns used to produce plots with a maximum of 101	none
qminpl	user-defined minimum concentration for plotting (kg/m^3)	none
qmaxpl	user-defined maximum concentration for plotting (kg/m^3)	none
round	machine unit round-off error	none
rel	relative error tolerance for convergence	none

The following description is excerpted from the "readme.txt" file that accompanies the source code. This description outlines the installation and execution procedures for the Fireball code package along with the generated output files. At the time of this report, the Fireball code package version number is 1.6, dated 3/12/97.

Files required for execution:

fireball.for - The main source code for fireball physics and control.

cetsub.for - The source code for the chemical equilibrium thermodynamic (CET) solver. This NASA code has been modified for use as a subroutine in the Fireball code.

maeros2s.for - The source code for the aerosol physics solver. This is the MAEROS2 code developed at Sandia which has been modified for use as a subroutine in the Fireball code.

fireball.in - The main input file for the Fireball code.

cetsub.in - The input file for the CET subroutine.

thermo.bin - The thermodynamic data used by the CET subroutine. This file is in binary format for use on a DOS-based machine. An ascii-to-binary converter program (asci2bin) is provided to convert the ascii data file (thermo.dat) to binary format on different machines.

transp.bin - The transport property data used by the CET subroutine. This file is in binary format for use on a DOS-based machine. An ascii-to-binary converter program (asci2bin) is provided to convert the ascii data file (transp.dat) to binary format on different machines.

maeros2s.in - The input file for the aerosol physics subroutine.

massdist.in - An optional input file that provides the initial PuO_2 mass distribution.

Supplemental files:

thermo.dat - An ascii file containing thermodynamic data which can be converted to a binary file for other operating systems using the asci2bin code.

transp.dat - An ascii file containing transport data which can be converted to a binary file for other operating systems using the asci2bin code.

asci2bin.for - Compile, link, and execute this program to convert thermo.dat and transp.dat ascii files to thermo.bin and transp.bin binary files, which are required for fireball execution. This is a one-time operation.

makefile - A make file for use with Lahey F77L EM/32 Fortran compiler.

Installation:

Copy all the required files to a directory of choice, such as \fireball. If using the Lahey compiler, just type make at the DOS prompt.

If not using Lahey, some lines must be changed. In subroutine **fbinput** of file "fireball.for," search for "Lahey". The open statement uses

carriage control = 'fortran'

to indicate how to treat carriage control data in the output file. Other compilers have different formats for this purpose. Also, similar lines in subroutine **uopen** of file "cetsub.for" and in file "maeros2s.for" must be modified. Also, the execution time output is based on a call to **timer**, which is a Lahey compiler subroutine; the calls to **timer** should be replaced with the appropriate subroutines if a different compiler is used. Now, compile files "fireball.for", "cetsub.for", and "maeros2s.for" and link their object files to create an executable named "Fireball.exe", or whatever you prefer. Specify the desired input parameters in files "fireball.in", "cetsub.in", and "maeros2s.in", and then execute Fireball.

Output files:

The output is currently written to sixteen text files:

fireball.out - This file contains the supplied input along with a few other calculated parameters based on that input. Also included are messages printed during execution that indicate the current status of the simulation.

fireball.dat - This file contains tab delimited calculated data for import into a spreadsheet or graphics package for plotting. The 17 columns of data are as follows:

1) time (s)
2) timestep (s)
3) fireball temperature (K)
4) fireball surface heat flux (W/cm^2)
5) fireball emissivity
6) molar air fraction (moles of entrained air/total moles in fireball)
7) elevation of fireball center (cm)
8) radius of fireball (cm)
9) fireball rise velocity (cm/s)
10) fireball surface area (cm^2)
11) fireball volume (cm^3)
12) PuO_2 supersaturation ratio [$P(PuO_2)$/P(equilibrium)]
13) PuO_2 vapor mass in the fireball from all particles (g)
14) PuO_2 mass loss from all rock particles (g)
15) total PuO_2 particle mass in all aerosol bins (g)
16) total particle mass (all components) in all aerosol bins (g)

17) fireball energy content (J) determined as the fireball enthalpy times the fireball moles. This number may be negative depending on the datum for enthalpy.

structt.dat - This file contains tab delimited data for the *nstruct* structures immersed in the fireball for import into a spreadsheet or graphics package for plotting.

The *nstruct*+2 columns of data are as follows:

1) - time (s)
2) - total vaporized structure mass (g)
3) - structure # 1 temperature (K)
⋮
nstruct+2) - structure # *nstruct* temperature (K)

apuo2t.dat - This file contains tab delimited temperature data for the aerosol particles immersed in the fireball for import into a spreadsheet or graphics package for plotting.

The *nabins*+1 columns of data are as follows:

1) - time (s)
2) - temperature of aerosol particles in bin # 1 (K)
⋮
nabins+1) - temperature of aerosol particles in bin # *nabins* (K)

rpuo2t.dat - This file contains tab delimited temperature data for the large PuO_2 rock particles immersed in the fireball for import into a spreadsheet or graphics package for plotting. The *nrbins*+1 columns of data are as follows:

1) - time (s)
2) - temperature of rock particles in bin # 1 (K)
⋮
nrbins+1) - temperature of rock particles in bin # *nrbins* (K)

apuo2v.dat - This file contains tab delimited heterogeneous vaporization data for the aerosol particles immersed in the fireball for import into a spreadsheet or graphics package for plotting. A negative value indicates condensation. The *nabins*+1 columns of data are as follows:

1) - time (s)
2) - vaporization rate of aerosol particles in bin # 1 (g/s)
⋮
nabins+1) - vaporization rate of aerosol particles in bin # *nabins* (g/s)

rpuo2v.dat - This file contains tab delimited heterogeneous vaporization data for the large PuO_2 rock particles immersed in the fireball for import into a spreadsheet or graphics package for plotting. A negative value indicates condensation. The *nrbins*+1 columns of data are as follows:

1) - time (s)
2) - vaporization rate of rock particles in bin # 1 (g/s)
⋮
nrbins+1) - vaporization rate of rock particles in bin # *nrbins* (g/s)

apuo2ml.dat - This file contains tab delimited PuO_2 mass loss data for the aerosol particles immersed in the fireball for import into a spreadsheet or graphics package for plotting. A negative value indicates addition of mass via condensation. The *nabins*+1 columns of data are as follows:

1) - time (s)
2) - PuO_2 mass loss from aerosol particles in bin # 1 (g)
⋮
nabins+1) - PuO_2 mass loss from aerosol particles in bin # *nabins* (g)

rpuo2ml.dat - This file contains tab delimited PuO_2 mass loss data for the rock particles immersed in the fireball for import into a spreadsheet or graphics package for plotting. A negative value indicates addition of mass via condensation. The *nrbins*+1 columns of data are as follows:

1) - time (s)
2) - PuO_2 mass loss from rock particles in bin # 1 (g)
⋮
nrbins+1) - PuO_2 mass loss from rock particles in bin # *nrbins* (g)

puo2m.dat - This file contains the mass (g) of PuO_2 for each of the aerosol bins. Both original and condensed PuO_2 are included in this total. Again, the data is tab delimited for import into a spreadsheet or graphics package for plotting. The *nabins*+1 columns of data are as follows:

1) - time (s)
2) - mass of PuO_2 in the aerosol particles in bin # 1 (g)
⋮
nabins+1) - mass of PuO_2 in the aerosol particles in bin # *nabins* (g)

puo2mf.dat - This file contains the mass fraction of PuO_2 for each of the aerosol bins. Mass fraction is defined as the mass of both original and condensed PuO_2 divided by the total mass of all components comprising the particle. Again, the data is tab delimited for import into a spreadsheet or graphics package for plotting. The *nabins*+1 columns of data are as follows:

1) - time (s)
2) - mass fraction of PuO_2 in the aerosol particles in bin # 1
⋮
nabins+1) - mass fraction of PuO_2 in the aerosol particles in bin # *nabins*

apartden.dat - This file contains the average density for the agglomerated particles in each aerosol bin (g/cm^3). Again, the data is tab delimited for import into a spreadsheet or graphics package for plotting. The *nabins*+1 columns of data are as follows:

1) - time (s)
2) - average density of the aerosol particles in bin # 1 (g/cm^3)
⋮
nabins+1) - average density of the aerosol particles in bin # *nabins* (g/cm^3)

cetsub.out - This file contains basic output related to the calculated chemical equilibrium solver (CET), along with any messages related to abnormal execution of the CET subroutine.

maeros2s.out - This file contains the computed output for the aerosol physics subroutine. It contains particle concentrations for each particle component along with additional information concerning agglomeration results. This file can get very large.

maeros2s.plt - This file basically contains the same information as maeros2s.out, but the data is provided in bar chart format.

maeros2s.msg - This file contains a summary of the information passed from Fireball to the aerosol solver.

Sample Results

The results from a hypothetical launch-abort fireball scenario are described here to demonstrate the simulation capabilities of the Fireball code package. This problem was selected for demonstration purposes and should not be considered as definitive, representative, or final. The Fireball code is intended to be executed parametrically to address the large uncertainties associated with the complex phenomena inherent to a launch-abort fireball. The results presented here are for just one simulation and should not be extrapolated or taken out of context.

The scenario selected is for a ground impact of a space vehicle. Thus not all of the rocket propellants are involved. The propellant mixes are based on an unpublished hydrodynamic calculation, which provides the timing information needed to specify combustion rates along with the quantity of entrained air during the combustion stage. The rates are based on the time it takes for the fuel and oxidants to come together during the impact. There are 24 reactant mixes specified in the "cetsub.in" file. Each mix is assumed to combust in a local burn front within the fireball. Submixes burn concurrently and are grouped within dotted lines as presented in the following table.

Table 10. Reactants for Space Vehicle Launch Abort

Mix	Reactants	Quantity (mol)	Burn interval (ms)
1	N_2O_4	312	0.0 – 43.65
	CH_6N_2	300	
2	CH_6N_2	208	
	N_2	2010	
	O_2	468	
3	N_2O_4	1610	43.65 – 86.87
	CH_6N_2	1550	
4	CH_6N_2	771	
	N_2	7460	
	O_2	1730	
5	N_2O_4	2710	86.87 – 130.3
	CH_6N_2	2600	
6	CH_6N_2	1460	
	N_2	14100	
	O_2	3290	
7	N_2O_4	3930	130.3 – 173.77
	CH_6N_2	3770	
8	CH_6N_2	2060	
	N_2	20000	

Mix	Reactants	Quantity (mol)	Burn interval (ms)
	O_2	4650	
9	N_2O_4	4550	173.77 – 217.16
	CH_6N_2	4370	
10	CH_6N_2	16900	
	N_2	15499	
	O_2	3820	
11	N_2O_4	2000	217.16 – 260.6
	CH_6N_2	1930	
12	CH_6N_2	512	
	N_2	4960	
	O_2	1150	
13	N_2O_4	2330	260.6 – 304.29
	CH_6N_2	2240	
14	CH_6N_2	390	
	N_2	3780	
	O_2	880	
15	N_2O_4	1600	304.29 – 347.63
	CH_6N_2	1540	
16	CH_6N_2	459	
	N_2	4450	
	O_2	1030	
17	N_2O_4	723	347.63 – 391.07
	CH_6N_2	695	
18	CH_6N_2	226	
	N_2	2180	
	O_2	508	
19	N_2O_4	394	391.07 – 434.33
	CH_6N_2	379	
20	CH_6N_2	173	
	N_2	1670	
	O_2	390	
21	N_2O_4	5.79	434.33 – 725.32
	CH_6N_2	5.57	
22	CH_6N_2	2.75	
	N_2	26.6	
	O_2	6.19	
23	N_2O_4	34.9	725.32 – 2480.0
	CH_6N_2	33.6	

Mix	Reactants	Quantity (mol)	Burn interval (ms)
24	CH_6N_2	16.6	
	N_2	161	
	O_2	37.5	

The "fireball.out" file provides a summary of the input parameters selected for this scenario. A listing of this file is presented in the following table:

Table 11. Listing of the "fireball.out" file for a Space Vehicle Scenario

```
FIREBALL CODE PACKAGE, Version 1.5

================== FIREBALL INPUT DATA ==================

PROBLEM TITLE:
Space Vehicle Fireball Simulation

INITIAL TIMESTEP:  1.00000E-05
PROBLEM STOP TIME (s):  2.00000E+01
PRINT FREQUENCY (timesteps):  100
MAXIMUM NUMBER OF TIMESTEPS ALLOWED:  10000
MAXIMUM NUMBER OF NEWTON ITERATIONS ALLOWED:  35
DESIRED RELATIVE ERROR FOR NEWTON ITERATIONS:  5.00000E-04
DESIRED TRUNCATION ERROR FOR RKF SOLVER:  3.00000E-02
MAXIMUM-ALLOWED TIMESTEP (s):  1.00000E-02
MINIMUM-ALLOWED TIMESTEP (s):  1.00000E-06

AMBIENT TEMPERATURE (K):   298.00
FIREBALL PRESSURE (atm):    1.000
INITIAL FIREBALL HEIGHT (cm):  0.0000E+00
INITIAL FIREBALL RISE VELOCITY (cm/s):  0.0000E+00
INITIAL SOOT MASS ADDED TO FIREBALL (g):  1.0000E+03

AIR ENTRAINMENT COEFFICIENT 1:  0.0000
AIR ENTRAINMENT COEFFICIENT 2:  0.2500
INITIAL DIRT MASS ADDED TO FIREBALL (g) :  1.0000E+02
DIRT ENTRAINMENT RATE 1 (g/s):  1.0000E+03
DIRT ENTRAINMENT RATE 2 (g/s):  1.0000E+01
DIRT DENSITY (g/cub.cm):  2.0000E+00

SOOT PARTICLE DIAMETER (cm):  2.0000E-04
AI2O3 PARTICLE DIAMETER (cm):  5.0000E-06
DIRT PARTICLE DIAMETER (cm):  5.0000E-03

EMISSIVITY OF PuO2 PARTICLES:  0.50000
EMISSIVITY OF SOOT PARTICLES:  0.90000
EMISSIVITY OF AI2O3 PARTICLES:  0.50000
EMISSIVITY OF DIRT PARTICLES:  0.60000

PuO2 PARTICLE INITIAL TEMPERATURE (K):  1520.00
PuO2 PARTICLE HEAT GENERATION RATE (J/cub.cm-s):     2.65
PuO2 PARTICLE MELT TEMPERATURE (K):  2698.00
```

CRITICAL SUPER SATURATION RATIO: 4.00
PuO2 SURFACE TENSION (J/sq.cm): 5.2500E-05
DELAY TIME FOR INJECTION OF PuO2 PARTICLES INTO THE FIREBALL (s): 0.0000
DYNAMIC SHAPE FACTOR FOR ALL PARTICLES: 1.2000
ROCK CUTOFF DIAMETER FOR QUASI-STEADY HEAT TRANSFER (cm): 1.0000E-03
FIREBALL RESIDENCE TIME FOR PuO2 ROCK PARTICLES (s): 50.0000

NUMBER OF ALUMINUM ALLOY STRUCTURES: 5
STRUCTURE RESIDENCE TIME IN FIREBALL (s): 100.000
STRUCTURE SURFACE EMISSIVITY: 0.600
CONVECTION HEAT TRANSFER COEFFICIENT (J/s-sq.cm-K): 5.00000E-02

#	AREA (sq.cm)	MASS (g)	STRUCTURE NAME
1	3.36260E+05	7.89264E+05	Centaur Attachment
2	5.66850E+06	4.53600E+06	Payload Fairing
3	5.03474E+06	5.94806E+06	Stage 1
4	9.69611E+05	1.33993E+06	Space Vehicle
5	1.62664E+06	3.19425E+06	Stage 2

TOTAL STRUCTURE SURFACE AREA (sq.cm): 1.36358E+07
TOTAL STRUCTURE MASS (g): 1.58075E+07

START TIME FOR AEROSOL PHYSICS SOLUTION: 0.00
TIME INTERVAL FOR AEROSOL UPDATE (s): 5.00000E-01
TEMPERATURE INTERVAL FOR AEROSOL UPDATE (K): 80.00
NUMBER OF BINS FOR AEROSOL PHYSICS: 14
NUMBER OF ROCK BINS FOR HEAT TRANSFER: 7
MINIMUM AEROSOL PARTICLE DIAMETER (cm): 1.0000E-06
MAXIMUM AEROSOL PARTICLE DIAMETER (cm): 1.0000E-02
MAXIMUM ROCK PARTICLE DIAMETER (cm): 1.0000E+00
TOTAL PuO2 MASS THAT ESCAPES (g): 1.0000E+01
RUPTURE SIZE (cm): 1.0000E+00
PARTICLE ESCAPE FACTOR: 1.00000

PARTICLE MASS DISTRIBUTIONS FROM WEIBULL

BIN#	MASS FRACTION	D (cm)	Number	MASS (g)
1	0.000003	1.3895E-06	2.2004E+12	2.9672E-05
2	0.000006	2.6827E-06	5.8937E+11	5.7197E-05
3	0.000011	5.1795E-06	1.5786E+11	1.1025E-04
4	0.000021	1.0000E-05	4.2281E+10	2.1253E-04
5	0.000041	1.9307E-05	1.1325E+10	4.0967E-04
6	0.000079	3.7276E-05	3.0331E+09	7.8965E-04
7	0.000152	7.1969E-05	8.1230E+08	1.5220E-03
8	0.000293	1.3895E-04	2.1752E+08	2.9332E-03
9	0.000565	2.6827E-04	5.8238E+07	5.6518E-03
10	0.001089	5.1795E-04	1.5586E+07	1.0886E-02
11	0.002095	1.0000E-03	4.1680E+06	2.0950E-02
12	0.004026	1.9307E-03	1.1129E+06	4.0261E-02
13	0.007715	3.7276E-03	2.9634E+05	7.7151E-02
14	0.014703	7.1969E-03	7.8471E+04	1.4703E-01
Aerosol bins above/Rock bins below				
15	0.027725	1.3895E-02	2.0560E+04	2.7725E-01
16	0.051226	2.6827E-02	5.2785E+03	5.1226E-01
17	0.091014	5.1795E-02	1.3031E+03	9.1014E-01
18	0.150019	1.0000E-01	2.9845E+02	1.5002E+00
19	0.214355	1.9307E-01	5.9254E+01	2.1435E+00
20	0.234014	3.7276E-01	8.9885E+00	2.3401E+00
21	0.155539	7.1969E-01	8.3012E-01	1.5554E+00

```
 TOTAL AEROSOL PARTICLE MASS FRACTION:  0.0308
 SUM OF ALL MASS FRACTIONS:  0.9547

ASSIGNED BIN NUMBER FOR SOOT:  9
ASSIGNED BIN NUMBER FOR ALUMINUM OXIDE:  3
ASSIGNED BIN NUMBER FOR DIRT:  13

================== SIMULATION RESULTS ==================

LIFTOFF OF INITIAL FIREBALL AT   1.0756 s (COMBUSTION STILL IN PROGRESS)
END OF COMBUSTION STAGE AT   2.4752 s
TOTAL VAPORIZED STRUCTURE MASS:  0.0000E+00 g
TOTAL MASS OF Al2O3 PARTICLES PRODUCED:  0.0000E+00 g
SUPPLEMENTAL SOOT MASS:  1.1123E+03 g
TOTAL SOOT MASS:  1.1123E+03 g
TOTAL DIRT MASS:  2.7377E+03 g
NET VAPORIZED PuO2 MASS:  5.0478E-07 g
TOTAL ENERGY LOST FROM FIREBALL:  3.5946E+09 J
FIREBALL HAS REACHED AMBIENT TEMPERATURE + 20
PROBLEM COMPLETED AT   18.7155 s (  9994 timesteps)
Program Execution Time (s):    129.240
```

In addition to the input parameters, this listing provides the timing sequence for some of the major events occurring in the simulation. The end of the combustion stage occurs at about 2.5 s and the average power radiated from the fireball during the combustion stage is about 1.45 GW. The simulation required 129 s on a 66 MH Pentium computer.

This calculation was performed using version 1.5 of the Fireball code package, dated 10/24/96. This version differs slightly from the latest, version 1.6 dated 3/12/97, as described in this report. The only difference is an error correction in the radiation model used for particles and aluminum structures. The error correction resulted in only a 0.4% change in the amount of plutonium vaporized and no change in the response of the aluminum structures. The minor error in version 1.5 only has an effect on the predicted response if the particle or structure surface emissivity is close to zero. Otherwise, the error is insignificant.

The calculated temperature of the fireball for this sample simulation is provided in Figure 5. The insert on this figure is included to show the temperature response for the first 0.4 s.

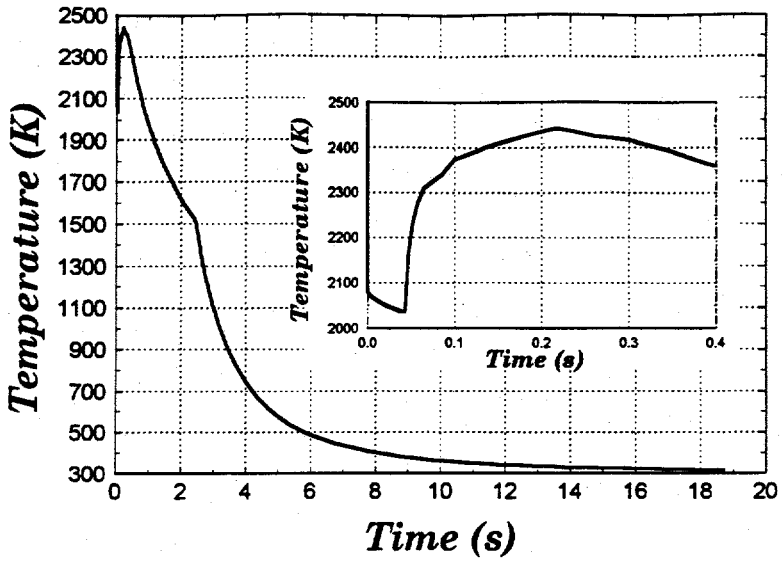

Figure 5. Fireball Temperature – Space Vehicle Scenario

The peak temperature of approximately 2500 K is reached at the end of the first time step (1.0×10^{-5} s). This temperature is essentially the adiabatic flame temperature for the first two concurrently-burning reactant mixes. The fireball cools rapidly at first due to this high temperature and because the surface area-to-volume ratio of the fireball is greatest when the fireball is smallest. (The surface area-to-volume ratio equals $3/r$ for a sphere.) As will be shown later, the emissivity of the fireball is also greatest at the time of fireball inception. As combustion proceeds, the fireball grows rapidly and the rate of energy loss decreases. At just before 0.05 s, new more-energetic reactant mixes are introduced that cause the fireball temperature to increase to a local maximum of 2450 K at about 0.22 s. The temperature then resumes dropping as thermal radiation losses exceed combustion energy input. At the end of the combustion stage (2.4752 s), energy input ceases and rapid air entrainment begins as the fireball lifts from the ground. The fireball cools very rapidly at this time.

Figure 6 shows the fireball emissivity and the entrained-air mole fraction as a function of time. The emissivity equals unity initially because of a "black hole" effect. In this scenario, plutonium, soot, and dirt particles are injected into the initially very small fireball. Thus the concentration of particles is very high, resulting in a high emissivity. As the fireball grows, the concentration decreases and the emissivity decreases to a local minimum of about 0.44. Dirt and soot injection continue along with the production of CO_2 and water vapor, which are the major contributors to gas emissivity. The emissivity rises again to a new maximum of about 0.72 and then decreases again as the fireball grows and cools. The air mole fraction shows that after lifting from the ground, the fireball rapidly entrains air. This curve does not include air added as a reactant and combusted. Thus the mole fraction is shown as zero during the combustion stage.

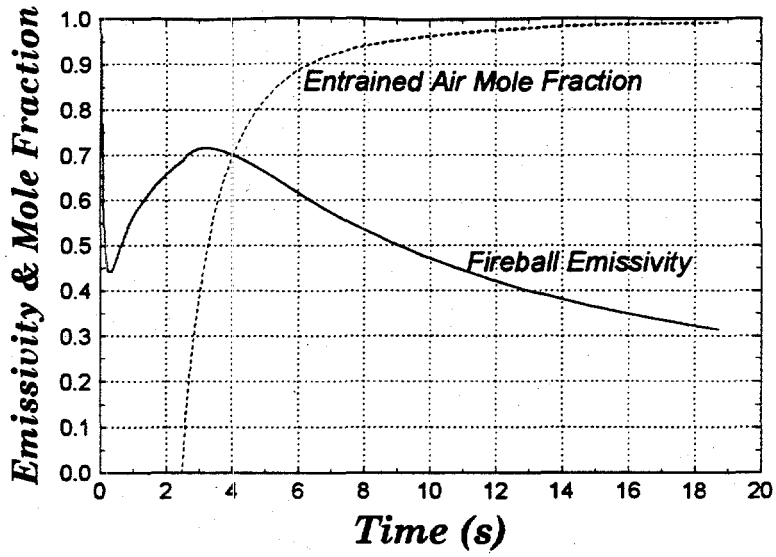

Figure 6. Fireball Emissivity and Entrained-Air Mole Fraction

The emissivity of the fireball is used in three ways: (1) to determine energy loss from the fireball, (2) to determine heat transfer between the aluminum-alloy structures and the fireball, and (3) to determine heat transfer between plutonium-bearing particles and the fireball. Plutonium vaporization is strongly dependent on the fireball emissivity. A higher fireball emissivity increases the rate of heat transfer to particles. But, because the fireball cools faster, less time is available for heat transfer. Particles also exchange heat with the ambient environment if the fireball emissivity is less than unity. Thus particles in a hot fireball may actually cool if the emissivity of the fireball is sufficiently low. A fireball model that simply specifies the fireball emissivity would not capture this coupled nonlinear phenomena.

Figure 7 shows the fireball radius and its elevation. The changing radius reflects the complicated combined influences of combustion-product gas generation, cooling, and air entrainment. Product gas generation increases the fireball radius, while radiative and convective cooling decrease the radius. The entrainment of air adds mass (increasing the radius) but also cools the fireball (decreasing the radius). The rate of growth and the rise velocity are greatest initially. The radius reaches a local minimum just before the end of the combustion stage and then increases as air entrainment ensues.

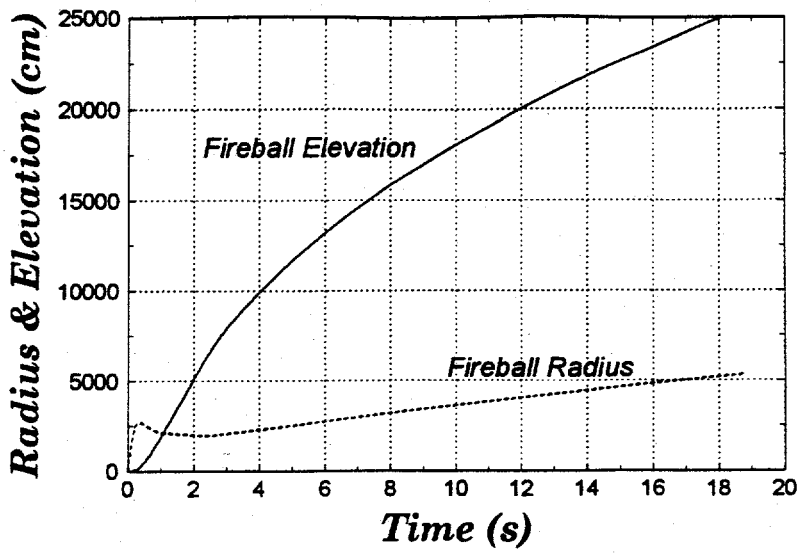

Figure 7. Fireball Radius and Elevation

The temperature of the aluminum-alloy structures is presented in Figure 8. For this relatively low-temperature short-duration scenario, none of the structures reach the melt temperature and there is no aluminum vapor production.

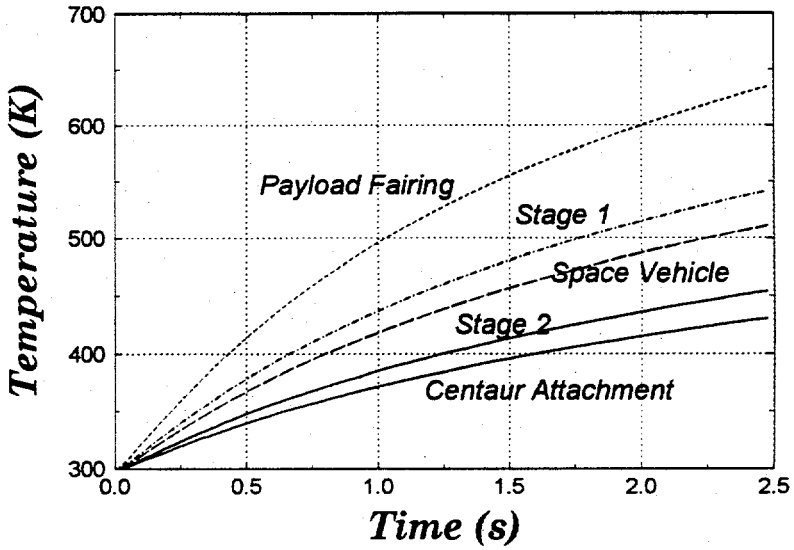

Figure 8. Aluminum-Alloy Structure Temperatures

Figure 9 shows the temperature response of the rock particles and the largest aerosol particle. The temperatures of the smaller aerosol particles are not shown to avoid clutter. However, the temperature trace for each successively-smaller particle moves closer to the fireball temperature trace. The initial particle temperature in the GPHS is assumed to be 1520 K. As expected, most of the rock particles do not increase significantly in temperature because of their relatively large heat capacity. In this scenario (and in most others), they contribute essentially no plutonium vapor to the fireball.

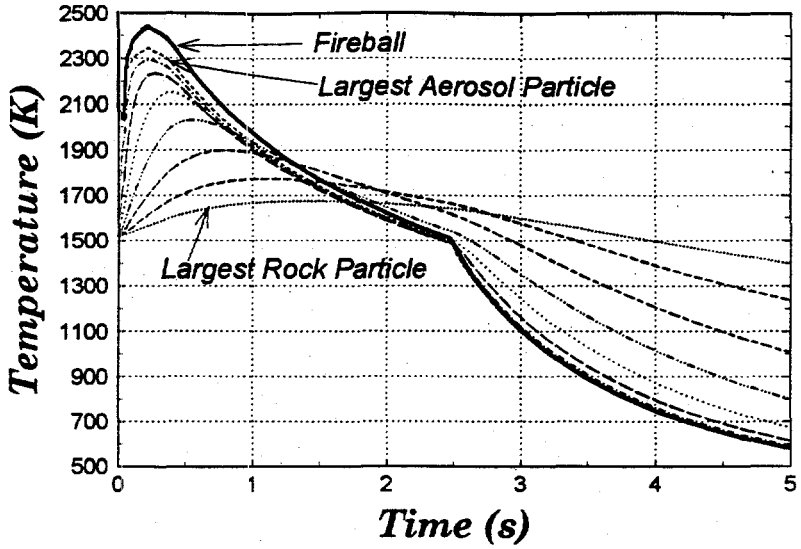

Figure 9. Particle Temperature Response

The plutonium vapor mass in the fireball is shown in Figure 10. The vapor mass levels (becomes constant) at about 0.8 s as vaporization and heterogeneous condensation equilibrate. By 1 s, vaporization is essentially over as a small amount of heterogeneous condensation onto the larger particles continues. At around 1.6 s, the fireball temperature has dropped sufficiently to initiate homogeneous condensation. All of the plutonium vapor is condensed by 2.5 s. Because not all of the rocket propellants are involved, this space-vehicle ground-impact scenario is rather benign. Thus the fireball temperature is relatively low and burn duration is relatively short, resulting in not much plutonium vaporization.

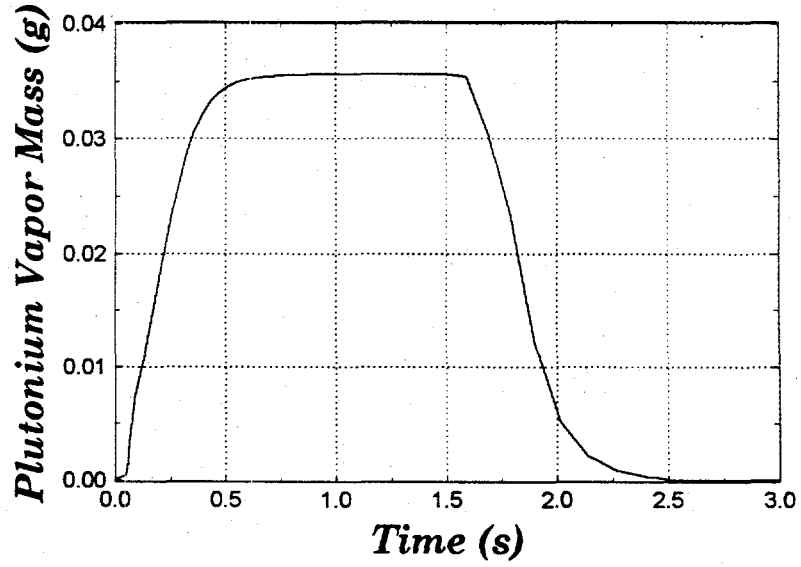

Figure 10. Plutonium Vapor Mass in the Fireball

The initial and final plutonium particle mass distributions are provided in the next two figures (linear scale for Figure 11 and logarithmic scale for Figure 12), for the 14 aerosol bins selected for this simulation. The higher the bin number (corresponding to larger particles), the smaller the amount of mass lost. The net mass lost is indicated by the difference between the initial and final masses. Thus bin 10 mass is reduced more from vaporization than bin 11, and so forth. An exception occurs in bin 9, which is the bin to which soot from combustion is added. There are two effects attributable to the presence of soot. First, the emissivity (and hence heat transfer) of the agglomerated particles in this bin is increased relative to plutonium-only particles. Thus more vaporization occurs initially from this bin than would if soot were not present. Second, the soot particles serve as heterogeneous condensation sites. Thus as the fireball cools, a larger share of condensation occurs in this bin than would otherwise. Similar effects occur in bin 13 to which entrained dirt is added. However, the effects are not as significant for the large particles in this bin because they don't increase in temperature as much and because they offer much less surface area for heterogeneous condensation.

The particles in bins 7 and 8 do not completely vaporize; however, they decrease in size sufficiently that their remaining mass is moved into bin 6. This accounts for the mass remaining in this bin at the end of the simulation. Essentially all of the mass in bins 1 through 5 is vaporized early in the fireball simulation. Homogeneous condensation produces very small particles that are then introduced into bin 1. Thus much of the plutonium vapor has been transported down into the smallest-sized particles by homogeneous condensation. Agglomeration then moves some of this mass up to bin 2. However, because the fireball cools relatively fast in this scenario, insufficient time is available for significant agglomeration.

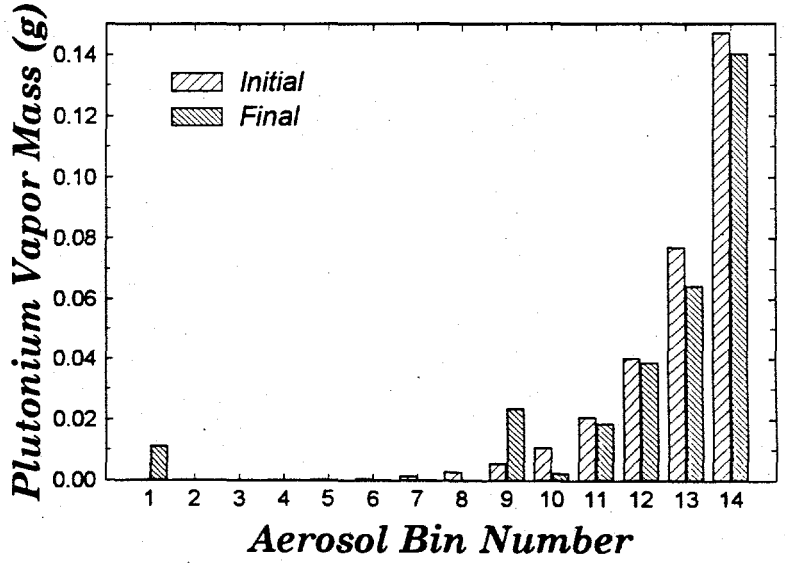

Figure 11. Plutonium Mass Distribution (Linear Scale)

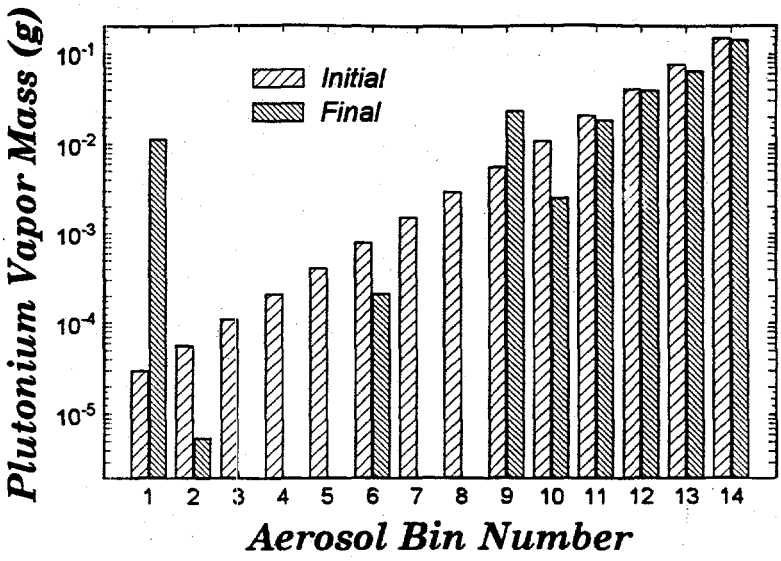

Figure 12. Plutonium Mass Distribution (Logarithmic Scale)

The mass distribution plots demonstrate the complicated nature of particle response in a fireball environment and highlight the need for an integrated treatment of the various processes occurring.

Several other scenarios were investigated, including those that produced hotter and longer-duration fireballs. In general, the results shared many of the same traits as demonstrated for the space vehicle scenario and are briefly mentioned here.

Plutonium vaporization occurs mostly during the first second of the fireball, when temperatures are highest. Particles less than about 5 μm in diameter usually completely vaporize while the larger rock particles vaporize a negligible amount. Vaporization and condensation (both homogeneous and heterogeneous) occur simultaneously depending on the fireball and particle temperatures. Most of the vaporized plutonium mass homogeneously condenses to form very small particles. Some of the vaporized mass condenses heterogeneously onto other available particles, such as soot, dirt, and aluminum oxide. The extent to which heterogeneous condensation precludes homogeneous condensation depends strongly on the size and quantity of available particles, such as soot and dirt. Agglomeration produces larger particles; however, this process does not continue very long because the fireball is rapidly cooling and growing due to air entrainment.

An abbreviated parametric study indicates that the particle size distribution results are most sensitive to combustion pressure, dynamic shape factor, dirt and soot particle size, and air entrainment coefficients. These general results are not based on extensive analyses and should not be considered final; however, they do provide a good starting point for additional investigations.

Summary, Comments and Recommendations

The Fireball code package simulates the integrated response of plutonium debris exposed to a hypothetical launch-abort fireball. The code includes coupled models for fireball physics and chemistry, thermodynamics, aerosol physics, particle heat transfer, structure heat transfer, plutonium vaporization and condensation (both homogeneous and heterogeneous), aluminum vaporization and combustion, soot generation, and dirt entrainment. This fast-running code provides many input options to support risk assessment studies, and represents a significant improvement over previous models.

The Fireball code includes several simplifying assumptions and approximations. This was necessitated by the very limited time available for development and the requirement for fast execution speed to support parametric investigations. Several comments and recommendations are offered regarding its development to provide guidance on code evaluation and continued development efforts.

As described in the appropriate sections, the CET89 and Maeros2 codes were employed to perform the chemical equilibrium thermodynamic and aerosol physics calculations, respectively. These codes were converted to callable subroutines and integrated with the remaining fireball models. The decision to use these codes was based primarily on the limited time available for development. The general acceptance of these codes in the technical community, along with significant validation of both also entered into the decision. Drawbacks to the use of these codes include the additional computational overhead associated with the many features not required for fireball simulations, and the use of coding methods not consistent with modern coding practice.

CET was originally developed in 1967 using Fortran, with many modifications made since. The Fortran language in 1967 was very limited, resulting in difficult-to-follow code by today's standards. The replacement of the CET subroutine with a fireball-specific code module would greatly increase the efficiency and maintainability of the Fireball code.

Another improvement would be to replace the equilibrium thermodynamics combustion model with a kinetic rate-dependent model. For most fireball scenarios of interest, the time it takes for fuel and oxidant to come together is much longer than the time required for the chemical reaction to proceed because of the high temperatures involved. However, certain scenarios may require inclusion of the kinetic rate dependencies in addition.

Maeros2 was developed in the early 1970s and also contains much difficult-to-follow code. It would also be desirable to replace this subroutine with a new aerosol physics model, perhaps using a finite element approach to more efficiently handle the section coefficient integrals. Including plutonium vaporization and

condensation models directly into the aerosol physics model should also be considered. As mentioned in the Aerosol Physics Section, only a single particle density is employed for all aerosol bins. The numerical approach in Maeros2 is not amenable to accommodating average densities for each bin, further supporting the need for an alternative aerosol physics model. There are numerous other advantages and reasons for creating a new fireball-specific aerosol physics model. However, the initial sensitivity studies mentioned in this report indicate that agglomeration is not a major influence on the evolution of plutonium-bearing particle distributions. Thus a new model may not be warranted. However, a definitive decision would require a systematic and thorough study.

A considerable amount of time was spent validating the CET subroutine, as used in the Fireball code. The Maeros2 subroutine was also checked for proper execution within the Fireball code package. However, a more exhaustive testing of this subroutine would be desirable.

The strategy for managing the movement of particles between bins as a result of vaporization and condensation can modify the final particle distribution results. Only a single strategy was implemented in the Fireball code. It would be desirable to investigate other strategies for managing particle bin changes.

The fireball physics model can be improved in a number of ways. First, the geometry of the fireball can be modified to account for a stem using a two-control-volume model. However, the available fireball-modeling literature from the petroleum industry indicates that the improvement in temperature prediction is not large. A still-more complicated approach would be to implement a multiple-volume fireball model. This would allow zones of different temperature and particle concentrations. Work is currently in progress in the nuclear safety community to develop multiple-volume aerosol physics models that could support this improvement. However, it does not appear that this would be worthwhile considering the complexities involved in a highly turbulent fireball. Again, more thorough sensitivity studies should be performed to further explore this.

A useful improvement to the fireball physics model would be the addition of wavelength dependencies for the thermal radiation heat transfer calculations involving the fireball, particles, and structures. This is warranted by the fact that absorption of radiation in many combustion gases and gas mixtures is strongly wavelength dependent. This spectral dependency can be addressed with a "band" radiation heat transfer model and would require the introduction of a model to calculate gas mixture absorption coefficients as a function of temperature, pressure, and constituent partial pressures. The effects of suspended particles could also be incorporated with the use of Mie scattering models. Gas mixture absorption coefficient and particle scattering models are readily available;[30] however, implementation into the Fireball code framework would be required.

The plutonium vaporization model can be improved by the inclusion of the effects of chlorides, carbides, and nitrides on the plutonium vapor pressure. Also, the inclusion of vapor phase hydrates should be considered. Sensitivity studies should address the importance of these modifications. The plutonium homogeneous condensation model can also be improved. Currently, rate effects are ignored. Models are available to include rate effects and such a model could easily be incorporated into the Fireball code package. As mentioned in the Homogeneous Condensation Section, a model more sophisticated than that in the Fireball code does not make a significant difference based on experience with several reactor safety codes. Implementation of a rate dependent model into the Fireball code is probably warranted, however, because the fireball environment is different from a reactor containment and because such a model would be relatively easy to include.

Currently, particles of soot, dirt, and aluminum oxide are assigned a single diameter value by the user. Thus all particles of a certain type have the same diameter. It would be desirable to instead allow a distribution of sizes to be specified for each particle type. Thus any particles added during the simulation would be assigned to the appropriate bin based on this distribution. It would also be desirable to include an additional particle component to account for the possible presence of solid propellant rocket exhaust particles.

In the current Fireball code version, a single user-specified shape factor is used for all particle bins to account for non-spherical particle shapes. This factor directly affects agglomeration, particle heat transfer, and fireball emissivity. A desired improvement would be to allow different shape factors to be specified for each bin and for each of the modeled processes.

As with any computer code, there are numerous minor improvements that can be implemented to improve efficiency, maintainability, robustness, and ease-of-use. Results post-processing capabilities would also be desirable. Although much effort was expended in ensuring that all submodels work properly as implemented, individual submodels and their integration into the entire package should be further explored for a variety of fireball scenarios. Detailed parametric investigations using the Fireball code package, for a wide variety of fireball scenarios, can provide a wealth of information concerning fireball simulations and provide invaluable guidance for future development work.

The Fireball code represents a considerable improvement over models used previously for launch-abort analysis. The many physical and chemical processes occurring in a fireball are integrated to allow the simulation of the entire fireball scenario with a single code. Integration of the various process models also captures the complex interdependencies inherent to such nonlinear phenomena. The code also offers numerous input parameters that allow the user to simulate a variety of launch-abort scenarios. This flexibility facilitates parametric investigations,

providing a valuable tool for advancing our understanding of plutonium-bearing particle behavior in a fireball environment.

References

1. Bonnie McBride, *CET89 – Chemical Equilibrium with Transport Properties, 1989*, Lewis Research Center, COSMIC Program # LEW-15113, 1989.
2. Sanford Gordon and Bonnie J. McBride, *Computer Program for Calculation of Complex Chemical Equilibrium Compositions, Rocket Performance, Incident and Reflected Shocks, and Chapman-Jouguet Detonations*, NASA Lewis Research Center, COSMIC Program # LEW-15113, NASA SP-273, March 1976.
3. Fred Gelbard, *Maeros Users Manual*, NUREG/CR-139, SAND80-822.
4. Frank M. White, *Fluid Mechanics*, Second Edition, McGraw-Hill Book Company, 1986.
5. H. C. Hottel and F. P. Broughton, *Ind. Eng. Chem.*, 4 (1932) 166.
6. Robert Siegel and John R. Howell, *Thermal Radiation Heat Transfer*, Second Edition, Hemisphere Publishing Corporation, 1981.
7. Steven C. Chapra and Raymond P. Canale, *Numerical Methods for Engineers*, Second Edition, McGraw-Hill Book Company, 1988.
8. Robert C. Reid, John M. Prausnitz, Bruce E. Poling, *The Properties of Gases & Liquids*, Fourth Edition, McGraw-Hill Book Company, 1987.
9. J. S. Turner, *Buoyancy Effects in Fluids*, Cambridge University Press, 1973.
10. F. Gelbard and J. W. Seinfeld, *J. Colloid and Interface Science*, 78 (1980) 485.
11. Frank P. Incropera, David P. DeWitt, *Introduction to Heat Transfer*, John Wiley & Sons, 1985.
12. William C. Hinds, *Aerosol Technology – Properties, Behavior, and Measurement of Airborne Particles*, John Wiley & Sons, 1982.
13. D. K. Green, J.K. Fink, and L. Leibowitz, "Vapor Pressures and Vapor Compositions in Equilibrium with Hypo-stoichiometric Plutonium Dioxide at High Temperatures," ANL-CEN-RSD-82-1, Argonne National Laboratory, Argonne, IL, June, 1982.
14. P.E. Blackburn, *J. Nuclear Materials*, 46 (1973) 119.
15. D. C. Williams, "Vaporization of Radioisotope Fuels in Launch Vehicles," SC-RR-71 0118, Sandia National Laboratories, Albuquerque, NM, December 1971.
16. R. J. Ackermann, R.L. Faircloth and M.H. Rand, *J. Phys. Chem.* 70 (1964) 3698.
17. A. Sheth and L. Leibowitrz, "Equation of State and Transport Properties of Uranium and Plutonium Nitrides in the Liquid Region", ANL-AFP-12, Argonne National Laboratory, Argonne, IL, 1975.
18. O. H. Krikorian, *High Temperature-High Pressures*, 14 (1982) 387.

19. D. Pavone, "GPHS Safety Tests Particle Size Data Package", LACP-86-62, Los Alamos National Laboratory, Los Alamos, NM, May 1986.

20. S. Zwick, *J. Applied Physics*, 31 (1960) 1735.

21. R. Kucherov and L. Rikenglanz, "Doklady Akad Nauk SSR", 133 (1960) 1130.

22. M. Kulmala and T. Vesala, *J. Aerosol Science*, 22 (1991) 337.

23. Heames, T. J. et. al, "VICTORIA: A Mechanistic Model of Radionuclide Behavior in the Reactor Coolant System Under Severe Accident Conditions," NUREG/CR-5545, SAND90-0756, Rev. 1, Sandia National Laboratories, Albuquerque, NM, Dec. 1992.

24. Murata, K. K., et. al, "CONTAIN 1.2 Code Manual: A Computer Code for Severe Accident Analysis," Sandia National Laboratories report SAND94-2358.

25. D. R. Stull and H. Prophet, *JANAF Thermochemical Tables*, Second Edition, NSRDS-NBS 37, National Bureau of Standards, Washington, DC, June 1971.

26. E. T. Turkdogan, P. Grieveson, and L. J. Darken, *J. Phys. Chem.*, 67 (1963) 1647.

27. B. S. Haynes and H. Gg. Wagner, *Soot Formation*, Prog. Energy Combust. Sci. Vol. 7. pp. 229-273, Pergamon Press Ltd., 1981.

28. Walton, W. D., "In Situ Burning of Oil Spills: Mesoscale Experiments," NISTIR 6266 Building and Fire Research Laboratory, National Institute of Standards and Technology, US Department of Commerce, Technology Administration, Gaithersburg, Maryland, November, 1993.

29. R. J. Lipinski, et. al., "Uncertainty in Radionuclide Release Under Specific LWR Accident Conditions," Volume II, TMLB' Analyses, Sandia National Laboratories, SAND84-0410, February 1985.

30. Weiming Li, Timothy W. Tong, Dean Dobranich, and Louis A. Gritzo, *A combined narrow- and wide-band model for computing the spectral absorption coefficient of CO_2, CO, H_2O, CH_4, C_2H_2, and NO*, Journal of Quantitative Spectroscopy & Radiative Transfer, Volume 54, Number 6, December 1995.

Bibliography

The following citations provide a comprehensive compendium of relevant technical literature. The citations in this bibliography, along with the references, served as the basis for much of the fireball modeling presented in this report, and as such serve as a resource for future development efforts. The citations are grouped according to the major topic of reference.

Thermodynamics of Plutonium Vaporization

1. D. R. Stull and H. Prophet, JANAF Thermochemical Tables, Second Edition, NSRDS-NBS37, National Bureau of Standards, Washington, D.C., 1971.
2. M. W. Chase et al., *J. Phys. Chem. Ref. Data*, 3 (1974) 311.
3. M. W. Chase et al., *J. Phys. Chem. Ref. Data*, 4 (1975) 1.
4. M. W. Chase et al., J. *Phys. Chem. Ref. Data*, 11 (1982) 695.
5. B. E. Bader, A. B. Donaldson, and H.C. Hardee, *J. Spacecraft*, 8 (1971) 1216.
6. H. A. Wriedt, *Bulletin of Alloy Phase Diagrams*, 11 (1990) 184.
7. B. Riley, Sci. Ceram., 5 (1970) 83.
8. T. D. Chikalla, C. E. McNeilly, and R.E. Skavdahl, *J. Nucl. Mater.*, 12 (1964) 131.
9. E. A. Aitkin and S. K. Evans, *A Thermodynamic Data Program Involving Plutonium and Urania at High Temperatures*, GEAP-5672, General Electric Corp., Vallecitos, CA, 1968.
10. W. L. Lyon and W. E. Baily, *J. Nuclear Mater.*, 22 (1967) 332.
11. T. M. Bessman and T. B. Lindemer, *J. Nucl. Mater.*, 130 (1985) 489.
12. A. Nakamura, *J. Nuclear Mater*, 201 (1993) 17.
13. M. V. Krishnaiah and P. Sriramamurti, *J. American Ceramic Society*, 67 (1984) 568.
14. P. E. Blackburn and C. E. Johnson, "Chemical Modelling of Uranium, Plutonium, and Oxygen Redistribution in Oxide Fuels by Vapour Transport and Diffusion," *Thermodynamics of Nuclear Materials*, 1974, p. 17, volume 1, International Atomic Energy Agency, Vienna, Austria, 1975.
15. T. M. Bessman, *J. Nuclear Mater.*, 144 (1987) 141.
16. D. K. Green, J. K. Fink, and L. Leibowitz, *Vapor Pressures and Vapor Compositions in Equilibrium with Hypostoichiometric Plutonium Dioxide at High Temperatures*, ANL-CEN-RSD-82-1, Argonne National Laboratory, Argonne, IL, June 1982.

17. M. Tetanbaum, "Thermodynamic Aspects of the Plutonium-Oxygen System," paper 8, p. 109 in *Plutonium Chemistry*, W. T. Carnall and G. R. Choppin, editors, ACS Symposium Series 216, American Chemical Society, Washington, D.C., 1983.

18. G. C. Swanson, *Oxygen Potential of Uranium-Plutonium Oxides as Determined by Controlled Atmosphere Thermogravimetry*, LA-6083-T, Los Alamos Scientific Laboratory, Los Alamos, NM, October 1975.

19. Panel on Thermodynamics of Plutonium Oxides, *The Plutonium-Oxygen and Uranium Plutonium-Oxygen Systems: A Thermochemical Assessment*, Technical Reports Series No. 79, International Atomic Energy Agency, Vienna, Austria, 1967.

Kinetics of Plutonium Dioxide Vaporization

1. R. L. Steinberger and R. E. Treybal, *AIChE J.*, 6 (1960) 227.
2. L. A. Baker, *Canadian Met. Quarterly*, 7 (1968) 217.
3. S. Zwick, *J. Appl. Phys.*, 31 (1960) 1735.
4. R. Kucherov and L. Rikenglanz, *Doklady Akad. Nauk* SSR, 133 (1960) 1130.
5. M. Kulmala and T. Vesala, *J. Aerosol Sci.*, 22 (1991) 337.
6. D. Pavone, *GPHS Safety Tests Particle Size Data Package*, LACP-86-62, Los Alamos National Laboratory, Los Alamos, NM, May 1986.
7. D. C. Williams, *Vaporization of Radioisotope Fuels in Launch Vehicle Abort Fires*, SC-RR-71 0118, Sandia Laboratories, Albuquerque, NM, December 1971.
8. J. O. Hirschfelder, C. F. Curtiss, and R.B. Bird, *Molecular Theory of Gases and Liquids*, John Wiley and Sons, 1954.
9. P. D. Neufeld, A .R. Janzen, and R. A. Aziz, *J. Chem. Phys.*, 57 (1972) 1100.
10. O. H. Krikorian et. al., "Evaluation of Actinide Volatilities in Mixed Waste Processors: Interim Report," UCRL-ID-111352, Lawrence Livermore Laboratory, Livermore, CA, August 1992.

Fireball Description

1. B. E. Bader, A. B. Donaldson, and H. C. Hardee, "Liquid-Propellant Rocket Abort Fire Model," *J. Spacecraft*, 8 (1971) 1216.
2. B. A. Boughton and J. M. DeLaurentis, *Description and Validation of ERAD: An Atmospheric Dispersion Model for High Explosive Detonations*, SAND92-2069, Sandia National Laboratories, Albuquerque, NM, October 1992.
3. J. B. Gayle and J. W. Bransford, *Size and Duration of Fireballs from Propellant Explosions*, NASA TM X-53314, George C. Marshall Space Flight Center, Huntsville, AL, August 1965.
4. A. B. Willoughby, C. Wilton, and J. Mansfield, *Liquid Propellant Explosive Hazards, Volume 3, Prediction Methods*, NTIS AD 855 087, URS Research Co., Burlingame, CA, December 1968.
5. H. Lamb, *Hydrodynamics*, 6th Edition, Dover, 1945.
6. J. S. Turner, *Buoyancy Effects in Fluids*, Cambridge University Press, 1973.
7. B. R. Morton, G. Taylor, and J. S. Turner, *Proceedings of the Royal Society* (London), A234 (1956) 1.
8. R. T. Haslam and H.C. Hottel, *Trans. ASME* 50 (1928) 9.

Condensation

1. S.K. Loyalka, *Progress in Nuclear Energy*, 12 (1983) 1.
2. S. K. Dua, P.Brand, E. Karg, and J. Heyder, *Aerosol Science and Technology*, 21 (1994) 170.
3. S. C. Saxena and R. K. Joshi, *Thermal Accommodation and Adsorption Coefficients*, Hemisphere Publishing Co., 1981.
4. M. M. R.Williams and S. K. Loyalka, *Aerosol Science Theory and Practice*, Pergamon Press, 1991.
5. S. K. Loyalka, *Physica*, A163 (1990) 813.

Aluminum Vaporization

1. A. B. Willoughby, C. Wilton, and J. Mansfield, *Liquid Propellant Explosion Hazards, Volume 3, Prediction Methods*, URS 652-35, AFRPL-TR-68-92, URS Research Co., Burlingame, CA, December 1968.
2. E. T. Turkdogan, P. Grieveson, and L. J. Darken, *J. Phys. Chem.*, 67 (1963) 1647.
3. *Heat Transfer Data Book*, Genium Publishing Co., Schnectady, NY, 1984.
4. Y. S. Touloukian and R. W. Powell, C. Y. Ho, and P. G. Klemens, *Thermophysical Properties of Matter, Volume 1, Thermal Conductivity Metallic Elements and Alloys*, IFI Plenum, 1970.
5. Y. S. Touloukian and D. P. DeWitt, *Thermophysical Properties of Matter, Volume 7, Thermal Radiative Properties of Metallic Elements and Alloys*, IFI Plenum, 1970.
6. J. Szekely and N. J. Themelis, *Rate Phenomena in Process Metallurgy*, Wiley-Interscience, 1971.
7. S. Zwick, *J. Appl. Phys.*, 31 (1960) 1735.
8. R. Kuchrov and L.Rikenglaz, *Doklady Akad. Nauk SSR*, 133 (1960) 1130.
9. J. P Hirth and G. M. Pound, *Condensation and Evaporation -- Nucleation and Growth Kinetics*, Pergamon Press, 1963.
10. C. R. Wilke and C. Y. Lee, *Industrial and Engineering Chemistry*, 47 (1955) 1253.
11. A. L. Hines and R. N. Maddox, *Mass Transfer Fundamentals and Applications*, Prentice Hall, Inc., 1985.
12. R. C. Reid, J. M. Prousnitz, and B. E. Poling, *The Properties of Gases and Liquids*, Fourth Edition, McGraw-Hill Book Co., 1987.
13. R. W. Hermsen and R. Dunlap, *Combustion and Flame*, 13 (1963) 253.
14. R. Becker and W. Doering, *Anu. Phys.* (Leipzig). 24 (1935) 719.
15. J. Loethe and G. M. Pound, *J. Chem. Phys.*, 36 (1962) 2080.
16. J. Feder, K. C. Russel, J. Loethe, and G. M. Pound, *Adv. Phys.*, 15 (1966) 111.
17. H. Reiss, J. I. Katz, and E. R. Cohen, *J. Chem. Phys.*, 48 (1968) 5553.
18. H. Reiss, *J. Statistical Physics*, 2 (1970) 83.
19. D. A. Powers, J. E. Brockmann, and A. W. Shiver, *VANESA: A Mechanistic Model of Radionuclide Release and Aerosol Generation During Core Debris Interactions with Concrete*, NUREG/CR-4308, SAND 85-1370, Sandia National Laboratories, Albuquerque, NM, July 1986.

20. A Chatterjae, M. Kerker, and D. D. Cooke, *J. Colloid and Interfacial Science*, 53 (1975) 71.

21. M. B. Ranade, D. T. Wasan, and R. Davies, *AIChE J.*, 20 (1974) 273.

22. R. J. Ollerenshaw, *Fundamental Processes Involved in the Formation of Metallurgical Fume*, Warren Spring Laboratory, Sterenage, Hertfordshire, United Kingdom, 1978.

23. G. A. Nicholson and M. Kerker, "Brownian Coagulation of Aerosols at Low Knudsen Number, "*Faraday Symposium of the Chemical Society*, No. 7, *Fogs and Smokes*, (1974) pp. 133-144.

24. T. E. Ramabharan, T. W. Peterson, J. H. Seinfeld, *AIChE J*, 22 (1976) 840.

25. E. R. Buckle, *J. Microscopy*, 114, Pt. 2 (1978) 205.

26. C. G. Granqvist and R.A. Buhram, *Solid State Communications* 18 (1976) 123.

27. J. D. Holmgren, J. O. Gibson, and C. Sheer, *J. Electrochemical Society* ,111 (1964) 362.

Entrainment of Particles

1. A. Alonso, R. Bolado, and E. Hontanon, *Aerosol Resuspension in the Reactor Cooling System of LWR's Under Severe Accident Conditions*, EUR-13789 EN, Joint Research Centre, Ispara, Italy, July 1991.
2. M. Corn, "Adhesion of Particles," Chapter 11.
3. G. A.Sehmel, *Environmental International*, 4 (1980) 107.
4. P. Belly, *Sand Movement* by Wind, AD 429785 (1964).
5. M. Corn and F. Stein, *Amer. Ind. Hygiene* Assoc. J., 26 (1965) 325.
6. R. A. Bagnold, *Intl. J. Air Pollution*, 2 (1960) 357.
7. D. Hall, *J. Fluid Mechanics*, 187 (1988) 451.
8. P. G. Saffman, *J. Fluid Mechanics*, 22 (1965) 385.
9. K. L. Johnson, K. Kendall, and A. D. Roberts, *Proc. Royal Society (London)*, A324 (1971) 301.
10. A Frometin, *Particle Resuspension from a Multi-Layer Deposit by Turbulent Flow*, PSI-Bericht, Nr. 38, September 1989.
11. M. W. Reeks, J. Reed, and D. Hall, *J. Phys. D applied Physics*, 21 (1988) 574.
12. F. P. Ricou and D. B. Spalding, J. *Fluid Mechanics*, 11 (1961) 21.
13. M. C. Kordecki and C. Orr, *Arch. Env. Health*, 1 (1960) 1.
14. M. Corn and F. Stein, *Amer. Ind. Hyg. Assoc. Journal*, 26 (1965) 325.
15. R. J. Garde, *Turbulent Flow*, John Wiley and Sons, 1994.
16. H. Y. Wen and G. Kasper, *J. Aerosol Science*, 20 (1989) 483.
17. D. A. Braeten, K. T. Paus, and R. H. Shaw, *J. Aerosol Science*, 21 (1990) 613.
18. J. Wu, *J. Fluid Mechanics*, 34 (1968) 91.

Aerosol Behavior in a Fireball

1. F. Gelbard and J. W. Seinfeld, *J. Colloid and Interface Science*, 78 (1980) 485.
2. K. E. Washington et al., *Reference Manual for the CONTAIN 1.1 Code for Containment Severe Accident Analysis*, NUREG/CR-5715, SAND 91-0835, Sandia National Laboratories, Albuquerque, NM, July 1991.
3. N. A. Johns, *The Evaluation of the MAEROS Section Coefficients*, PWR/SAMAS/P(87) 57, AEE Winfrith, October 1987.
4. J. D. Klett and M. H. Davis, *J. Atmospheric Science*, 30 (1973) 107.
5. M. M. R. Williams and S. K. Loyalka, *Aerosol Science Theory and Practice*, Pergamon Press, 1991.
6. D. A. Powers, K. E. Washington, S. B. Burson, and J. L. Sprung, *A Simplified Model of Aerosol Removal by Natural Processes in Reactor Containments*, NUREG/CR-6189, SAND94-0417, Sandia National Laboratories, Albuquerque, NM.
7. H. R. Pruppacher and J. D. Klett, *Microphysics of Clouds and Precipitation*, Reidel, 1978.
8. N. A. Fuchs, *The Mechanics of Aerosols*, Pergamon, 1964.
9. P. G. Saffman and J. S. Turner, *J. Fluid Mechanics*, 1 (1956) 16.
10. M. M. R. Williams and S. K. Loyalka, *Aerosol Science Theory and Practice*, Pergamon, 1989.
11. B. H. McDonald, "Assessing Numerical Methods Used in Nuclear Aerosol Transport Models," in *Proceedings of Water-cooled Reactor Aerosol Code Evaluation and Uncertainty Assessment*, E. della Loggia and J. Royen, Editors, EUR-11351 EX, Commission of the European Communities, Luxembourg, 1988.
12. D. J. Rader, *J. Aerosol Science*, 21 (1990) 161.
13. S. C. Saxena and R. K. Joshi, *Thermal Accommodation and Adsorption Coefficients*, Hemisphere Publishing Co., 1991.
14. F. O. Goldman and H. Y. Wachman, *J. Chem. Phys.*, 46 (1967) 2376.
15. H-C. Hansson and M. S. Ahlberg, *J. Aerosol Science*, 16 (1985) 69.
16. M. D. Allen, O. R. Moss, and J. K. Briant, *J. Aerosol Science*, 10 (1978) 43.
17. W. Stober, *Aerosol Science*, 2 (1971) 453.
18. J. Kops, G. Dibbets, L. Hermans, and J. F. Van de Vate, J. *Aerosol Science*, 6 (1975).

19. J. F. Van de Vate, W. F. Van Leeuwen, A. Plomp, and H.C. D. Smet, *J. Aerosol Science*, 11 (1980) 67.

20. S. R. Forrest and T. A. Witten, *J. Phys.* A, 12 (1979) L109.

21. P. Meakin, *J. Chem. Phys.*, 81 (1984) 4637.

22. R. Richter, L. M. Sanders, and Z. Cheng, *J. Colloid Interface Science*, 100 (1984) 203.

23. J. Feder, T. Jossang and E. Rosenquist, *Phys. Rev. Letters*, 53 (1984) 1403.

24. J. E. Martin, D. W. Schaefer, and A. Hurd, *Phys. Rev.*, A33 (1986) 3540.

25. R. D. Mountain, G. W. Mulholland, and H. Baum, *J. Colloid and Interface Science*, 114 (1986) 67.

26. R. J. Samson, G. W. Mulholland, and J. W. Gentry, *Langmuir*, 3 (1987) 272.

27. A. J. Hurd and W. L. Fowler, *J. Colloid Interface Science*, 122 (1988) 178.

28. H. X. Zhang, C. M. Sorensen, E. R. Ramer, B. J. Oliver, and J. F. Merkin, *Langmuir*, 4 (1988) 867.

29. G. W. Mulholland, R. J. Samson, R. D. Mountain, and M. H. Ernst, *Energy and Fuels*, 2 (1988) 481.

30. F. Legaffre, *J. Aerosol Science*, 20 (1989) 857.

31. P. Meakin, B. Donn, and G. W. Mullholland, *Langmuir*, 5 (1989) 510.

32. C. M. Megardis and R. A. Dobbins, *Combustion Science and Technology*, 71 (1990) 95.

33. T. T. Charelampopoulos and H. Chang, *Combustion and Flame*, 87 (1991) 89.

Shape Factors

1. D. Pavone, *GPHS Safety Tests Particle Size Data Package*, LACP-86-62, Los Alamos National Laboratory, Los Alamos, NM, May 1986.
2. M. E. O'Neill, *Proc. Cambridge Philosophical Society*, 65 (1969) 543.
3. R. Hill and G. Power, *Quarterly J. Mechanics and Applied Mathematics*, 9 (1956) 313.
4. D. Leith, *Aerosol Science and Technology*, 6 (1987) 153.
5. C-T. Lee and D. Leith, *J. Aerosol Science*, 20 (1989) 503.
6. J. Wadell, *J. Geology*, 41 (1939) 310.
7. B. D. Bowen and J. H. Masliyah, *Canadian J. Chemical Engineering*, 51 (1973) 8.
8. Cited in R. Clift, J. R. Grace, and M. E. Weber, *Bubbles, Drops and Particles*, Academic Press, 1978.
9. A. D. Ah Chin, J. Portz, M. Ward, J. K. Beddow, and A. F. Vetter, *Powder Technology*, 48 (1986) 59.
10. N. N. Clark, P. Gabriele, S. Shuker, and R. Turton, *Powder Technology*, 59 (1989) 69.
11. T. L. Thompson and N. N. Clark, *Powder Technology*, 67 (1981) 57.
12. J. S. McNown and J. Malaika, *Transactions American Geophysical Union*, 31 (1951) 74.
13. W. B. Kunkel, *J. Appl. Phys.*, 19 (1948) 1056.
14. J. R. Heiss and J. Coull, *Chemical Engineering Progress*, 48 (1952) 133.
15. E. S. Pettyjohn and E.B. Christiansen, *Chemical Engineering Progress*, 44 (1948) 157.
16. P. N. Blumberg and C. M. Mohr, *AIChE Journal*, 14 (1968) 331.
17. R. Hill and G. Power, *Q. J. Mech and Appl. Math.*, 9 (1956) 313.
18. M. M. R. Williams and S. K. Loyalka, *Aerosol Science: Theory and Practice*, Pergamon Press, 1991.
19. B. Aschenbrenner, *J. Sedimentary Petrology*, 26 (1956) 15.
20. L. I. Briggs, D. S. McCulloch, and F. Moser, J. *Sedimentary Petrology*, 32 (1962) 645.
21. D. W. Luerkens, J.K. Beddow, and A. F. Better, "Theory of Morphological Analysis," p. 3 in *Particle Characterization in Technology, Volume II, Morphological Analysis*, J.K. Beddow, editor, CRC Press. See also D. W.

Luerkens, *Theory and Application of Morphological Analysis: Fine Particles and Surfaces*, CRC Press, 1991.

22. N. N. Clark, *Powder Technology*, 51 (1987) 243.
23. G. H. Ganser, *Powder Technology*, 77 (1993) 143.
24. A. Haider and O. Levenspiel, *Powder Technology*, 58 (1989) 63.
25. J. G. de la Torre and V. A. Bloomfield, *Quarterly Reviews of Biophysics*, 14 (1981) 81.
26. E. B. Christiansen and D. H. Barker, *Amer. Institute of Chemical Engineers Journal*, 11 (1965) 145.

Notes

Notes

Distribution:

2 Haliburton NUS
Attn: H. Firstenburg,
B. Bartram
910 Clopper Road
Gaithersburg, MD 20878

2 Orbital Sciences Corporation
Attn: R. Carpenter, E. Skrabek
20301 Century Blvd. MS A-35
Germantown, MD 20874

1 Teledyne Brown Energy Systems
Attn: D. Anderson
10707 Gilroy Road
Hunt Valley, MD 21031

4 Lockheed Martin Missiles & Space
Attn: L. DeFillipo, D. Hemler
MS 29B12
Building B – Valley Forge
P. O. Box 8555
Philadelphia, PA 19101

1 Foils Engineering
Attn: M. Eck
25731 Ridge Road
Damascus, MD 20872

1 University of New Mexico
Attn: M. S. El-Genk
Department of Chemical and Nuclear Engineering
Albuquerque, NM 87131-1341

3 JHU/APL, MS 6-385
Attn: D. Conn, P. Brenza,
E. Lucero
Johns Hopkins Road
Laurel, MD 20723

1 Lamb Associates .
Attn: E. Johnson
1017 Glen Arbor Court
Dayton, OH 45459-5421

3 U.S. Department of Energy
Attn: D. Owings, L. Rutger,
B. Cook
MS NE-50
19901 Germantown Road
Germantown, MD 20874

2 Lockheed Martin Missiles & Space
Attn: R. Rosko, C. Chang
MS 20B14
Building B – Valley Forge
P. O. Box 8555
Philadelphia, PA 19101

2 Lockheed Martin Missiles & Space
Attn: N. A. Dean, C. P. Ha
4041 N. First St.
San Jose, CA 95134

1 AFSA/SEWA
Attn: B. E. Hickman, Col.
9700 Avenue G, Bldg 24499
Kirtland AFB, NM 87117-5670

1 NASA HQ/Code QS
Attn: J. W. Lyver
Room 5T80
300 E Street, SW
Washington, DC 20546-0001

1 Department of Energy HQ
Code EH-32
Attn: D. Pyatt
19901 Germantown Road
Germantown, MD 20874

1 Attn: R. Pollard
Vitro; Suite 825
400 Virginia Ave.,SW
Washington, DC 20024

1 45th Space Wing/SEO
Attn: R. Stout
Bldg 423, Rm C310
1201 Minuteman Drive
Patrick AFB, FL 32925-5000

1 Research Triangle Institute
Attn: W. H. Boggs
3000 N. Atlantic Avenue, # 108
Cocoa Beach, FL 32931-5029

1 NASA/Marshall Space Flight
Center/CR-50
Attn: R. Gladwin
Huntsville, AL 35812

1 Los Alamos National Laboratory
Attn: J. Taylor
341 Potrillo Drive
Los Alamos, NM 87544

1 USEPA/CRD-LV
Attn: G. J. Martin, Capt.
Box 93478
Las Vegas, NV 89193-3478

1 US Nuclear Regulatory Commission, Research Division
Attn: J. Randall
Washington, D.C. 20555

1 Safety Factor Associates
Attn: M. V. Frank
Suite #106
4401 Manchester Avenue,
Encinitas, CA 92024

1 National Aeronautics and Space Administration, Johnson Space Center/Code EM
Attn: F. J. Benz
Houston, TX 77058-3696

1 Kennedy Space Center
Code RT-SOE
Attn: R. R. Gillett
KSC, FL 32899

1 5SLS/LMUE
Attn: J. A. Noe
Cape Canaveral AFS, FL 32899

2 AFSA/SENA
Attn: M. Thornton, LtCol, USAF
E. Baker, Capt., USAF
9700 Avenue G, Bldg 24499
Kirtland AFB, NM 87117-5670

1 The Aerospace Corporation
Attn: W. Ailor
Mail Stop M1-023
PO Box 92957
El Segundo, CA 90009-2957

1 NASA-Marshall Space Flight Center
Attn: B. J. Anderson
Mail Code EL-23
Huntsville, AL 35812

1 Attn: J. A. Sholtis, Jr.
2 Oso Drive
Tijeras, NM 87059-7632

1 Jason Associates Corporation
Attn: R. C. Nelson
3250 Port of Benton Blvd
Richland, WA 99352

1 Sandia National Laboratories
Attn: W. McCulloch
Org 6411, Mail Stop 0405
P.O. Box 5800
Albuquerque, NM 87185-0405

1 James R. Coleman Consulting, Inc
Attn: J. Coleman
826 Deadrick Road
Knoxville, TN 37920

1 NOAA/ATDD
Attn: W. R. Pendergrass
PO Box 2456
Oak Ridge, TN 37831

1 Attn: J. Leary
526 Hillside Ave.
Santa Fe, NM 87501

1	MS-0734	M. E. Tadros
1	MS-0736	N. R. Ortiz
1	MS-0739	F. Gelbard
1	MS-0739	D. C. Williams
5	MS-0744	D. A. Powers
1	MS-0744	A. C. Marshall
3	MS-0747	V. J. Dandini
1	MS-0747	K. M. Hays
1	MS-0747	G. D. Wyss
1	MS-0747	A. L. Camp
5	MS-0748	F. T. Harper
1	MS-0767	B. A. Boughton
1	MS-0827	J. E. Brockmann
1	MS-0828	P. J. Hommert
1	MS-0828	R. D. Skocypec
1	MS-0834	M. L. Hobbs
1	MS-0834	A. C. Ratzel
1	MS-0835	T. C. Bickel
7	MS-0835	D. Dobranich
1	MS-0835	R. C. Dykhuizen
1	MS-0835	V. J. Romero
1	MS-0836	S. R. Tieszen
1	MS-1081	D. K. Monroe
1	MS-9018	Central Technical Files, 8940-2
5	MS-0899	Technical Library, 4916
2	MS-0619	Review & Approval Desk for DOE/OSTI, 12690
1	DOE/EE-32	T. G. Marachaux
1	DOE/EE-222	S. Dillich